NASA TECHNICAL NOTE

NASA TN D-2622

c. 1

NASA TN D-2622

TECH LIBRARY KAFB, NM

0154654

TRANSONIC AERODYNAMIC CHARACTERISTICS OF A SERIES OF BODIES HAVING VARIATIONS IN FINENESS RATIO AND CROSS-SECTIONAL ELLIPTICITY

by Bernard Spencer, Jr., and W. Pelham Phillips

Langley Research Center

Langley Station, Hampton, Va.

NATIONAL AERONAUTICS AND SPACE ADMINISTRATION • WASHINGTON, D. C. • FEBRUARY 1965

TECH LIBRARY KAFB, NM

0154654

TRANSONIC AERODYNAMIC CHARACTERISTICS OF A SERIES OF BODIES HAVING VARIATIONS IN FINENESS RATIO AND CROSS-SECTIONAL ELLIPTICITY

By Bernard Spencer, Jr., and W. Pelham Phillips

Langley Research Center
Langley Station, Hampton, Va.

NATIONAL AERONAUTICS AND SPACE ADMINISTRATION

For sale by the Office of Technical Services, Department of Commerce,
Washington, D.C. 20230 -- Price $3.00

TRANSONIC AERODYNAMIC CHARACTERISTICS OF A SERIES OF BODIES HAVING VARIATIONS IN FINENESS RATIO AND CROSS-SECTIONAL ELLIPTICITY

By Bernard Spencer, Jr., and W. Pelham Phillips
Langley Research Center

SUMMARY

An investigation has been made in the Langley high-speed 7- by 10-foot tunnel to determine the longitudinal and lateral aerodynamic characteristics at transonic speeds of a series of low-wave-drag lifting bodies having variations in fineness ratio and cross-sectional ellipticity.

Increasing horizontal-to-vertical axis ratio for a body having a given fineness ratio results in increases in the variation of lift and lift-drag ratio with angle of attack at all test Mach numbers.

Increasing fineness ratio for a body with any given horizontal-to-vertical axis ratio results in slight reductions in the drag at zero lift at all test Mach numbers and large reductions in the transonic drag rise noted for the bodies. At all test Mach numbers, the highest values of lift-drag ratio obtained for any horizontal-to-vertical axis ratio occur for the body having the highest fineness ratio.

There are only minor effects of changing fineness ratio on the longitudinal center-of-pressure location for low angles of attack in the Mach number range of the investigation.

For the moment-reference-point location of the present investigation each of the bodies exhibited static directional instability with reductions in the level of directional instability indicated for increases in horizontal-to-vertical axis ratio. These reductions in directional instability were accompanied by corresponding increases in the variation of positive effective dihedral with increasing angle of attack for the Mach number range of the present investigation.

Changes in the sign of the side-force parameter were noted to occur as the horizontal-to-vertical axis ratio was increased for a body having a given fineness ratio. Progressive reductions in the angle of attack at which sign reversal occurs result from either increasing horizontal-to-vertical axis ratio for a given fineness ratio or increasing fineness ratio for a given horizontal-to-vertical axis ratio.

INTRODUCTION

The National Aeronautics and Space Administration is presently engaged in investigations to determine the longitudinal and lateral aerodynamic characteristics from low subsonic to hypersonic speeds of generalized lifting-body shapes with application as possible manned reentry configurations. (See refs. 1 to 10.) Research on low-fineness-ratio cones at supersonic speeds (ref. 5), a high-fineness-ratio low-wave-drag body at subsonic speeds (ref. 6), and a series of low-wave-drag bodies having variations in fineness ratio at supersonic speeds (ref. 10) has indicated that notable gains in performance may be realized from varying body cross section from circular to elliptic (elongations in the horizontal plane). These improvements in performance should improve maneuverability and range control throughout the range of Mach numbers to be encountered (as suggested in refs. 1 and 11). Improvement in the performance of the basic body should also be reflected in significant gains in overall performance during landing when these bodies are used in combination with wings having extremely low aspect ratio and high sweep, since the body will constitute a major portion of the lifting surface.

The present investigation was initiated to provide aerodynamic information from low subsonic through transonic speeds on the effects of changing fineness ratio and cross-sectional ellipticity on the aerodynamic characteristics for a series of bodies representing low-wave-drag shapes at hypersonic speeds, where the lateral coordinate varies as the 2/3 power of the longitudinal coordinate. Results of an investigation to determine the aerodynamic characteristics of these bodies at supersonic speeds are presented in reference 10.

Variations in horizontal-to-vertical axis ratio from 0.5 to 2.0 are included for effective body fineness ratios of 3, 5, and 7. Tests were conducted in the Langley high-speed 7- by 10-foot tunnel in a range of Mach numbers from 0.40 to 1.14, corresponding to a range of average test Reynolds number per foot from approximately 2.7×10^6 to 4.5×10^6. The angle-of-attack range varied from approximately -5° to 21° at angles of sideslip of 0° and 5°.

SYMBOLS

Longitudinal data are presented about the stability axes, and lateral data are presented about the body axes. The coefficients are nondimensionalized with respect to the body base area (constant for all configurations) and the base diameter of the circular-cross-section bodies, unless otherwise noted. The longitudinal location of the moment reference point was taken as 66.67 percent of the total length for each configuration. The vertical location of the moment reference point for each body is indicated in figure 1.

C_L lift coefficient, $\frac{\text{Lift}}{qS_b}$

C_D drag coefficient, $\frac{\text{Drag}}{qS_b}$

C_m pitching-moment coefficient, $\frac{\text{Pitching moment}}{qS_b d}$

C_l rolling-moment coefficient, $\frac{\text{Rolling moment}}{qS_b d}$

C_n yawing-moment coefficient, $\frac{\text{Yawing moment}}{qS_b d}$

C_Y side-force coefficient, $\frac{\text{Side force}}{qS_b}$

$C_{D,o}$ drag coefficient at zero lift

$C_{m,o}$ pitching-moment coefficient at zero lift

C_{L_α} lift-curve slope ($\alpha \approx 0^\circ$), per deg

C_{N_α} normal-force-curve slope ($\alpha \approx 0^\circ$), per deg

C_{m_α} longitudinal stability parameter, per deg

$C_{l_\beta} = \left(\frac{\Delta C_l}{\Delta \beta}\right)_{\beta=0^\circ,5^\circ}$, per deg

$C_{n_\beta} = \left(\frac{\Delta C_n}{\Delta \beta}\right)_{\beta=0^\circ,5^\circ}$, per deg

$C_{Y_\beta} = \left(\frac{\Delta C_Y}{\Delta \beta}\right)_{\beta=0^\circ,5^\circ}$, per deg

A aspect ratio $\frac{\left(2y_{max}\right)^2}{S_p}$

a length of semimajor axis of elliptic cross section, ft

b length of semiminor axis of elliptic cross section, ft

d	equivalent base diameter of bodies, $2\sqrt{a_{max}b_{max}}$
FR	body effective fineness ratio, l/d
l	total body length, ft
L/D	lift-drag ratio
$(L/D)_{max}$	maximum L/D obtained for a given body
M	Mach number
n	power body exponent in $y = y_{max}\left(\frac{x}{l}\right)^n$
q	free-stream dynamic pressure, lb/sq ft
r	local radius for circular body, ft
S_b	body base area, $\pi(d/2)^2$, 0.08727 sq ft
S_{cross}	cross-sectional areas of bodies, sq ft
S_p	body projected planform area, sq ft
S_{wet}	wetted area of bodies (excluding base area), sq ft
x	longitudinal coordinate of bodies, ft
$\frac{x_{cp}}{l}$	longitudinal center-of-pressure location ($\alpha = 0^\circ$), $\frac{x_o}{l} - \frac{\partial C_{m_\alpha}}{\partial C_{N_\alpha}}\left(\frac{d}{l}\right)$
x_r	longitudinal coordinate of moment reference point
y	lateral coordinate of bodies, $f(x,n)$; for example, $y = a$ for $\phi = 0^\circ$ and $y = b$ for $\phi = 90^\circ$
α	angle of attack, deg
$\alpha_{(C_{Y_\beta}=0)}$	angle of attack at which C_{Y_β} reverses sign
β	angle of sideslip, deg
ϕ	angle of roll about the body ordinate reference line, deg

Subscript:

max maximum

Configuration designations:

A circular body, $a/b = 1.0$

B elliptic body, $a/b = 1.5$

C elliptic body, $a/b = 2.0$

Configuration designation subscripts:

1 symmetrical bodies, $\phi = 0^\circ$

2 negatively displaced bodies, $\phi = 0^\circ$

4 symmetrical bodies, $\phi = 90^\circ$

MODELS

Three-view drawings of the body shapes used in the major portion of the present investigation are shown in figure 1, along with pertinent geometric characteristics and configuration designations. In these designations, the number preceding the configuration cross-section designation indicates effective fineness ratio, the letter indicates the cross-section ellipticity, and the subscript indicates the symmetry of the body. For example, $3A_1$ represents a symmetrical body with an effective fineness ratio of 3, a circular cross section, and $\phi = 0^\circ$. Photographs of the symmetrical bodies of revolution $3A_1$ and $5A_1$ and the elliptic symmetrical bodies $5C_1$ and $7C_1$ are shown in figure 2.

The body shapes of the investigation had effective fineness ratios of 3, 5, and 7, with effective fineness ratio being defined as $\frac{l}{2\sqrt{a_{max}b_{max}}}$. The body planforms followed a 2/3-power contour $y = y_{max}\left(\frac{x}{l}\right)^{2/3}$, which for circular cross sections represents a low-wave-drag body shape at hypersonic speeds. In varying the body cross sections from circular to elliptic the longitudinal distribution of cross-sectional area was held constant for a given fineness ratio as shown in figure 3. All bodies of the investigation had the same base area that has been used as the reference area.

The bodies with horizontal-to-vertical axis ratio of 0.5 were obtained by rotation of the symmetrical $a/b = 2.0$ bodies through a roll angle of $\phi = 90^\circ$.

Design ordinates of the symmetrical bodies are given in table I, and pertinent geometric characteristics of these bodies are presented in table II.

The negatively displaced bodies were formed by displacing each cross section vertically, so that the uppermost point of each section lay on the body reference line. (See fig. 1.)

TEST AND CORRECTIONS

The present investigation was conducted in the Langley high-speed 7- by 10-foot tunnel at Mach numbers from 0.40 to 1.14, corresponding to a range of average test Reynolds numbers per foot of approximately 2.7×10^6 to 4.5×10^6. The angle-of-attack range of the investigation was from approximately -5° to 21°.

The lateral stability parameters were obtained from test data taken over the angle-of-attack range at angles of sideslip of 0° and 5°; therefore, the sideslip derivatives were obtained between $\beta = 0^\circ$ and $\beta = 5^\circ$ and do not account for any nonlinearities which may exist in the intermediate range of sideslip angle. Forces and moments were measured by use of a six-component strain-gage balance.

On all bodies tested, transition was fixed at a distance of 0.5-inch aft of the body apex by a 1/8-inch-wide circumferential band of carborundum grains having a nominal diameter of 0.0117 inch. Transition was also fixed along the body length on the lower surface, at a distance from the body center line equal to one-half the perimeter at the maximum width.

Corrections to the angle of attack because of sting and balance deflection under load have been applied to the data, but no corrections for the effect of base pressure have been applied. No attempt has been made to correct the drag data for the induced effects of sting-support interference; however, the ratio of sting diameter to equivalent base diameter was relatively low (i.e., 0.3 or less). The maximum error (maximum at transonic speeds) resulting from sting effects on measured minimum drag is estimated to be of the order of ± 10 percent, based on indicated results shown in references 12 to 14.

RESULTS AND DISCUSSION

Presentation of Results

The basic longitudinal aerodynamic characteristics of the various bodies tested are presented in figures 4 to 13 with the lateral directional characteristics presented in figures 14 to 18 as functions of angle of attack. Table III is included to aid in locating basic data figures for the various bodies tested. Figures 19 to 22 present a summary of the longitudinal aerodynamic characteristics obtained from the basic data of the present investigation plotted as a function of Mach number and include the summary data of reference 10 at supersonic speeds. Figure 23 presents the effects of fineness ratio and ellipticity on the side-force characteristics of the various bodies tested.

Longitudinal Aerodynamic Characteristics

The effects of increasing a/b on the longitudinal aerodynamic characteristics of the symmetrical bodies having fineness ratios of 3, 5, and 7 at Mach numbers from 0.4 to 1.14 are presented in figures 4 to 8. Large increases in C_L, C_m, and C_D for given positive angles of attack result from a change from $a/b = 2.0$, $\phi = 90^\circ$ to $a/b = 2.0$, $\phi = 0^\circ$ at all test Mach numbers for each fineness ratio. These gains are primarily a result of the increases in planform area for a given fineness ratio. The increases in lift-curve slope (fig. 19(a)) are also a result of increases in aspect ratio accompanying a change from $a/b = 2.0$, $\phi = 90^\circ$ to $a/b = 2.0$, $\phi = 0^\circ$ for a given fineness ratio as illustrated in figure 19(b) where each value of lift-curve slope is based on the individual projected planform area. There are only slight effects of increasing Mach number from 0.40 to 2.86 on the lift characteristics for any given body tested. The lift characteristics in the range of Mach numbers from 1.5 to 2.86 were obtained from reference 10.

The variation of drag coefficient at zero lift with Mach number (fig. 20(a)) for the symmetrical bodies indicates an increasing trend in $C_{D,o}$ with increasing a/b with the coefficients based on a constant reference. These increases are directly in proportion to the increases in body wetted area realized from increasing a/b. When the coefficient is based on the individual body planform area, however, increases in $C_{D,o}$ for increasing a/b ($\phi = 90^\circ$) and decreases in $C_{D,o}$ for increasing a/b ($\phi = 0^\circ$) occur at all Mach numbers, as would be expected. The primary effect of increasing fineness ratio is large reduction in the drag-rise characteristics at transonic speeds for any given body. The decreases in $C_{D,o}$ for all bodies as Mach number is increased in the supersonic range are as expected, due primarily to the base drag of the bodies approaching zero as the Mach numbers approach hypersonic speeds.

Large increases in L/D result from increasing a/b ($\phi = 0^\circ$) for a body having any given fineness ratio throughout the angle-of-attack range at all Mach numbers. (See part d of figs. 4 to 8.) Increasing fineness ratio for a body with a given a/b results in further increases in L/D at a given angle of attack because of the large reductions in $C_{D,o}$, although the bodies with the lowest fineness ratios have the highest aspect ratios and, therefore, would be expected to have the lowest production of drag due to lift.

Figure 21 presents the variation of the maximum L/D values obtained for each of the bodies tested, as a function of Mach number, and includes results presented in reference 10 for Mach numbers from 1.5 to 2.86. At all Mach numbers, a maximum rearward shift in center-of-pressure location for low angles of attack of approximately 2 to 3 percent of body length results from changing $a/b = 2.0$, $\phi = 90^\circ$ to $a/b = 1.0$, $\phi = 90^\circ$ and generally smaller changes are noted from changing $a/b = 1.0$, $\phi = 0^\circ$ to $a/b = 2.0$, $\phi = 0^\circ$. (See fig. 22.) It is interesting to note that there are little or no effects of fineness ratio on the longitudinal center-of-pressure location.

A comparison of the variations of C_L, C_D, and C_m for the symmetrical and the negatively displaced bodies ($a/b = 1.0$ or 2.0, $\phi = 0^\circ$) shows the primary effect of displacement to be a decrease in angle of attack (for a given value of C_L, C_D, or C_m) by an increment approximately equal to the angular displacement of the body center line at all test Mach numbers (see figs. 9 to 13), with little or no effect on the maximum L/D obtained except on the angle of attack at which this value of (L/D) occurs. This body displacement may have possible application for providing positive values of $C_{m,o}$ for low-aspect-ratio wing-body configurations when the body shapes of the present investigation are employed as forebodies, without greatly penalizing the configuration $(L/D)_{max}$.

Lateral-Directional Characteristics

A comparison of the lateral-directional characteristics of the symmetrical bodies having fineness ratios of 3, 5, and 7 and variations in a/b from 1.00 to 2.00 ($\phi = 0^\circ$ and 90°) is presented in figures 14 to 16. Reductions in the level of directional instability result from changing $a/b = 2.0$, $\phi = 90^\circ$ to $a/b = 2.0$, $\phi = 0^\circ$ (figs. 15 and 16), with corresponding increases in the variation of $-C_{l_\beta}$ with increasing angle of attack at all test Mach numbers and all fineness ratios. Increasing fineness ratio results in increases in directional instability with considerable irregularity in the variation of C_{n_β} with increasing angle of attack noted above approximately 8° for all Mach numbers. This irregularity was also noted at supersonic speeds in reference 10.

The effects of body displacement on the lateral-directional characteristics of the configurations having a fineness ratio of 3 are presented in figure 17. Little or no effect on the variation of C_{n_β} or C_{l_β} with angle of attack is indicated for the test range of Mach numbers. Similar effects of displacement at angles of attack below 4° are exhibited for the bodies having a fineness ratio of 7 at all test Mach numbers (fig. 18); however, rather large variations in C_{n_β} result from body displacement at the higher angles of attack.

It is interesting to note for the symmetrical bodies that for a given fineness ratio, changes in the sign of the side-force parameter C_{Y_β} occur as a/b is increased ($\phi = 0^\circ$). (See figs. 14 to 16.) Progressive reductions in the angle of attack at which C_{Y_β} reverses sign result from either increasing a/b ($\phi = 0^\circ$) for a given fineness ratio, or increasing fineness ratio for a given a/b, as summarized in figure 23 for a Mach number of 0.40. This result was found to be true at all test Mach numbers and at a Mach number of 1.5 in reference 10. Above a Mach number of 1.5, however, this effect rapidly disappears. Changes in the sign of C_{Y_β} may enhance the directional stability characteristics for complete, low-aspect-ratio wing-body configurations which may employ these body shapes as fuselage forebodies.

CONCLUSIONS

An investigation has been made in the Langley high-speed 7- by 10-foot tunnel to determine the longitudinal and lateral aerodynamic characteristics at transonic speeds of a series of 2/3-power low-wave-drag bodies having variations in fineness ratio and cross-sectional ellipticity. The results of the investigation may be summarized in the following observations.

1. Increasing horizontal-to-vertical axis ratio for a body having a given fineness ratio results in increases in the variation of lift and lift-drag ratio with angle of attack at all test Mach numbers.

2. Increasing fineness ratio for a body with any given horizontal-to-vertical axis ratio results in reductions in the drag at zero lift at all test Mach numbers and large reductions in the transonic drag rise noted for the bodies. At all test Mach numbers, the highest values of lift-drag ratio obtained for any horizontal-to-vertical axis ratio occur for the body having the highest fineness ratio.

3. There are only minor effects of changing fineness ratio on the longitudinal center-of-pressure location for low angles of attack in the Mach number range of the investigation.

4. For the moment-reference-point location of the present investigation each of the bodies exhibited static directional instability with reductions in the level of directional instability indicated for increases in horizontal-to-vertical axis ratio. These reductions in directional instability were accompanied by corresponding increases in the variation of positive effective dihedral with increasing angle of attack for the Mach number range of the present investigation.

5. Changes in the sign of the side-force parameter were noted to occur as the horizontal-to-vertical axis ratio was increased for a body having a given fineness ratio. Progressive reductions in the angle of attack at which sign reversal occurs result from either increasing horizontal-to-vertical axis ratio for a given fineness ratio or increasing fineness ratio for a given horizontal-to-vertical axis ratio.

Langley Research Center,
National Aeronautics and Space Administration,
Langley Station, Hampton, Va., October 23, 1964.

REFERENCES

1. Rainey, Robert W., compiler: Summary of Aerodynamic Characteristics of Low-Lift-Drag-Ratio Reentry Vehicles From Subsonic to Hypersonic Speeds. NASA TM X-588, 1961.

2. Dennis, David H.; and Edwards, George G.: The Aerodynamic Characteristics of Some Lifting Bodies. NASA TM X-376, 1960.

3. Armstrong, William O.: Hypersonic Aerodynamic Characteristics of Several Series of Lifting Bodies Applicable to Reentry Vehicle Design. NASA TM X-536, 1961.

4. Carleton, W. E.; and Matthews, R. K.: The Aerodynamic Characteristics of Three Elliptical-Cone Lifting Bodies at Transonic Speeds. AEDC-TDR-63-53 (Contract No. AF 40(600)-1000), Arnold Eng. Develop. Center, Apr. 1963.

5. Jorgensen, Leland H.: Elliptic Cones Alone and With Wings at Supersonic Speeds. NACA Rept. 1376, 1958. (Supersedes NACA TN 4045.)

6. Spencer, Bernard, Jr.; and Phillips, W. Pelham: Effects of Cross-Section Shape on the Low-Speed Aerodynamic Characteristics of a Low-Wave-Drag Hypersonic Body. NASA TN D-1963, 1963.

7. Fuller, Dennis E.; Shaw, David S.; and Wassum, Donald L.: Effect of Cross-Section Shape on the Aerodynamic Characteristics of Bodies at Mach Numbers From 2.50 to 4.63. NASA TN D-1620, 1963.

8. Stivers, Louis S., Jr.; and Levy, Lionel L., Jr.: Longitudinal Force and Moment Data at Mach Numbers From 0.60 to 1.40 for a Family of Elliptic Cones With Various Semiapex Angles. NASA TN D-1149, 1961.

9. Eggers, A. J., Jr.; Resnikoff, Meyer M.; and Dennis, David H.: Bodies of Revolution Having Minimum Drag at High Supersonic Airspeeds. NACA Rept. 1306, 1957. (Supersedes NACA TN 3666.)

10. Spencer, Bernard, Jr.; Phillips, W. Pelham; and Fournier, Roger H.: Supersonic Aerodynamic Characteristics of a Series of Bodies Having Variations in Fineness Ratio and Cross-Section Ellipticity. NASA TN D-2389, 1964.

11. Grant, Frederick C.: Importance of the Variation of Drag With Lift in Minimization of Satellite Entry Acceleration. NASA TN D-120, 1959.

12. Stivers, Louis S., Jr.; and Levy, Lionel L., Jr.: Effects of Sting-Support Diameter on the Base Pressures of an Elliptic Cone at Mach Numbers From 0.60 to 1.40. NASA TN D-354, 1961.

13. Fuller, Dennis E.; and Langhans, Victor E.: Effect of Afterbody Geometry and Sting Diameter on the Aerodynamic Characteristics of Slender Bodies at Mach Numbers From 1.57 to 2.86. NASA TN D-2042, 1963.

14. Perkins, Edward W.: Experimental Investigation of the Effects of Support Interference on the Drag of Bodies of Revolution at a Mach Number of 1.5. NACA TN 2292, 1951. (Supersedes NACA RM A8B05.)

TABLE I.- DESIGN BODY ORDINATES FOR SYMMETRICAL BODIES

x, in.	a/b = 1.0	a/b = 1.5		a/b = 2.0	
	r, in.	a, in.	b, in.	a, in.	b, in.
Effective fineness ratio 3					
0	0	0	0	0	0
2	.606	.742	.495	.857	.428
4	.961	1.178	.785	1.360	.680
6	1.260	1.543	1.029	1.782	.891
8	1.526	1.869	1.246	2.158	1.079
10	1.771	2.169	1.446	2.505	1.252
12	2.000	2.449	1.633	2.828	1.414
Effective fineness ratio 5					
0	0	0	0	0	0
2	.431	.528	.352	.609	.305
4	.684	.838	.558	.967	.484
6	.896	1.098	.732	1.267	.634
8	1.086	1.300	.886	1.535	.768
10	1.260	1.543	1.029	1.782	.891
12	1.423	1.742	1.162	2.012	1.006
14	1.577	1.931	1.287	2.229	1.115
16	1.724	2.111	1.407	2.437	1.219
18	1.864	2.283	1.522	2.636	1.318
20	2.000	2.449	1.633	2.828	1.414
Effective fineness ratio 7					
0	0	0	0	0	0
2	.344	.422	.281	.488	.244
4	.547	.669	.446	.774	.387
6	.716	.877	.585	1.014	.507
8	.868	1.063	.708	1.228	.614
10	1.007	1.233	.822	1.424	.712
12	1.137	1.392	.928	1.608	.804
14	1.260	1.543	1.029	1.782	.891
16	1.377	1.687	1.125	1.948	.974
18	1.490	1.825	1.216	2.107	1.054
20	1.598	1.957	1.305	2.261	1.130
22	1.703	2.086	1.391	2.409	1.204
24	1.805	2.210	1.474	2.553	1.276
26	1.904	2.331	1.554	2.693	1.346
28	2.000	2.449	1.633	2.828	1.414

TABLE II.- BODY GEOMETRIC CHARACTERISTICS

[S_b = 12.5626 sq in.]

Body shape	A	Volume, cu in.	S_{wet}, sq in.	S_p, sq in.	$\frac{S_{wet}}{S_b}$	$\frac{S_p}{S_b}$
Effective fineness ratio 3						
A_1	0.5556	64.6667	92.0880	28.2000	7.3303	2.2924
B_1	.6803	64.6667	94.9104	35.2449	7.5550	2.8071
C_1	.7857	64.6667	100.3968	40.2828	7.9917	3.2320
C_4	.3928	64.6667	100.3968	20.1414	7.9917	1.6210
Effective fineness ratio 5						
A_1	0.3334	107.9550	151.1424	47.3333	12.0311	3.8207
B_1	.4082	107.9550	155.7936	58.4081	12.4013	4.6784
C_1	.4713	107.9550	164.7792	67.4713	13.1166	5.4025
C_4	.2357	107.9550	164.7792	33.2356	13.1166	2.7012
Effective fineness ratio 7						
A_1	0.2381	151.0000	211.1616	67.4666	16.8087	5.3490
B_1	.2862	151.0000	217.6416	83.5820	17.3245	6.6716
C_1	.3367	151.0000	230.2128	95.6598	18.3252	7.5635
C_4	.1683	151.0000	230.2128	47.3299	18.3252	3.7818

TABLE III.- INDEX FOR BASIC DATA FIGURES

Body shape	Effective fineness ratio	a/b	Displacement	ϕ, deg	Mach number	Figure
Longitudinal data						
A_1, B_1, C_1, and C_4	3, 5, and 7	1.0, 1.5, and 2.0	0	0 and 90	0.40	4
	3, 5, and 7	1.0, 1.5, and 2.0	0	0 and 90	.80	5
	3, 5, and 7	1.0, 1.5, and 2.0	0	0 and 90	.90	6
	3, 5, and 7	1.0, 1.5, and 2.0	0	0 and 90	1.00	7
	3, 5, and 7	1.0, 1.5, and 2.0	0	0 and 90	1.13	8
A_1, A_2, C_1, and C_2	3 and 7	1.0 and 2.0	0 and negative	0	0.40	9
	3 and 7	1.0 and 2.0	0 and negative	0	.80	10
	3 and 7	1.0 and 2.0	0 and negative	0	.90	11
	3 and 7	1.0 and 2.0	0 and negative	0	1.00	12
	3 and 7	1.0 and 2.0	0 and negative	0	1.13	13
Lateral data						
A_1, B_1, C_1, and C_4	3	1.0, 1.5, and 2.0	0	0 and 90	0.40 to 1.13	14
	5	1.0, 1.5, and 2.0	0	0 and 90	0.40 to 1.13	15
	7	1.0, 1.5, and 2.0	0	0 and 90	0.40 to 1.13	16
A_1, A_2, C_1, and C_2	3	1.0, 1.5, and 2.0	0 and negative	0 and 90	0.40 to 1.13	17
	7	1.0, 1.5, and 2.0	0 and negative	0 and 90	0.40 to 1.13	18

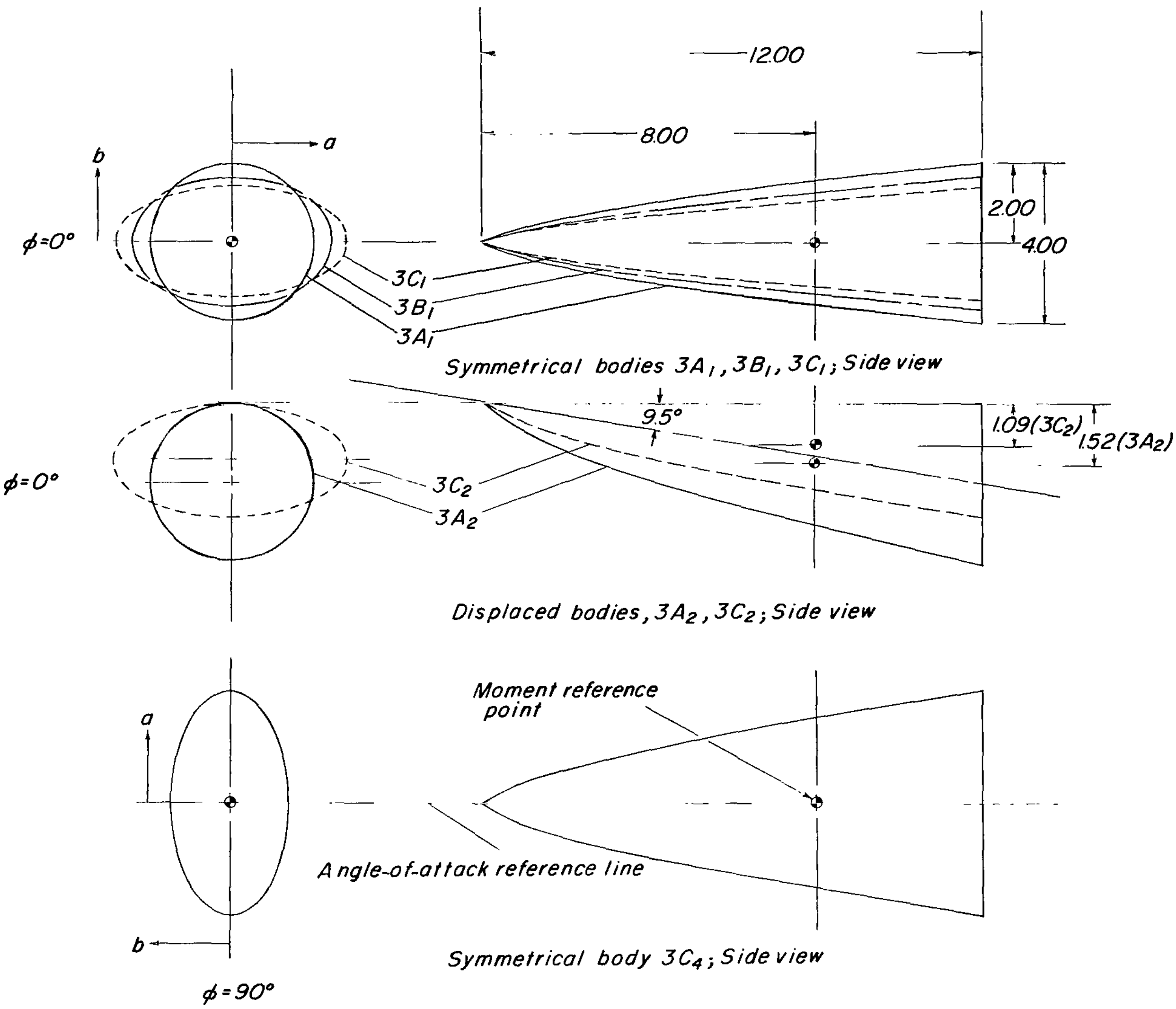

(a) Fineness ratio 3.0.

Figure 1.- Geometric characteristics of various bodies tested. All dimensions are in inches unless otherwise noted.

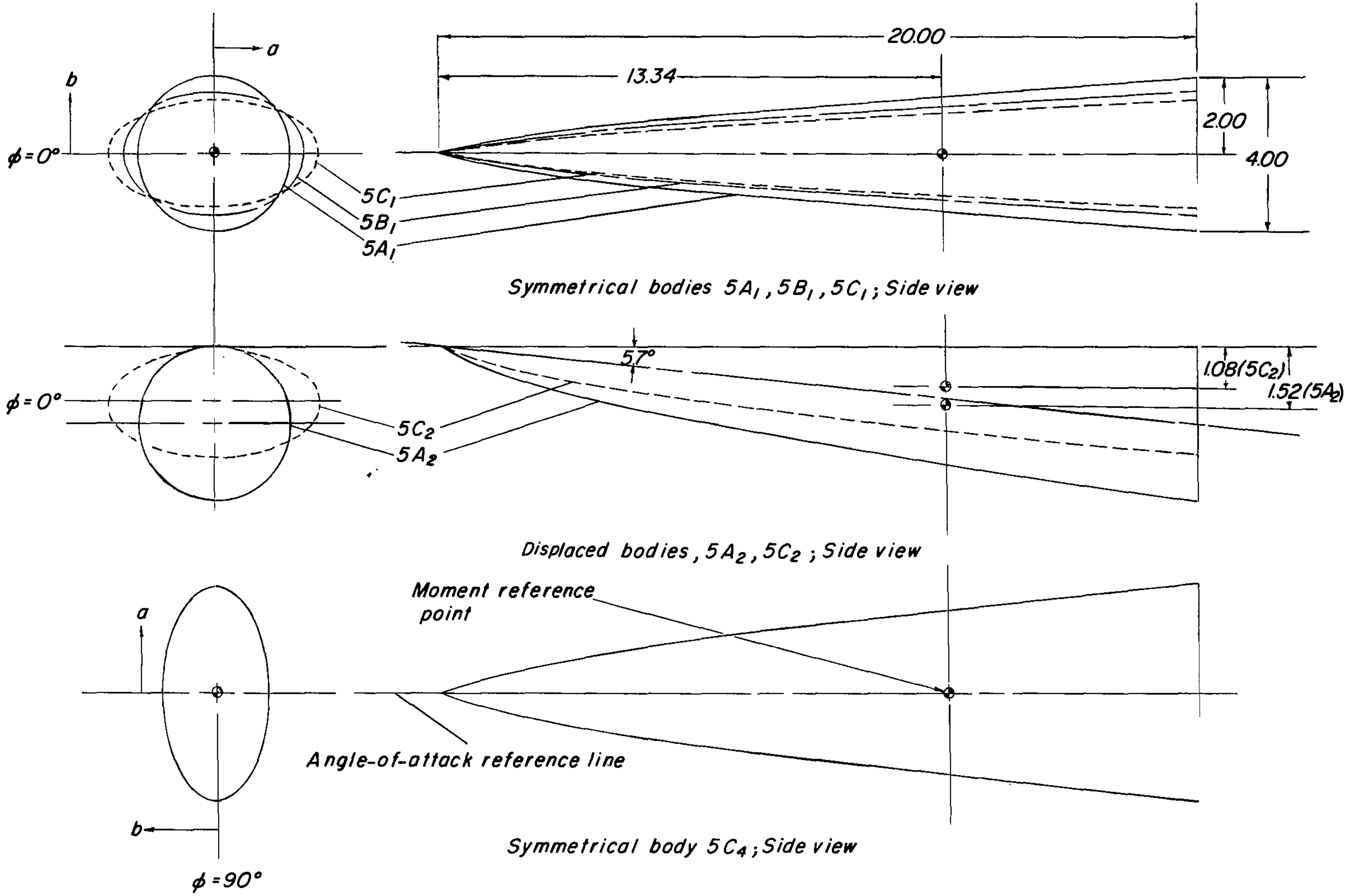

(b) Fineness ratio 5.0.

Figure 1.- Continued.

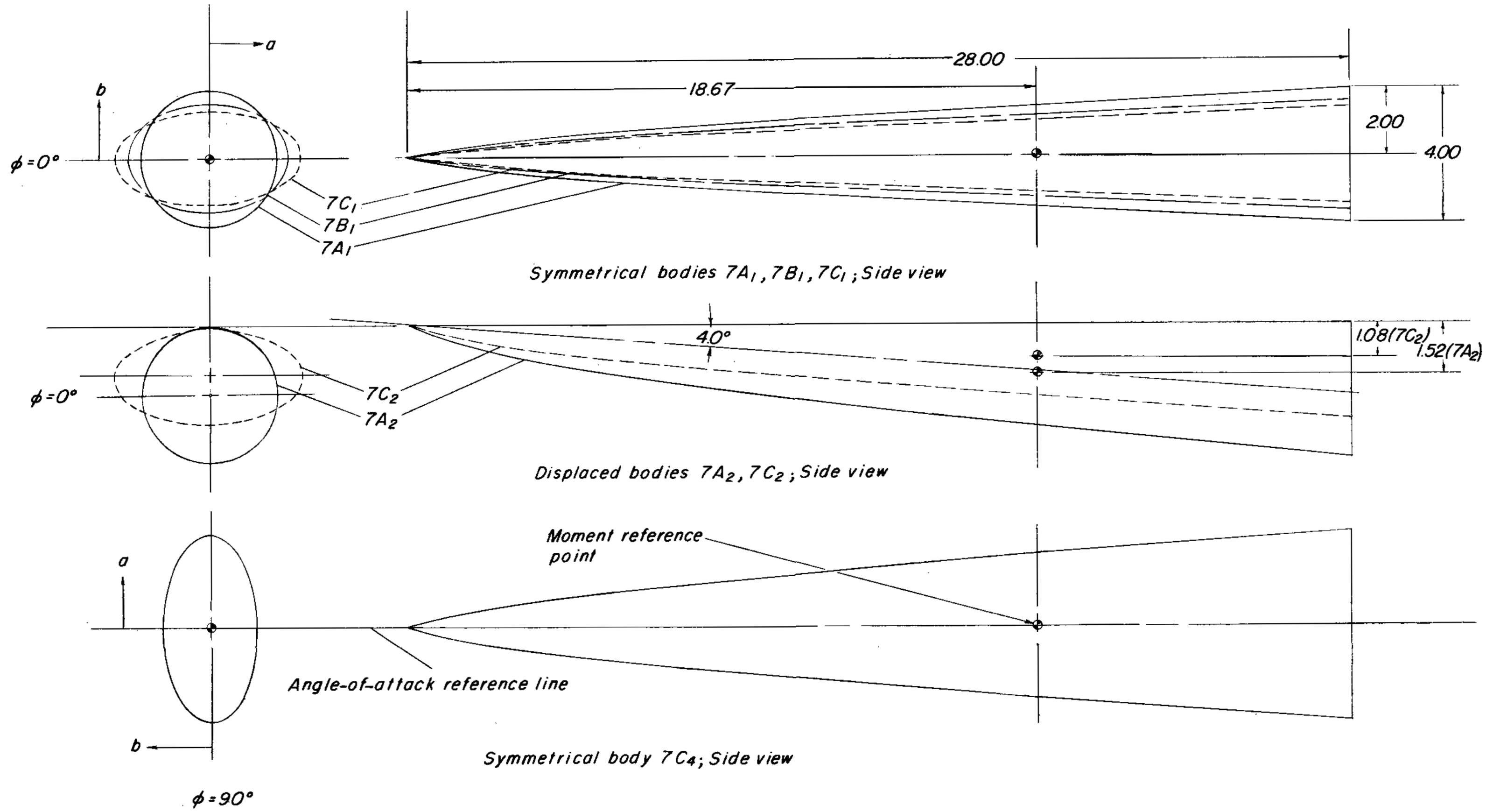

(c) Fineness ratio 7.0.

Figure 1.- Concluded.

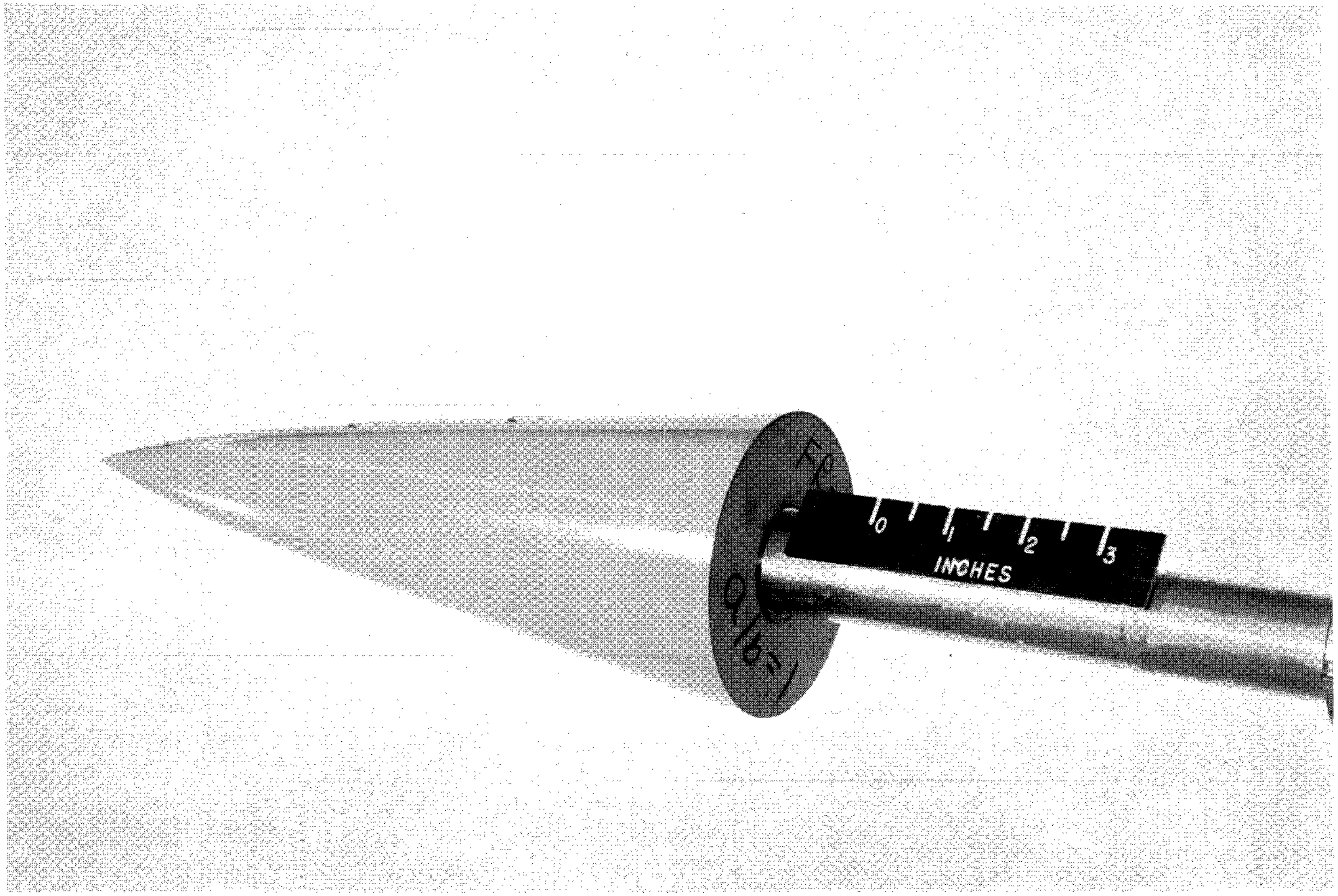

(a) Body $3A_1$. L-63-490

Figure 2.- Photographs of some body configurations tested.

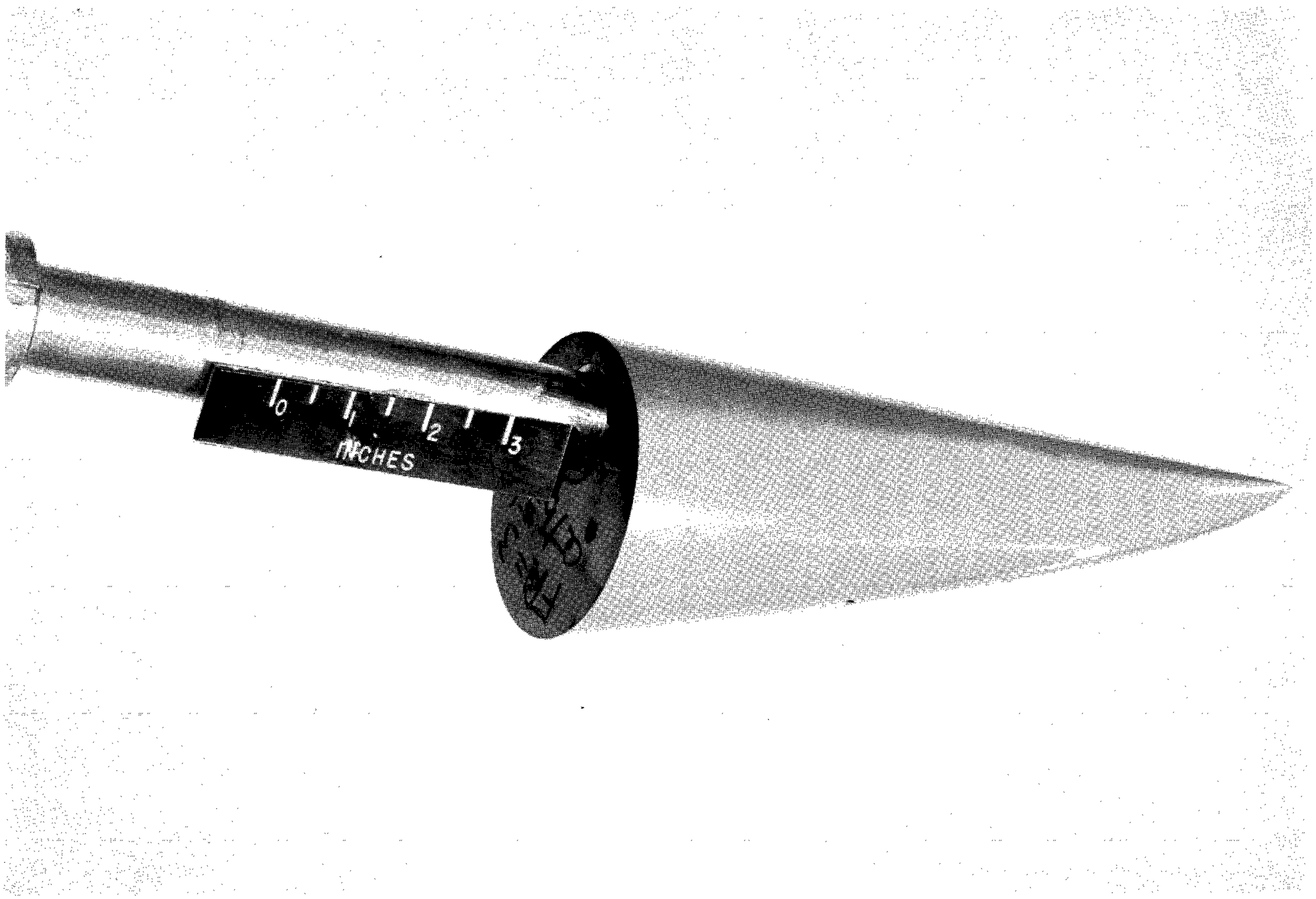

L-64-3031

(b) Body $3A_2$.

Figure 2.- Continued.

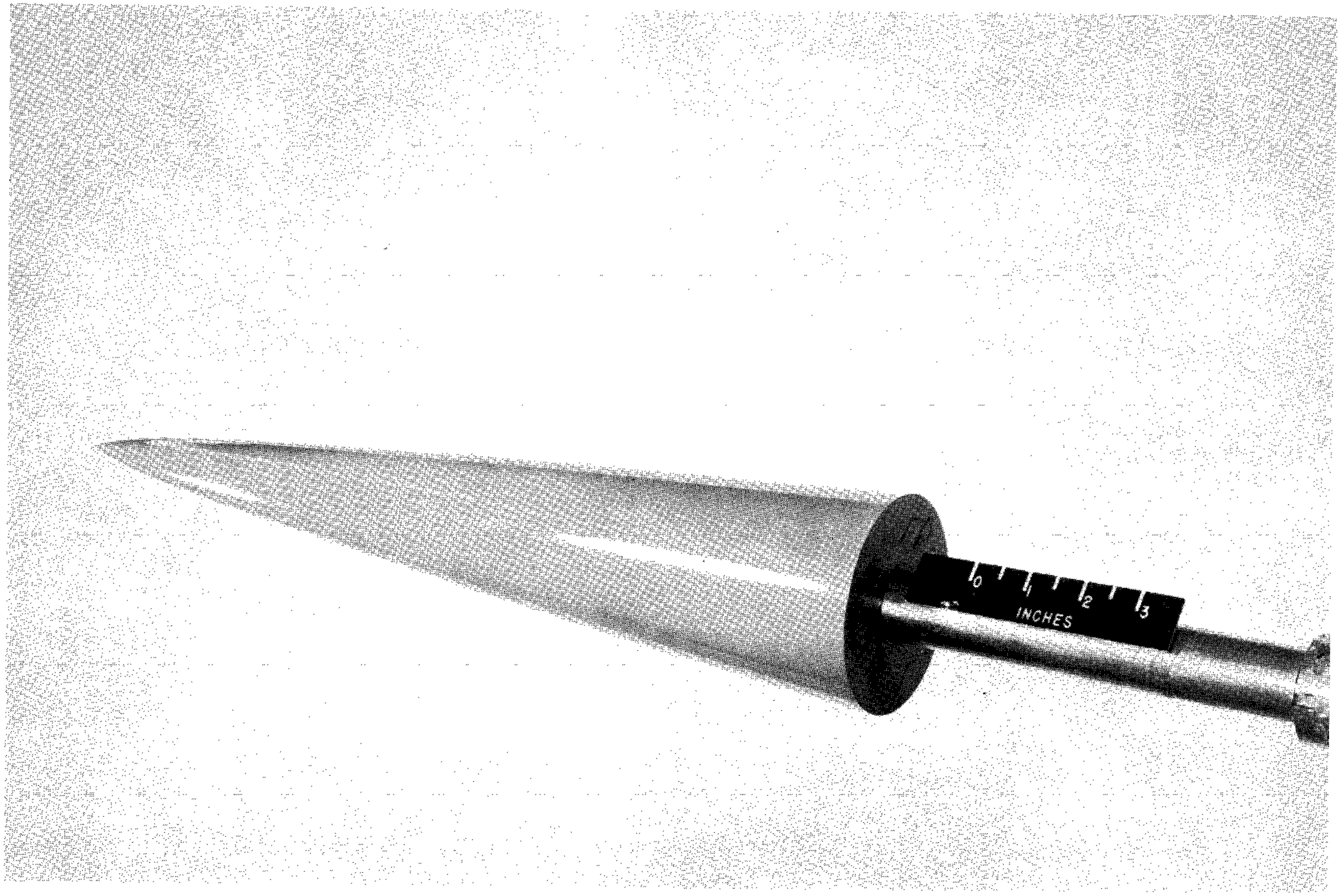

(c) Body $5A_1$.

L-63-487

Figure 2.- Continued.

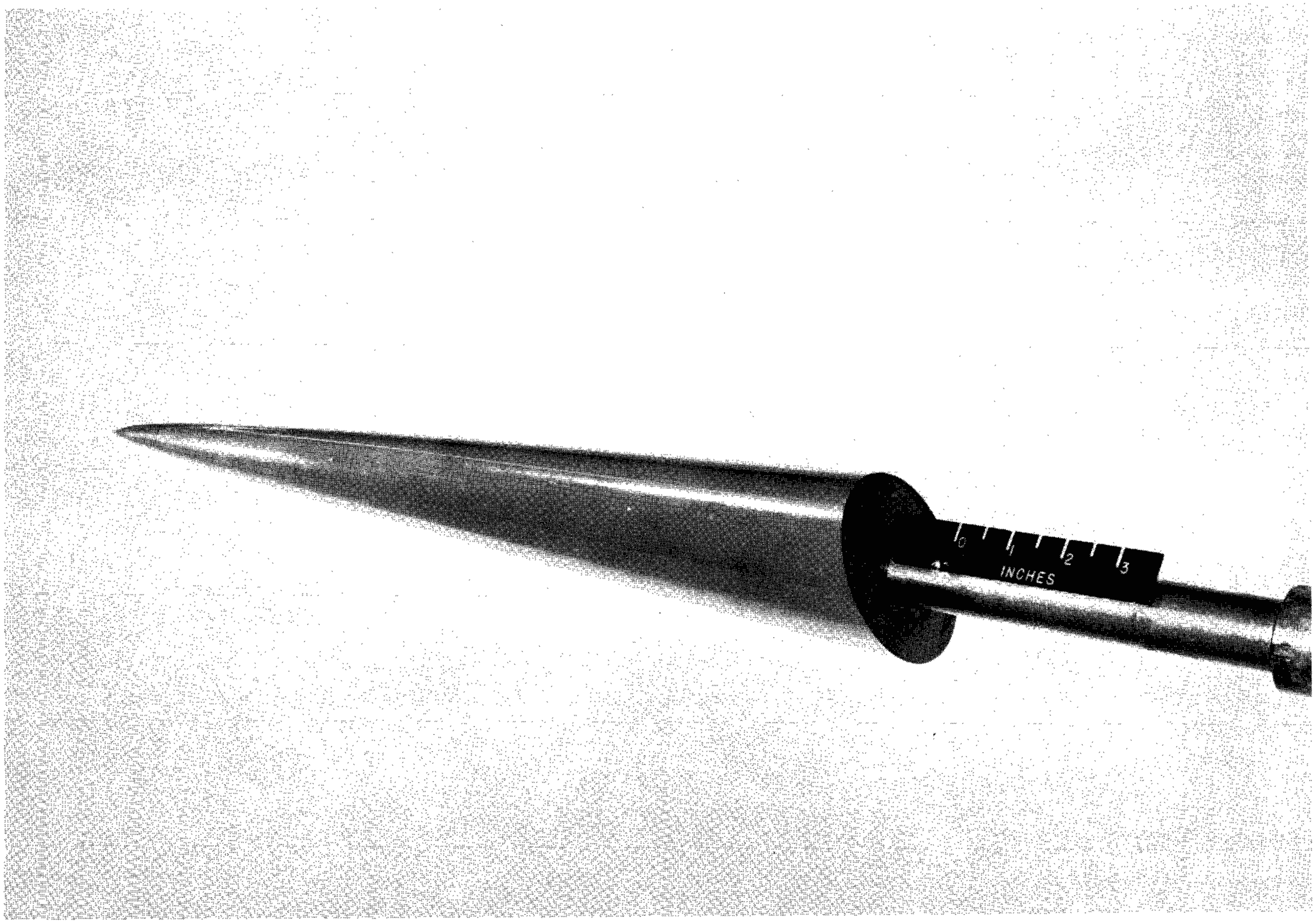

(d) Body $5C_1$. L-63-483

Figure 2.- Continued.

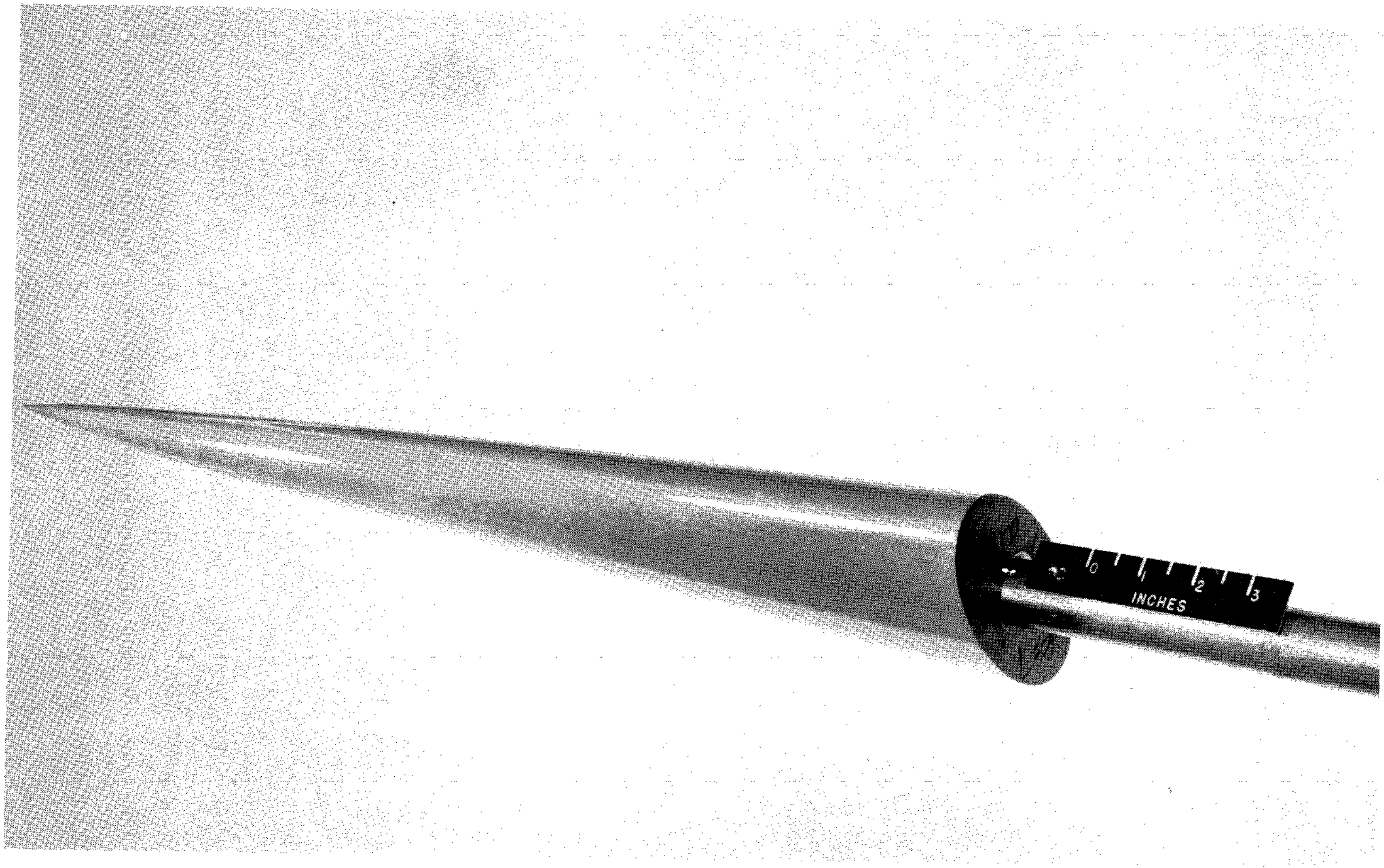

(e) Body $7C_1$.

L-63-486

Figure 2.- Concluded.

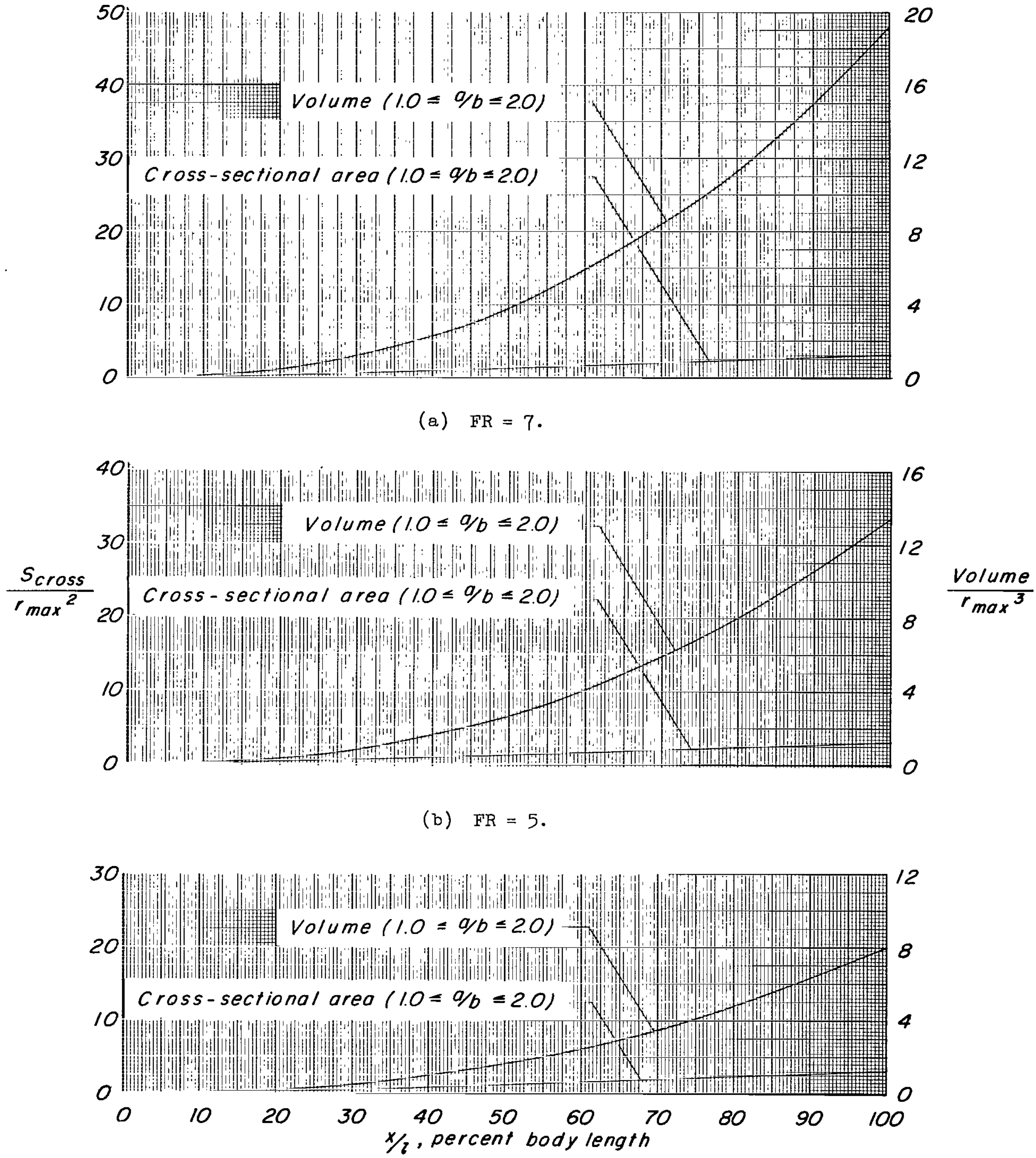

(a) FR = 7.

(b) FR = 5.

(c) FR = 3.

Figure 3.- Variation of cross-sectional area and volume distributions with body length.

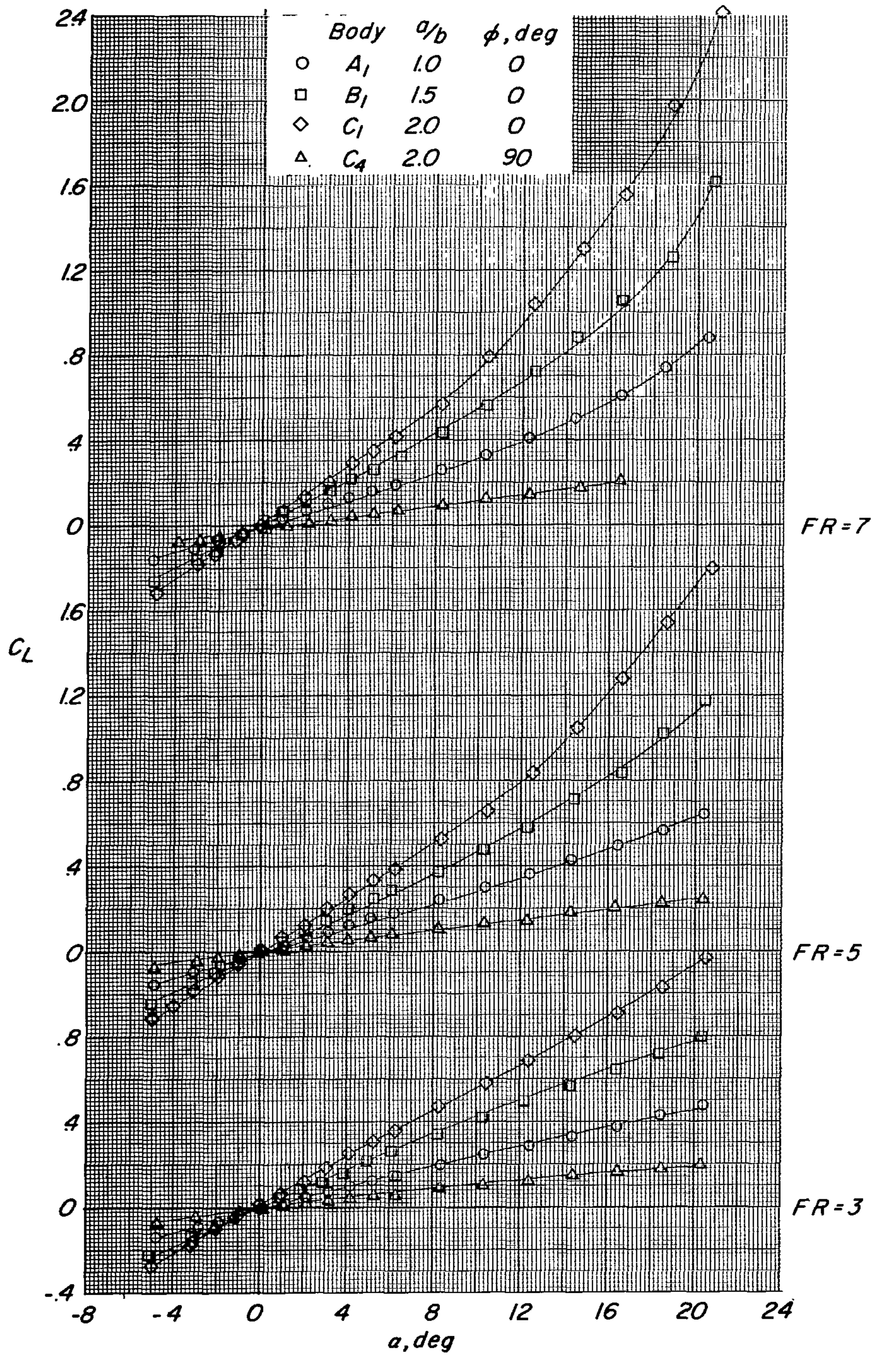

(a) C_L plotted against α.

Figure 4.- Effects of increasing a/b from 1.0 to 2.0 at $\phi = 0^\circ$ and 90° on longitudinal aerodynamic characteristics of symmetrical bodies. M = 0.40.

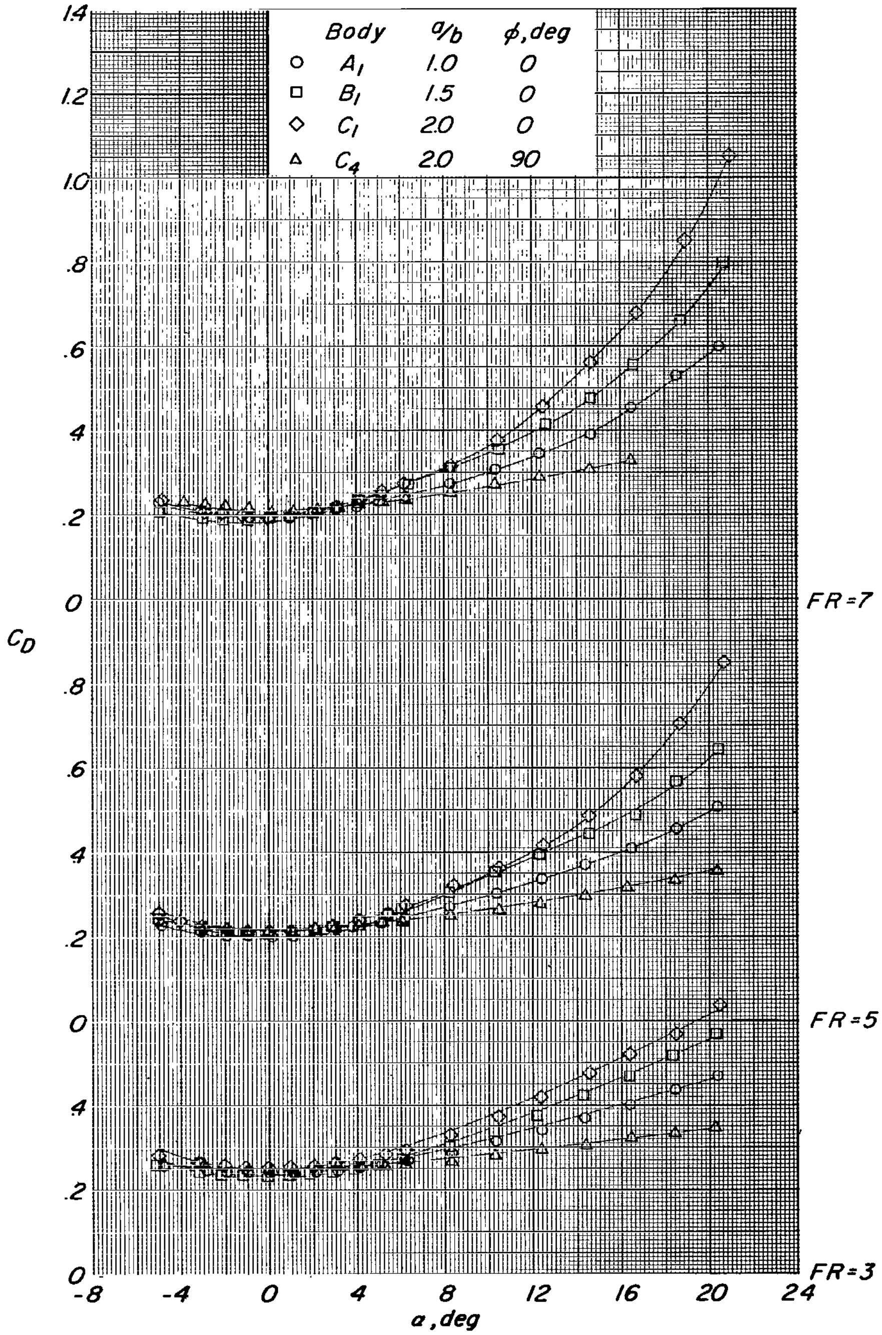

(b) C_D plotted against α.

Figure 4.- Continued.

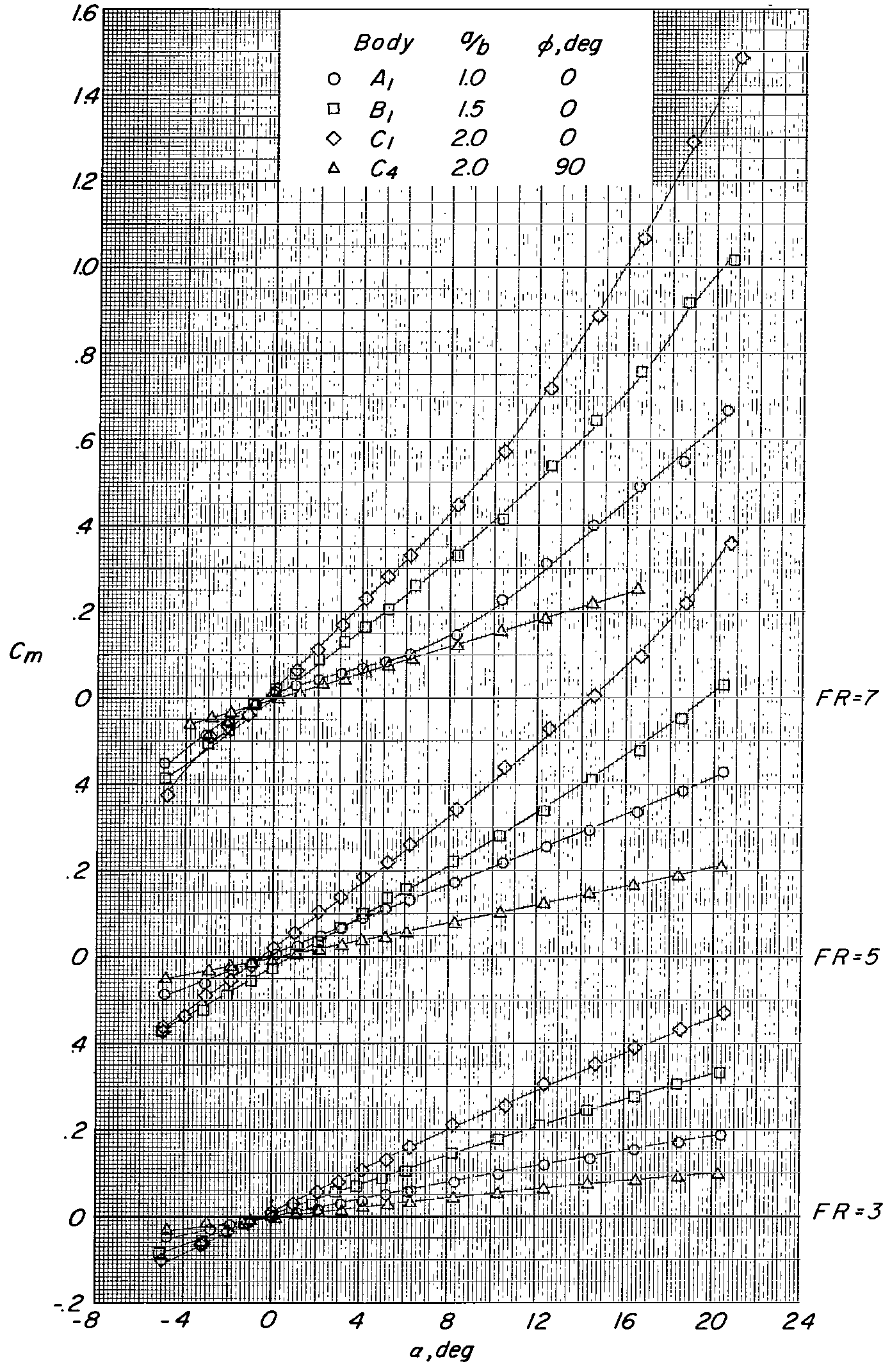

(c) C_m plotted against α.

Figure 4.- Continued.

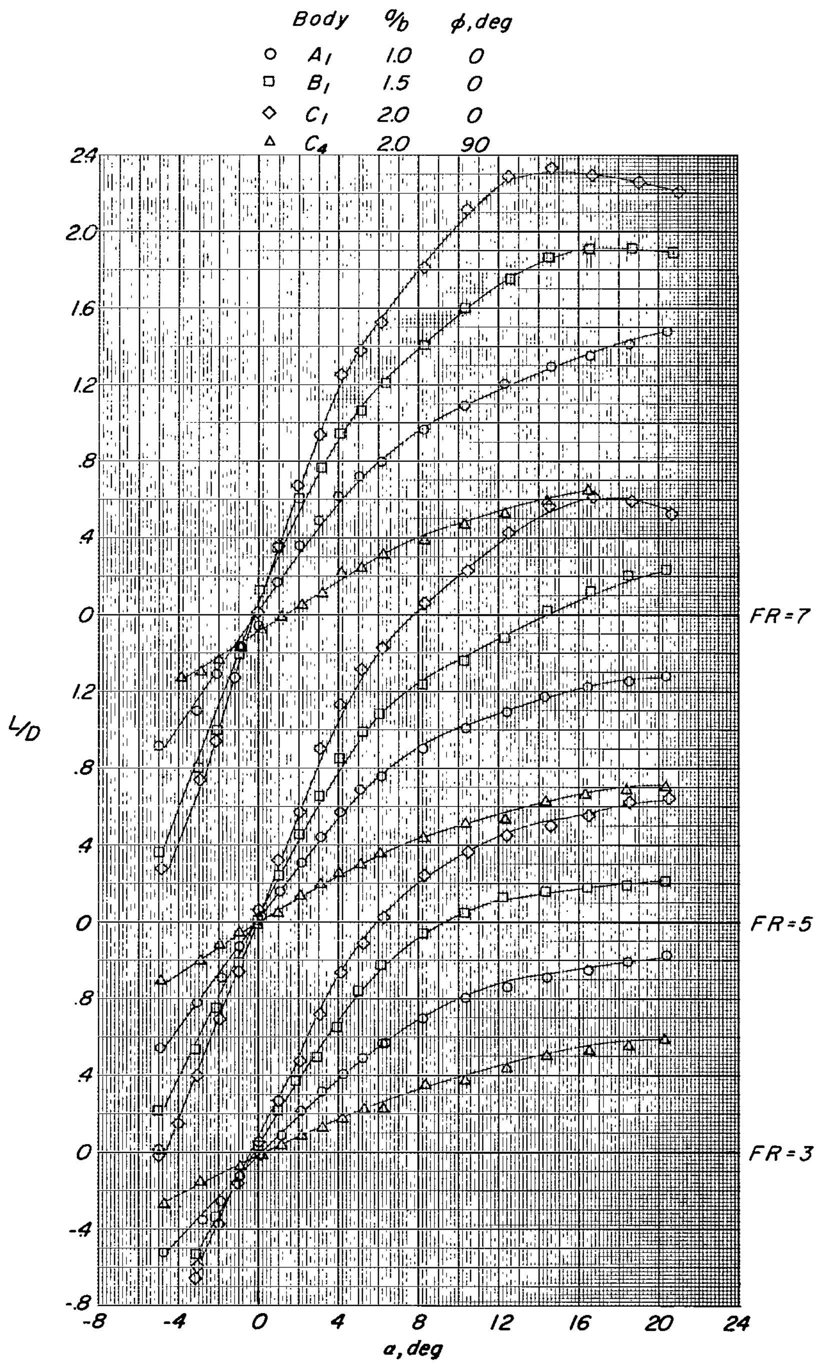

(d) L/D plotted against α.

Figure 4.- Concluded.

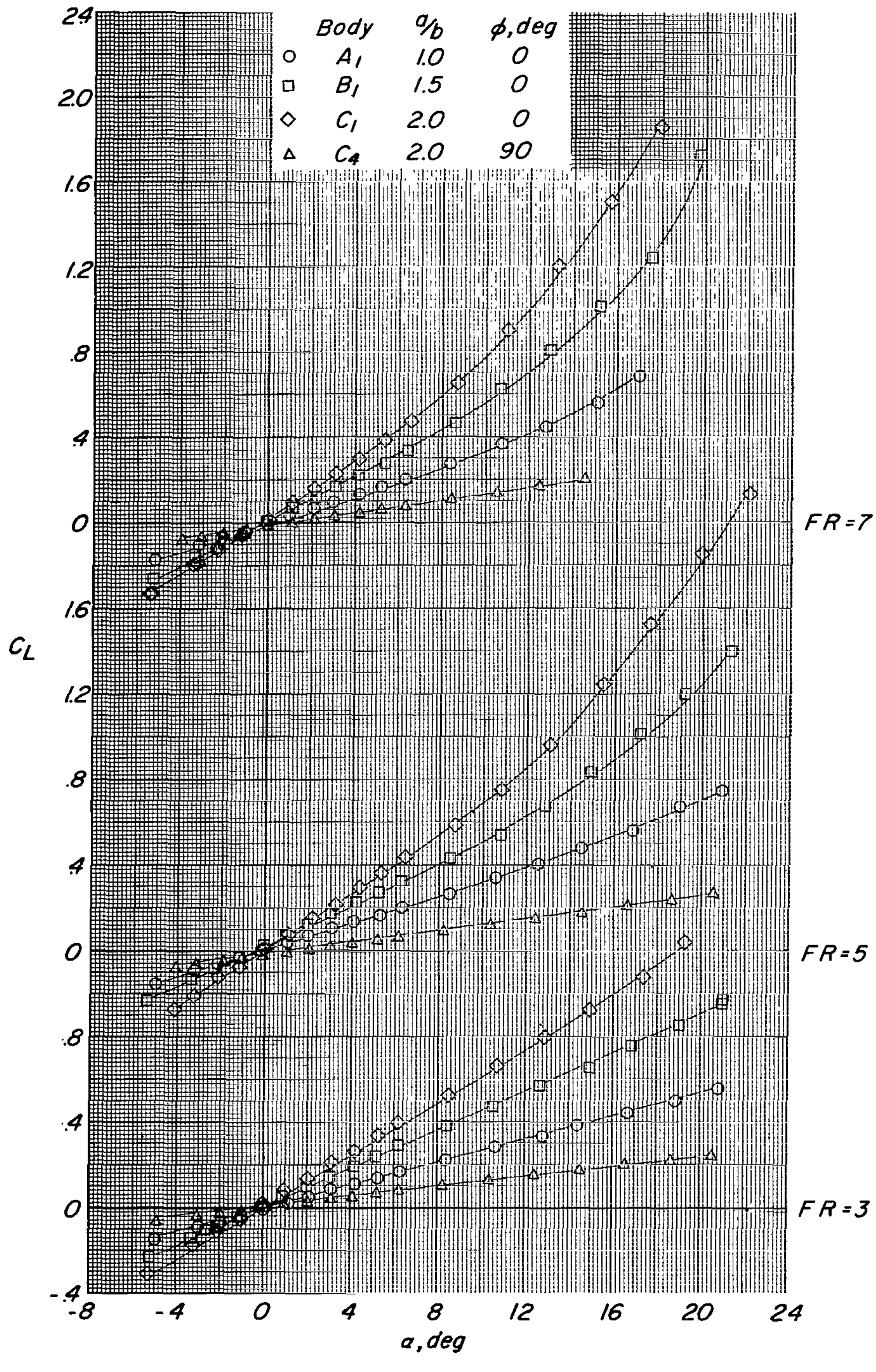

(a) C_L plotted against α.

Figure 5.- Effects of increasing a/b from 1.0 to 2.0 at $\phi = 0^\circ$ and 90° on longitudinal aerodynamic characteristics of symmetrical bodies. M = 0.80.

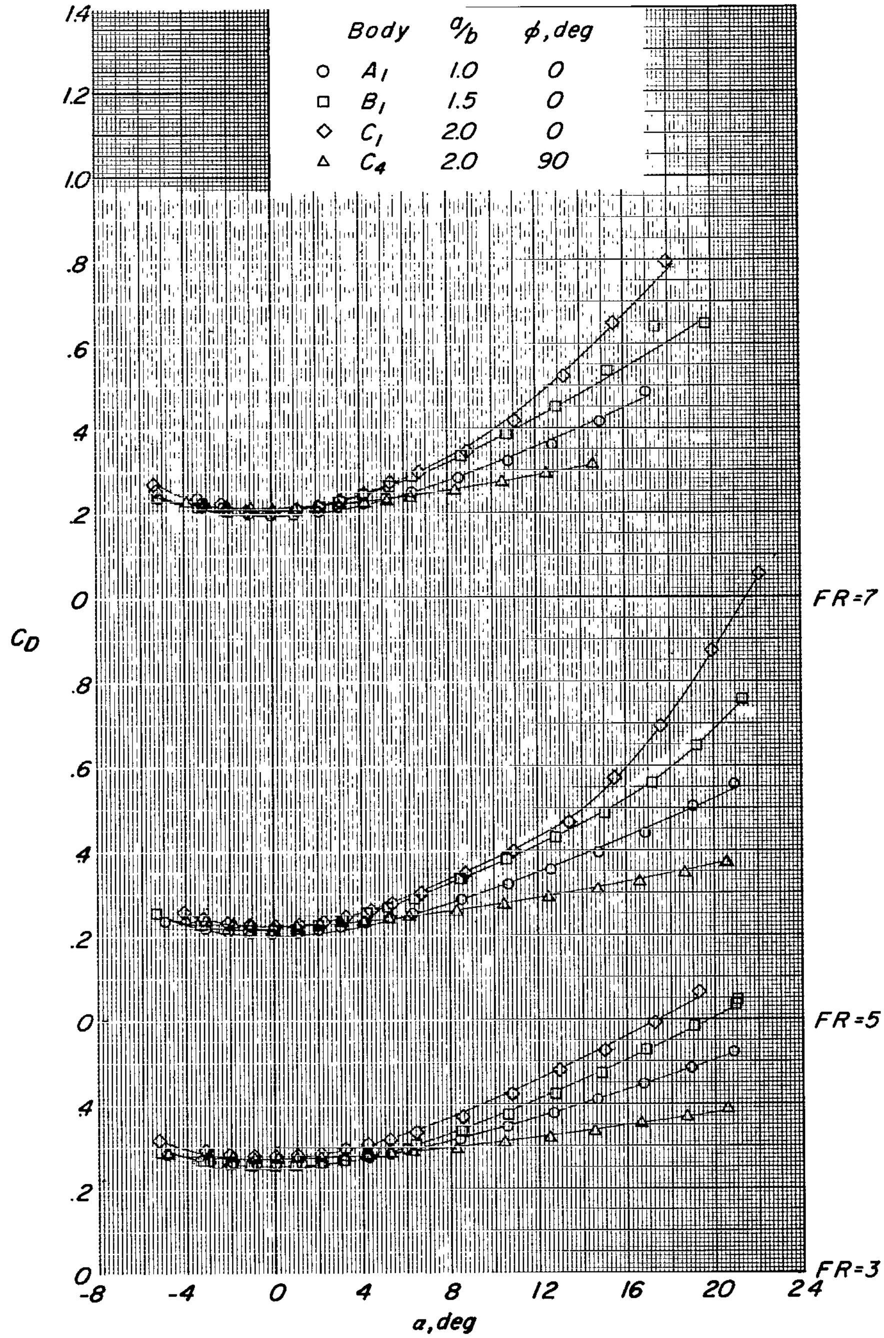

(b) C_D plotted against α.

Figure 5.- Continued.

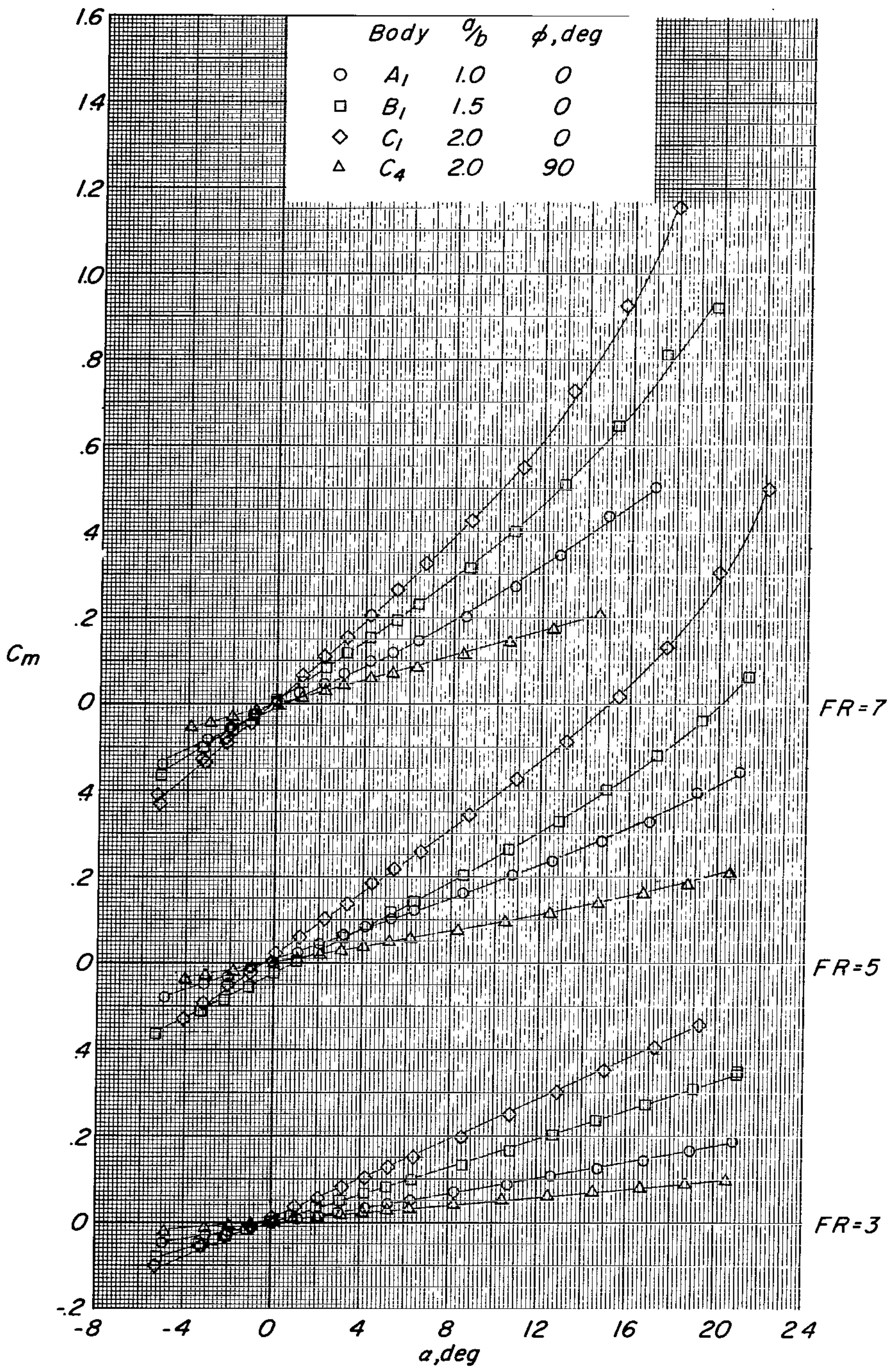

(c) C_m plotted against α.

Figure 5.- Continued.

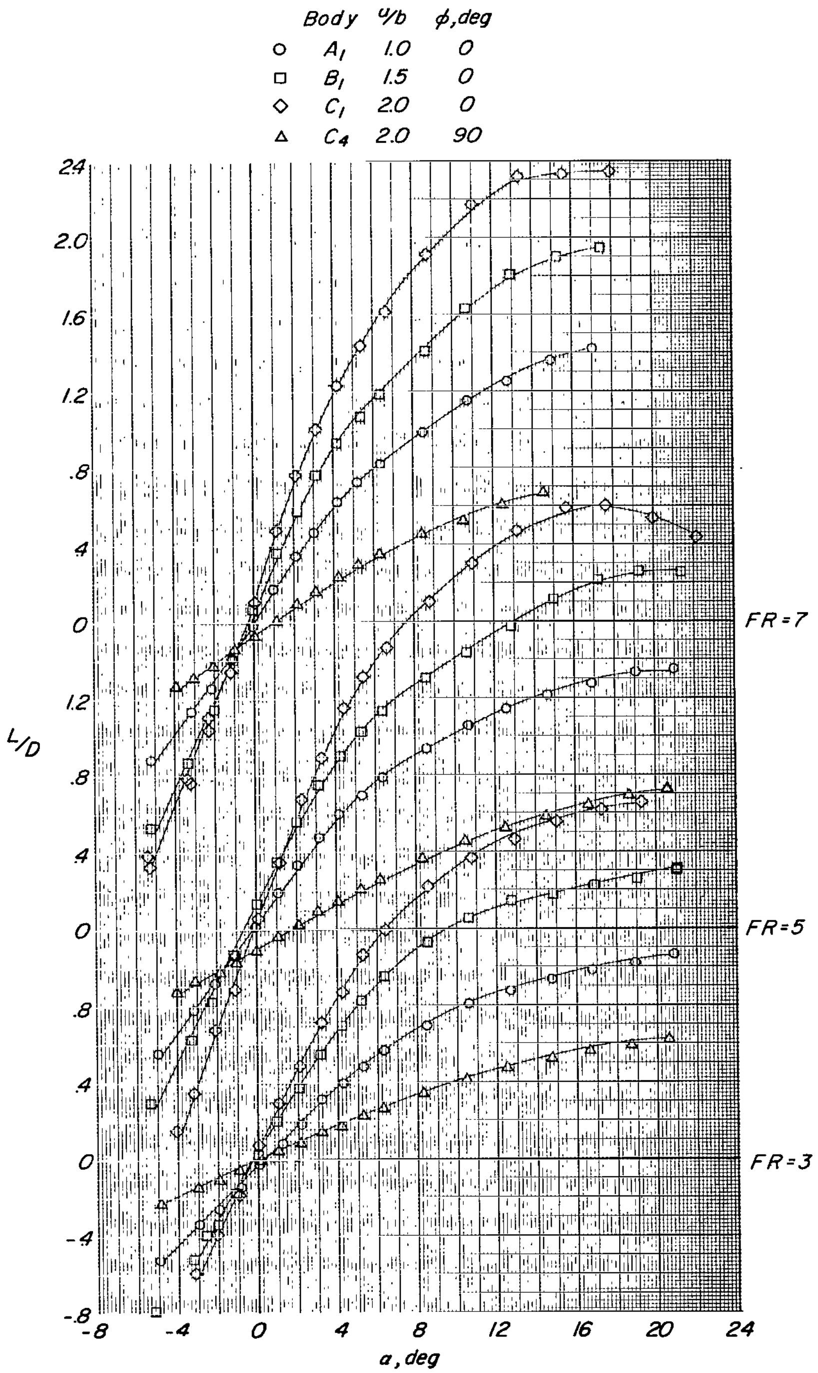

(d) L/D plotted against α.

Figure 5.- Concluded.

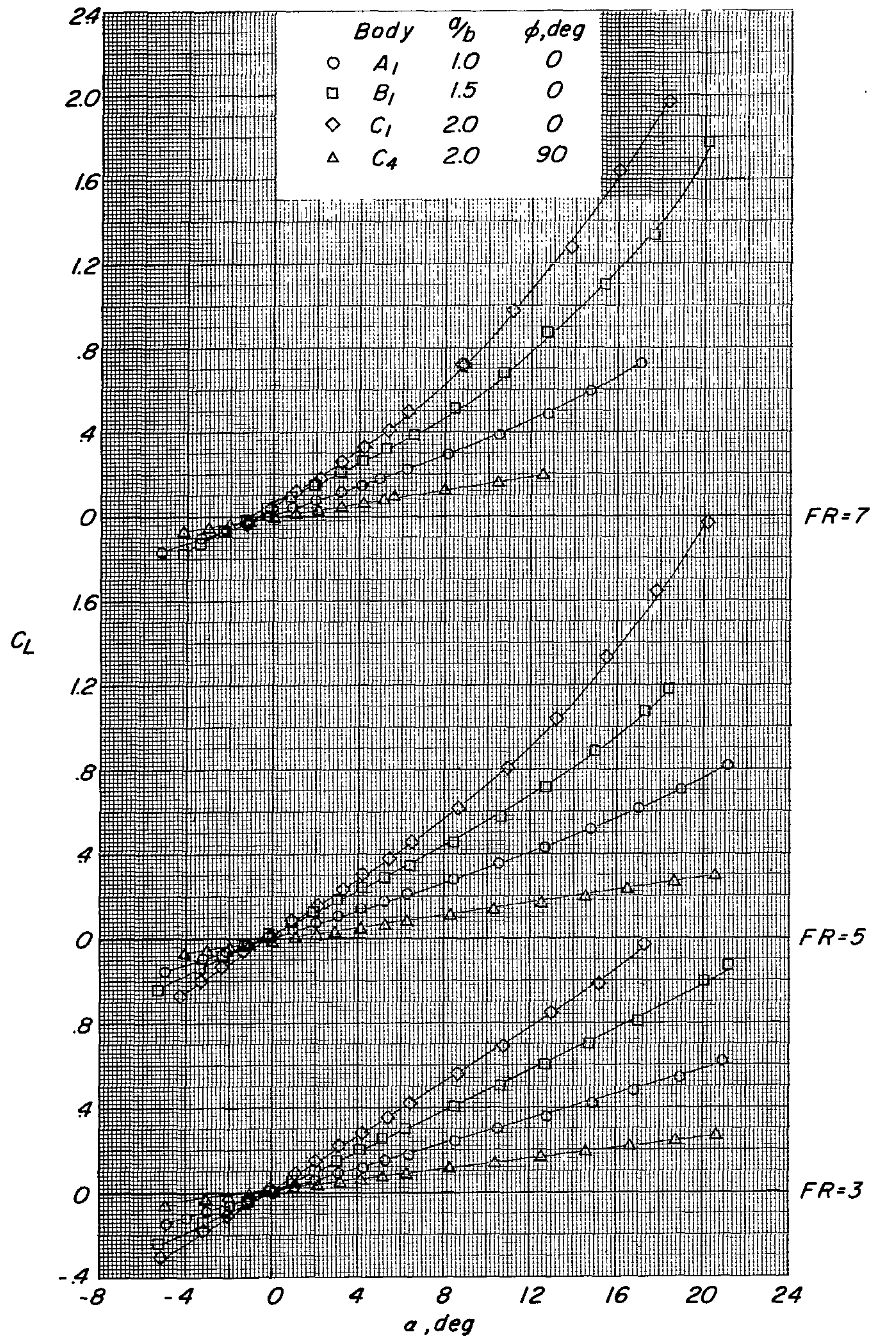

(a) C_L plotted against α.

Figure 6.- Effects of increasing a/b from 1.0 to 2.0 at $\phi = 0^\circ$ and 90° on longitudinal aerodynamic characteristics of symmetrical bodies. M = 0.90.

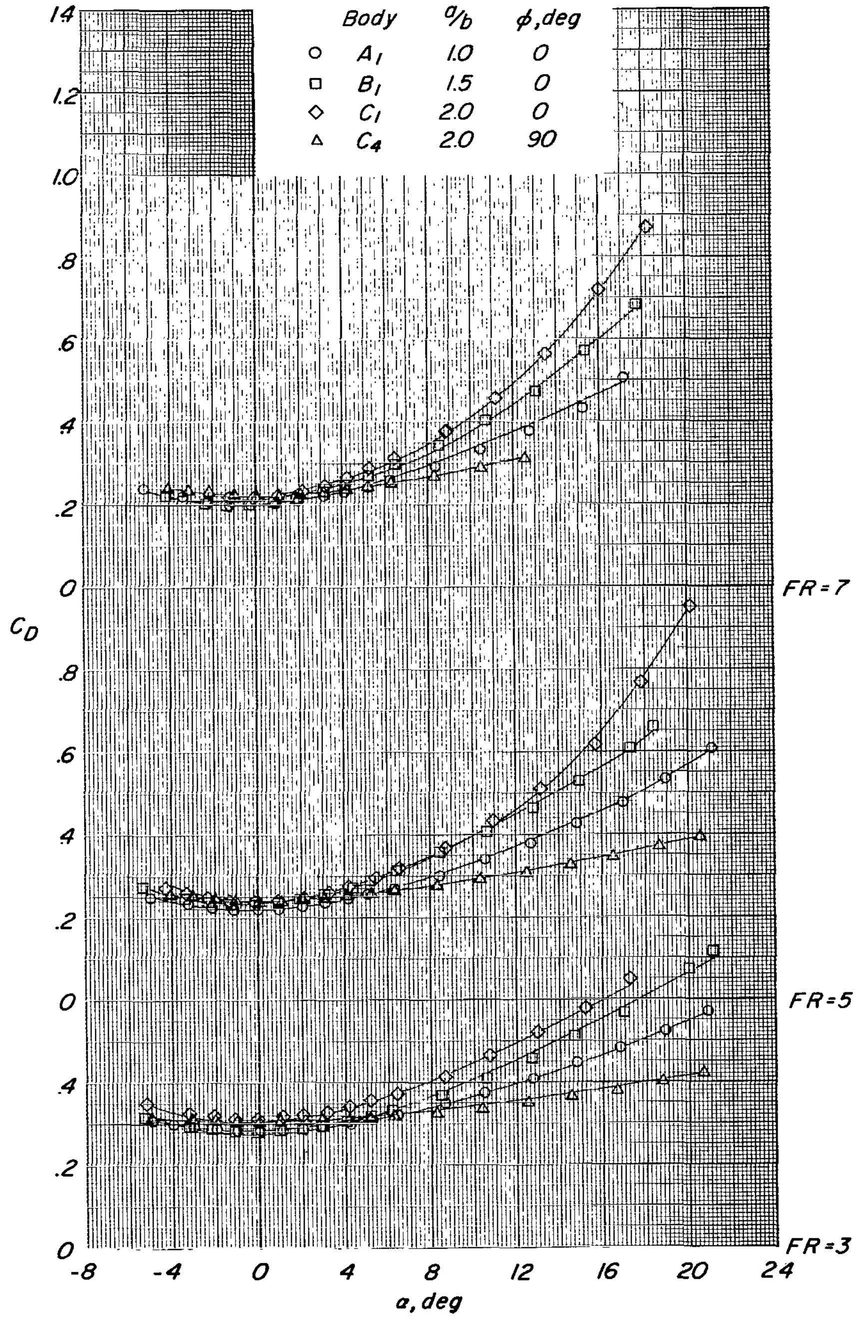

(b) C_D plotted against α.

Figure 6.- Continued.

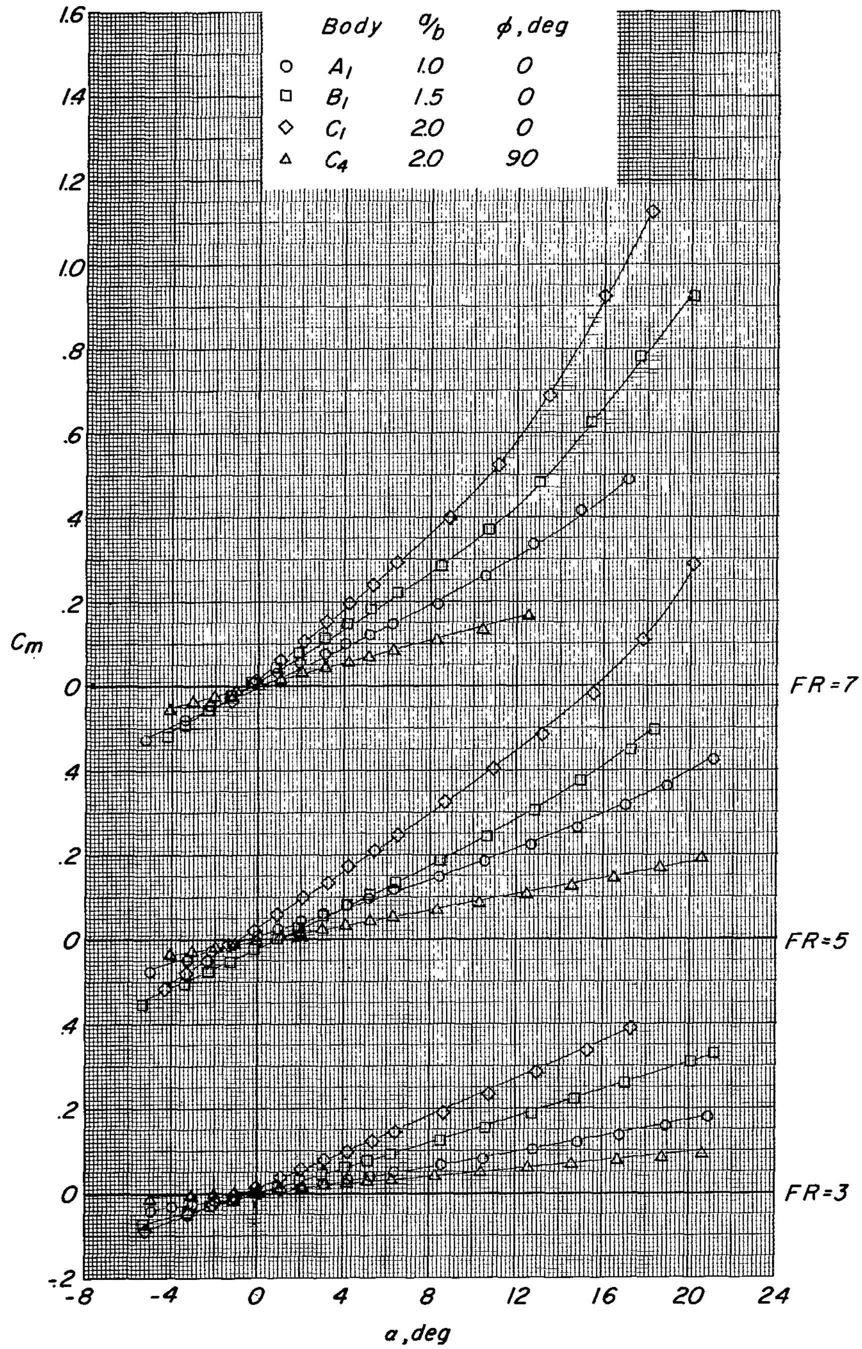

(c) C_m plotted against α.

Figure 6.- Continued.

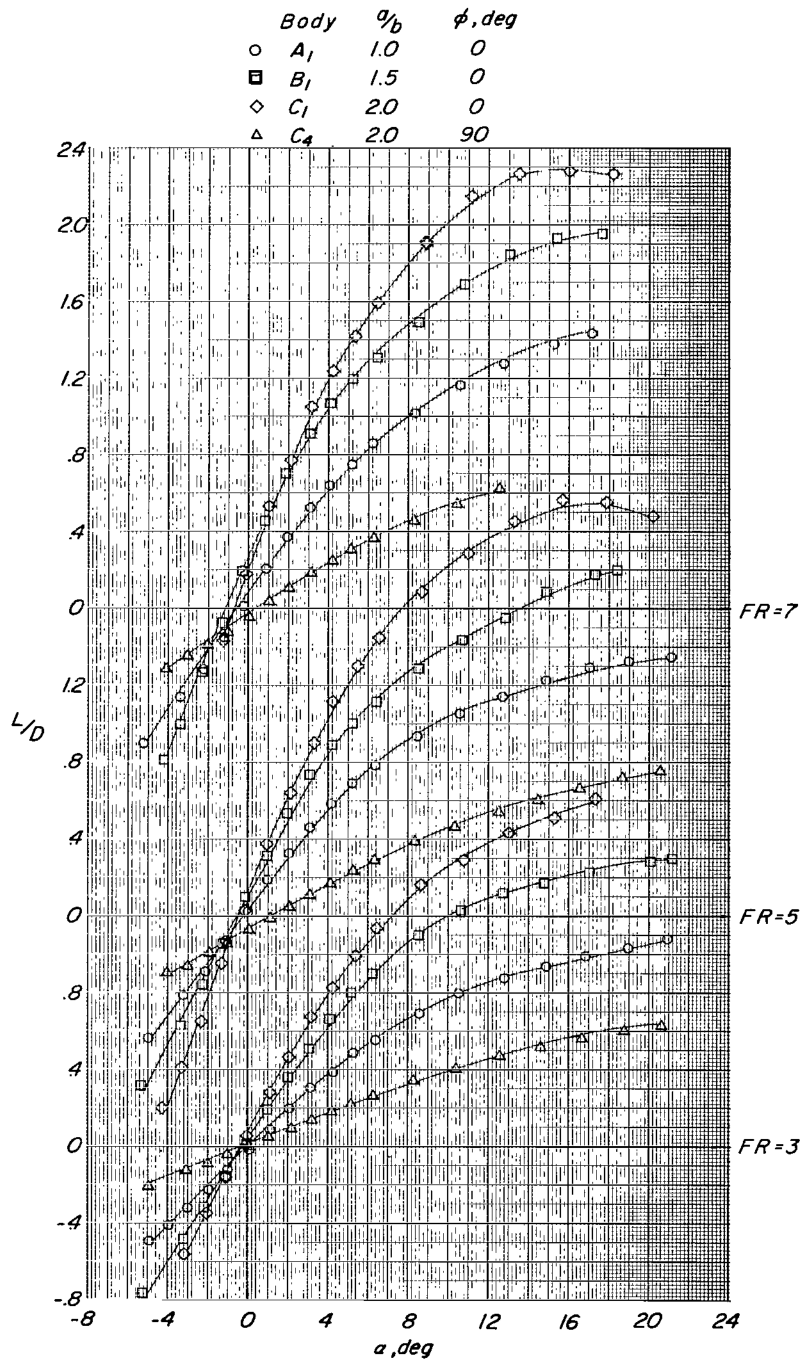

(d) L/D plotted against α.

Figure 6.- Concluded.

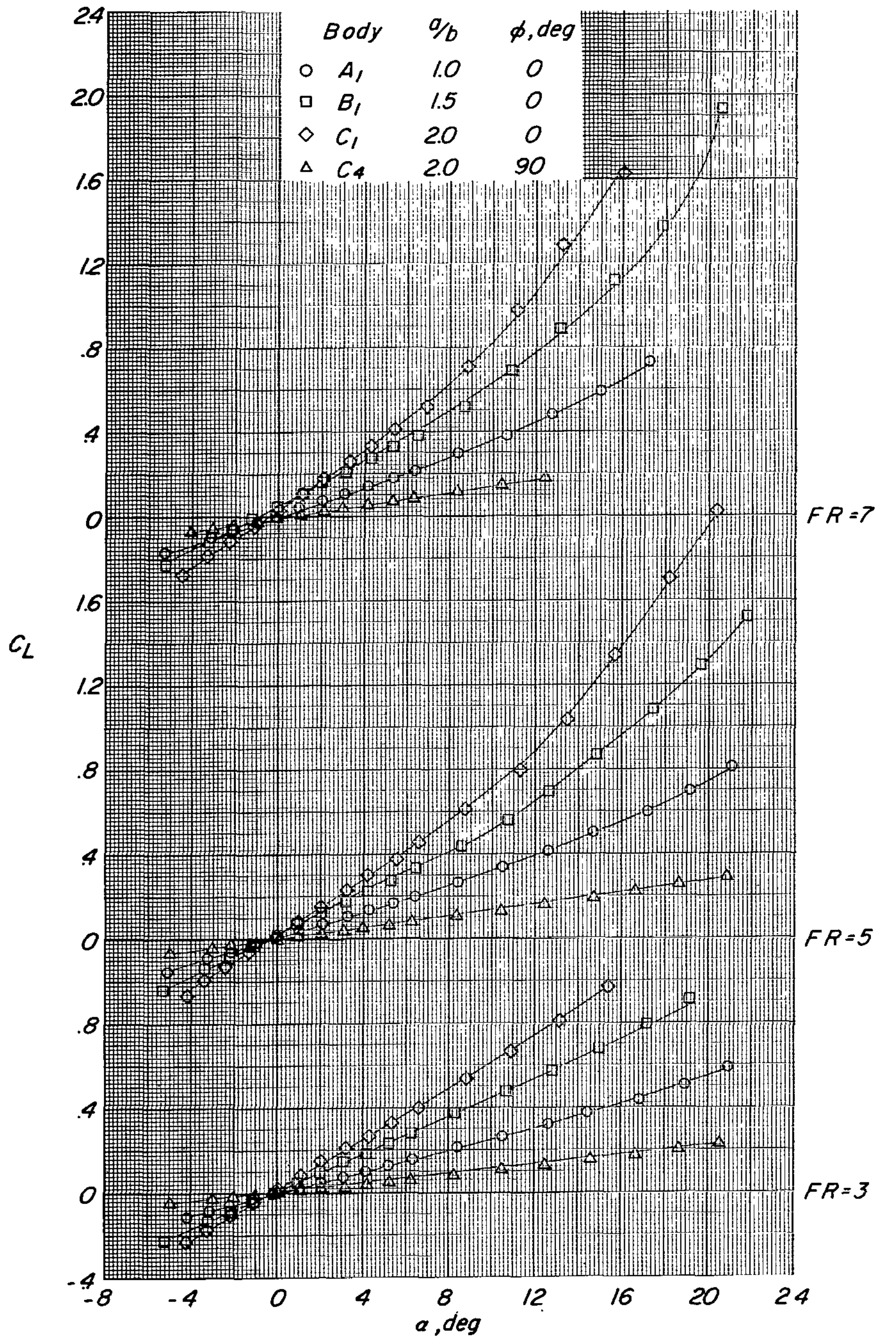

(a) C_L plotted against α.

Figure 7.- Effects of increasing a/b from 1.0 to 2.0 at $\phi = 0^\circ$ and 90° on longitudinal aerodynamic characteristics of symmetrical bodies. M = 1.00.

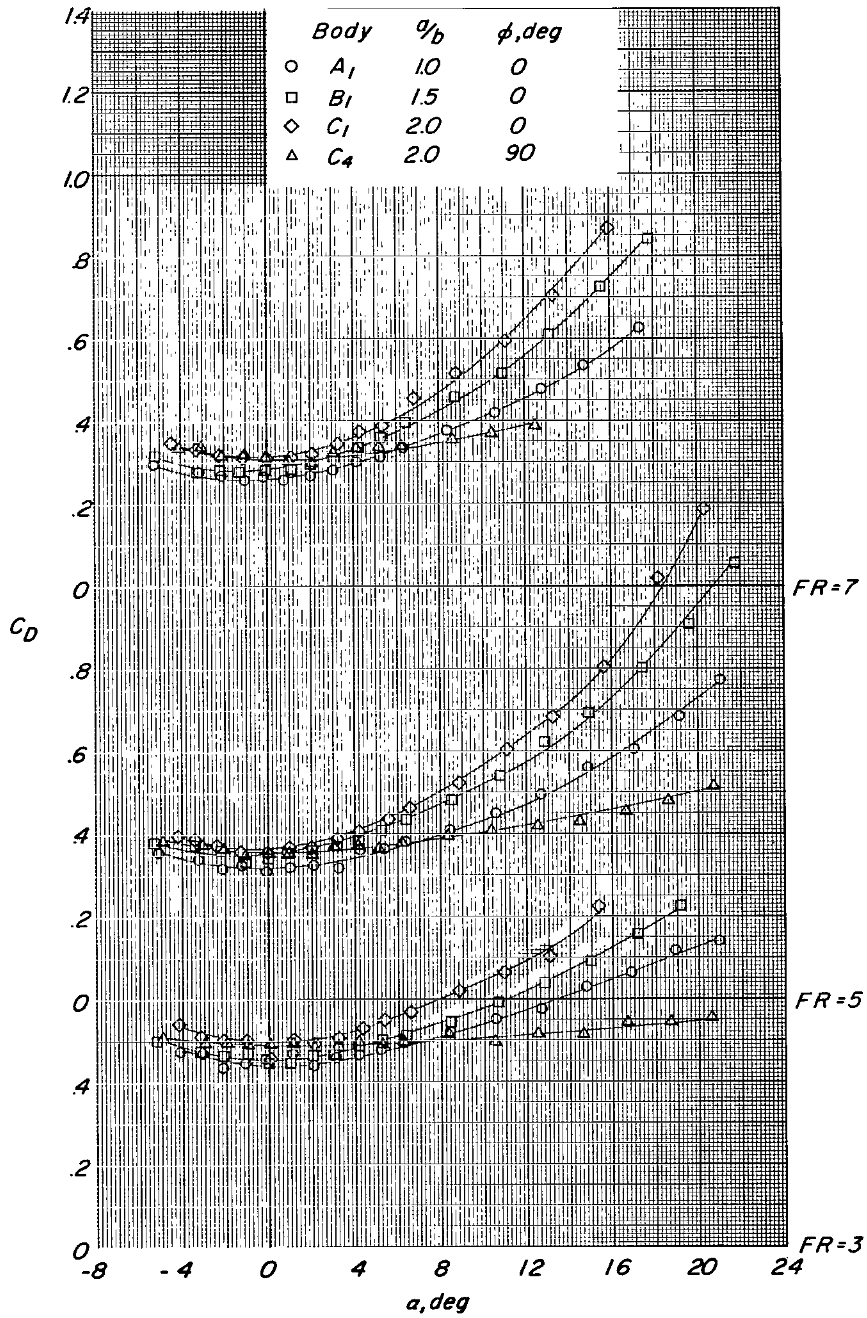

(b) C_D plotted against α.

Figure 7.- Continued.

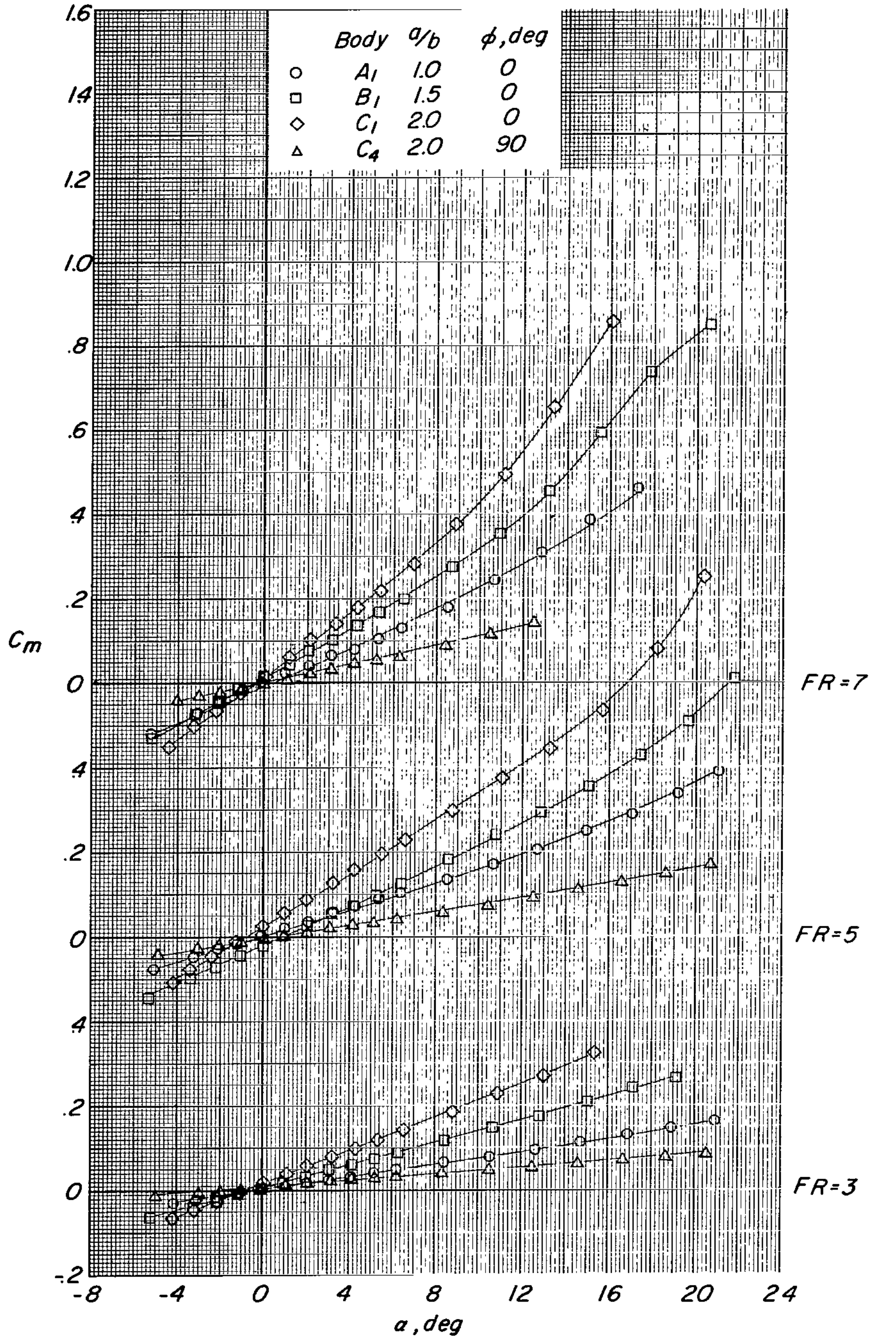

(c) C_m plotted against α.

Figure 7.- Continued.

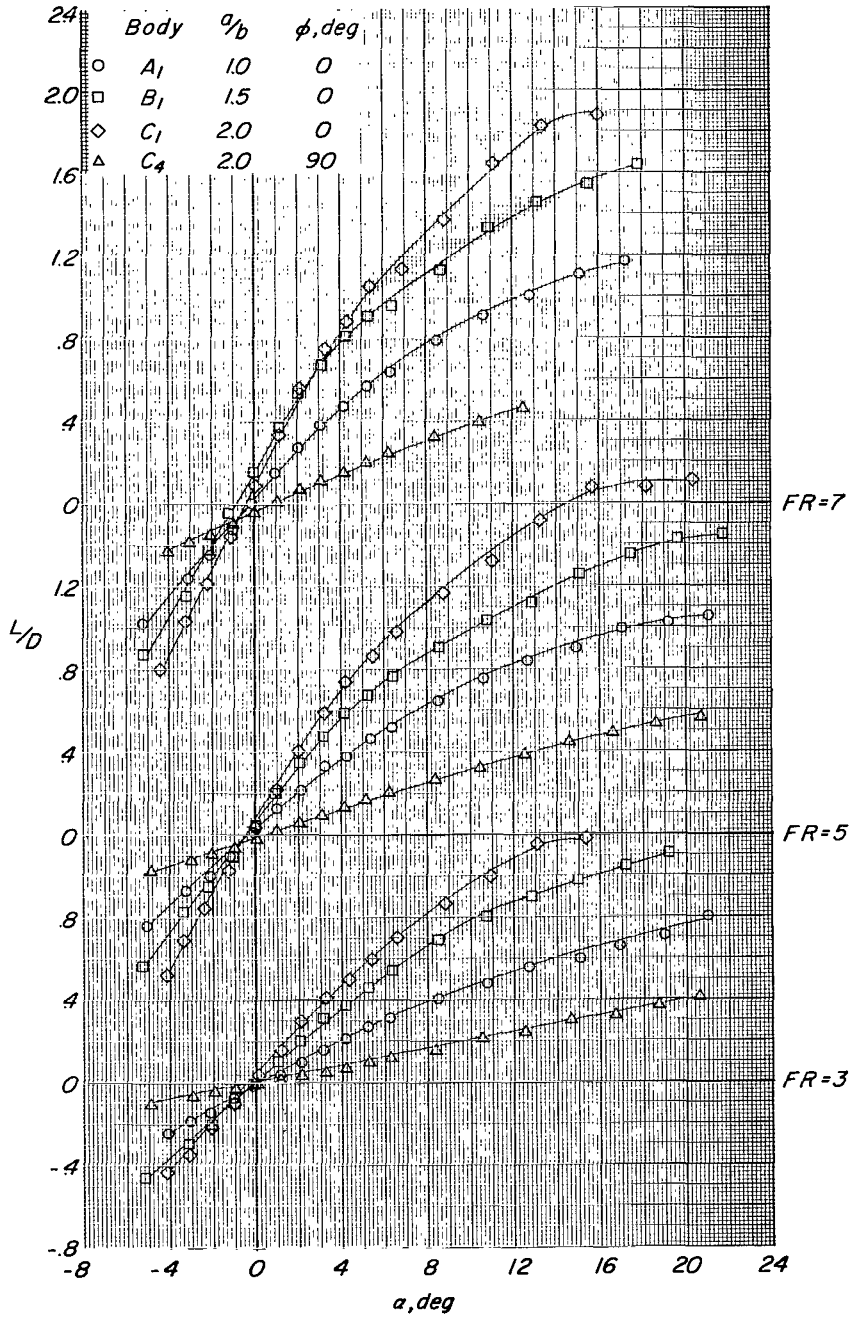

(d) L/D plotted against α.

Figure 7.- Concluded.

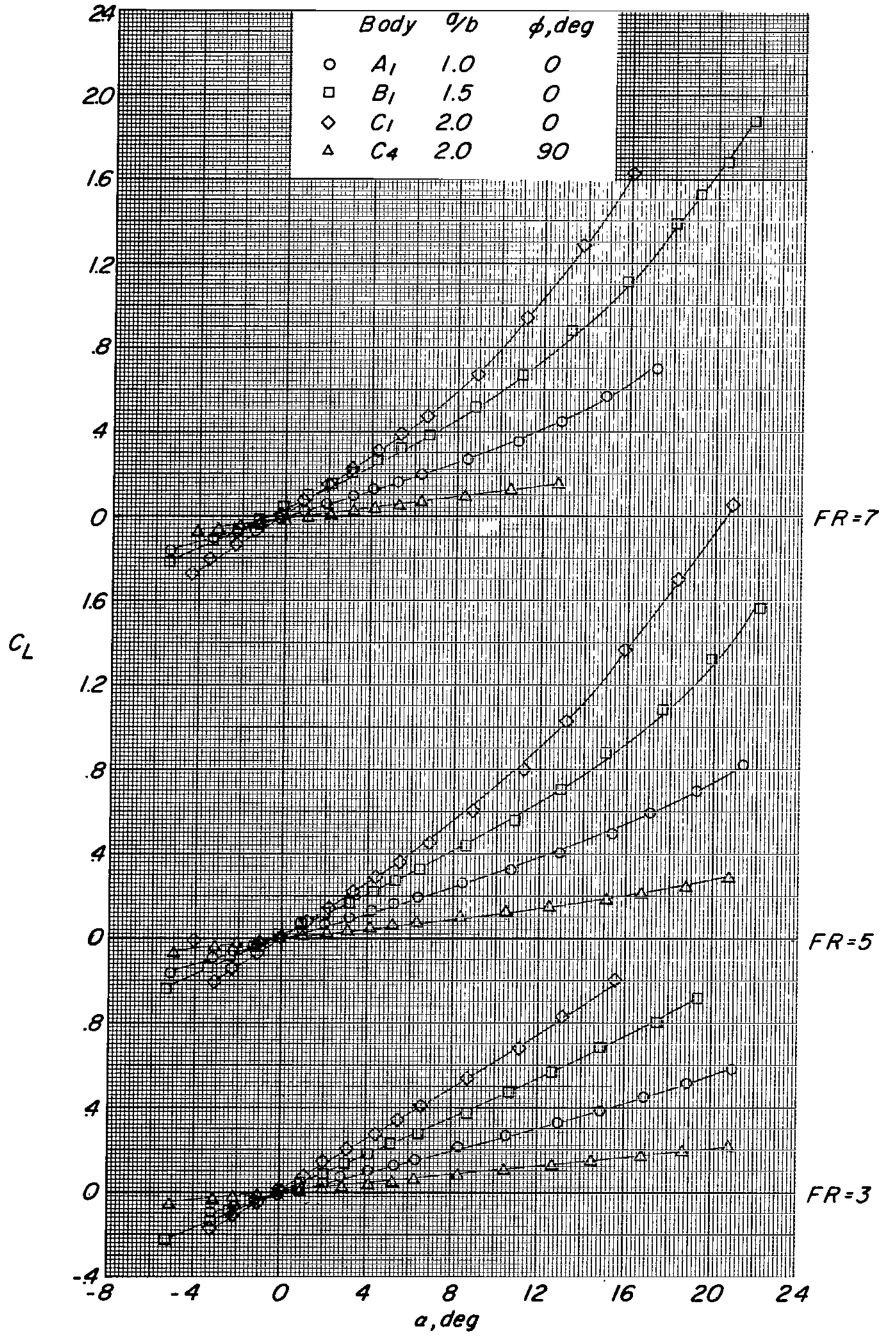

(a) C_L plotted against α.

Figure 8.- Effects of increasing a/b from 1.0 to 2.0 at $\phi = 0^\circ$ and 90° on longitudinal aerodynamic characteristics of symmetrical bodies. M = 1.14.

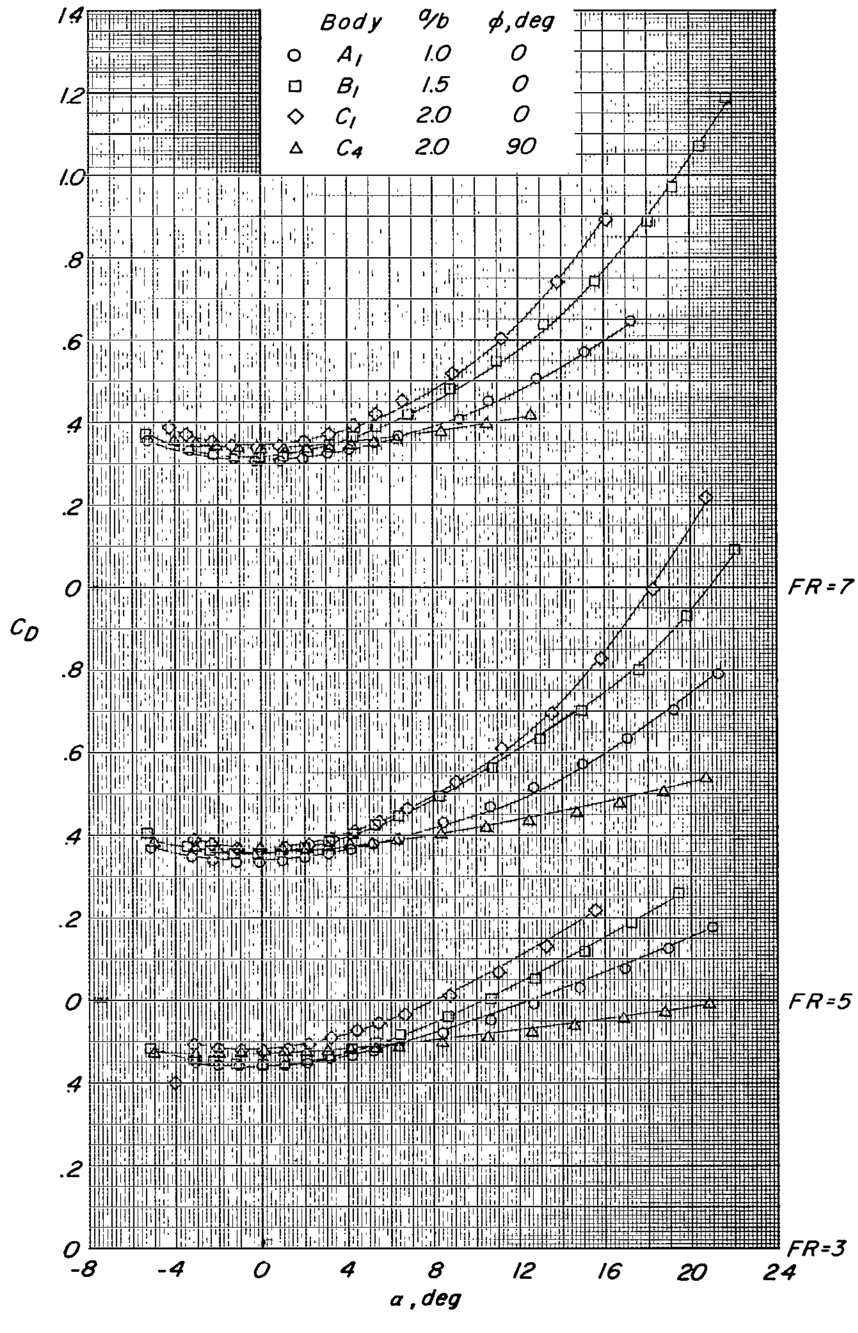

(b) C_D plotted against α.

Figure 8.- Continued.

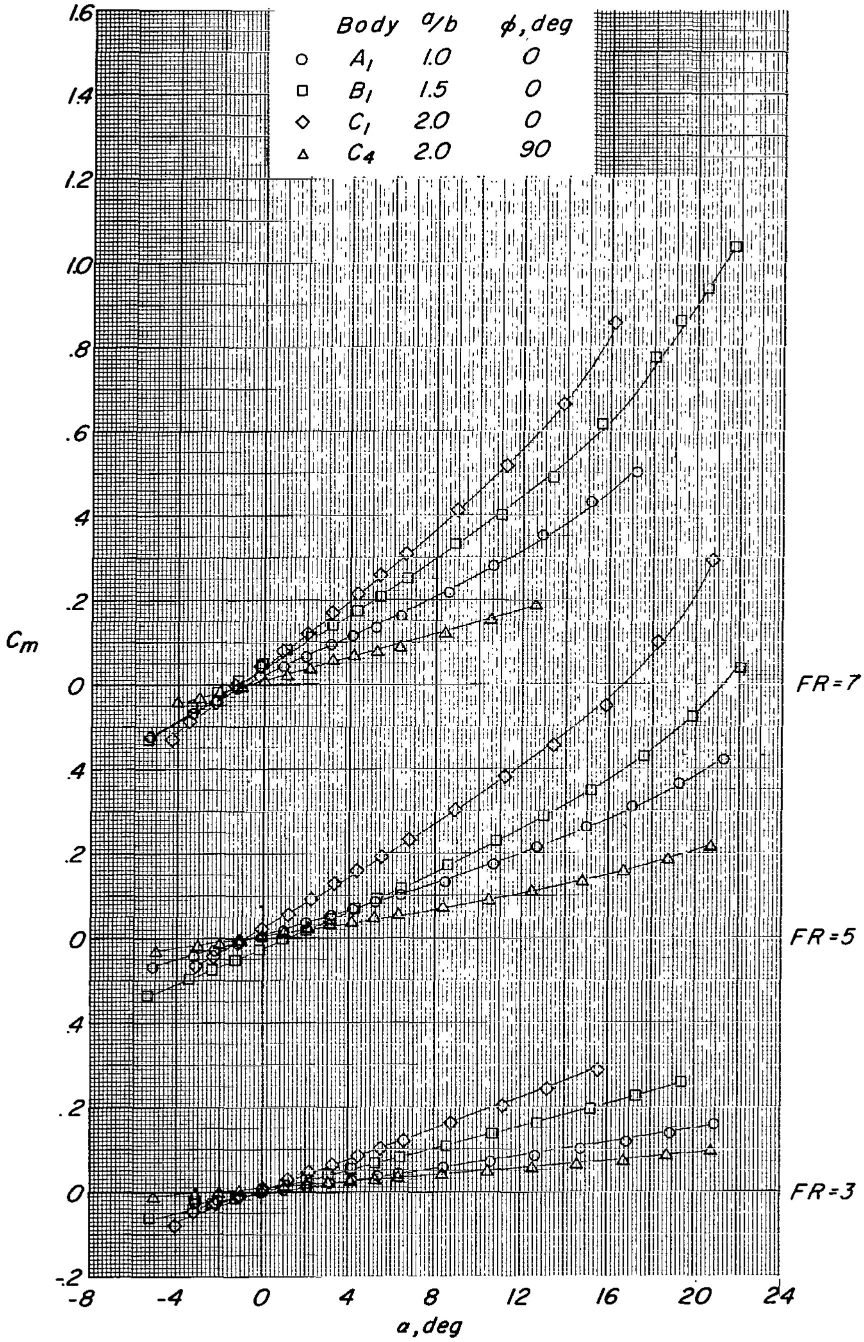

(c) C_m plotted against α.

Figure 8.- Continued.

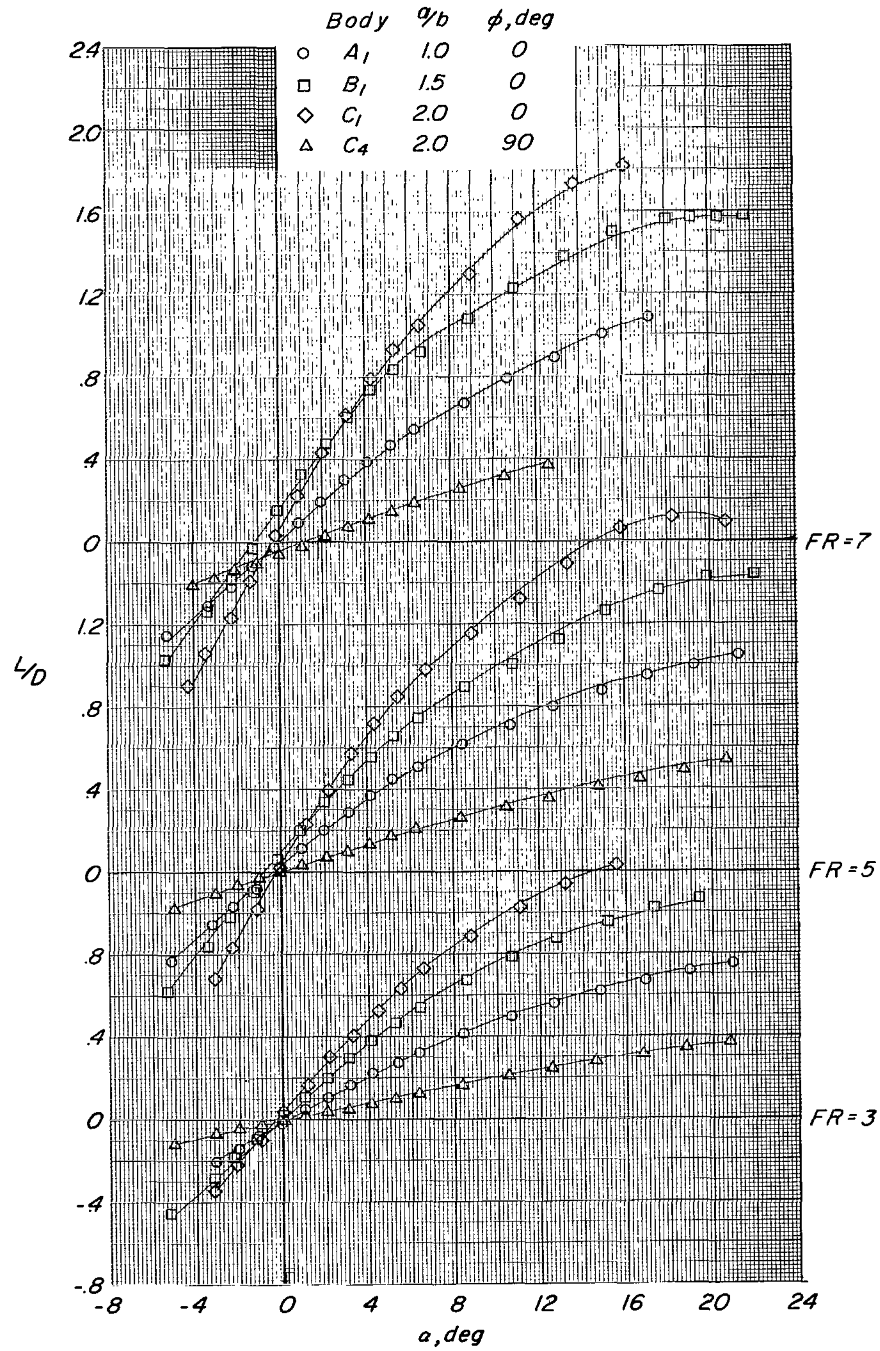

(d) L/D plotted against α.

Figure 8.- Concluded.

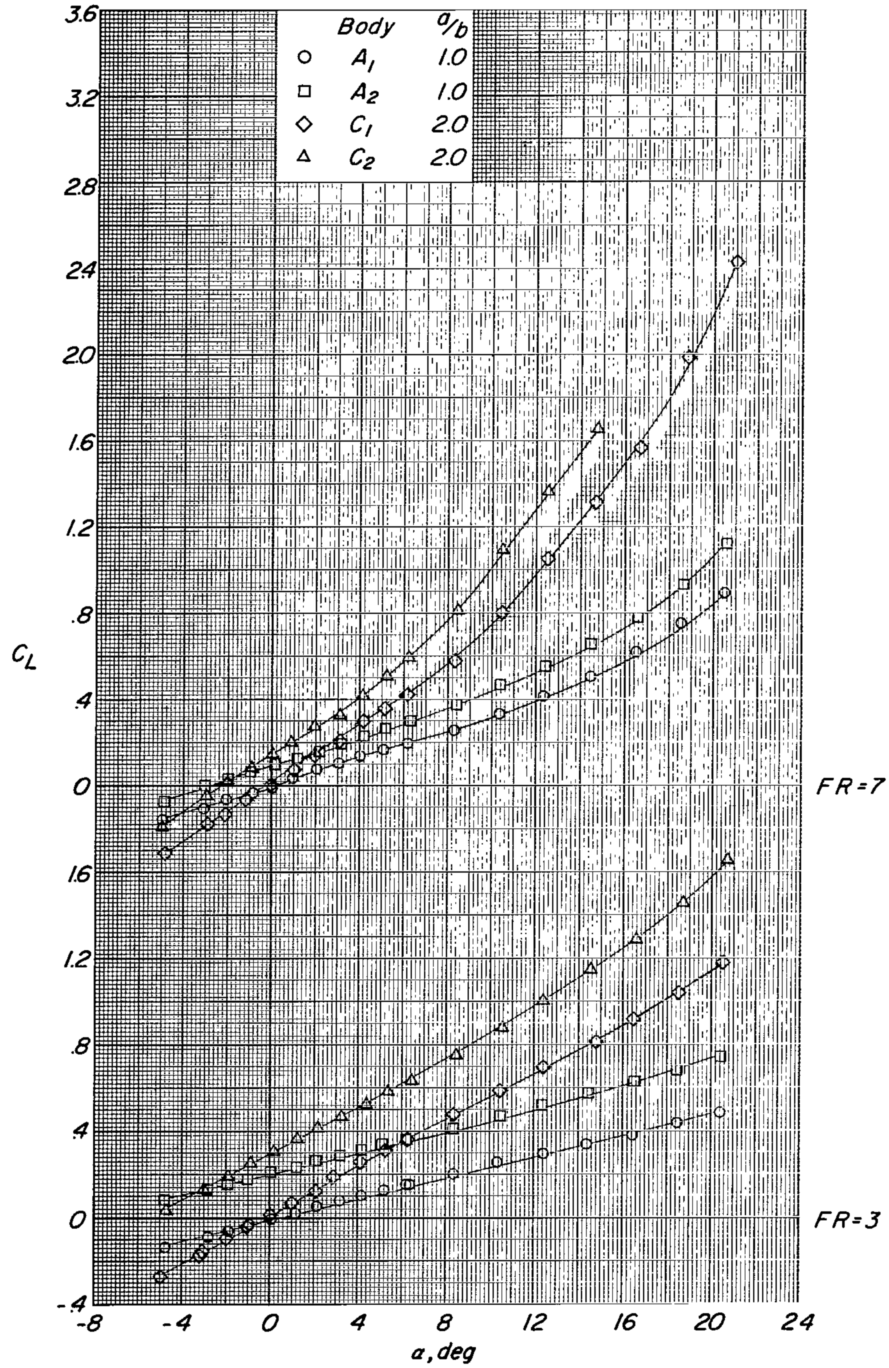

(a) C_L plotted against α.

Figure 9.- Effects of body section displacement on longitudinal aerodynamic characteristics of bodies having a/b = 1.0 and 2.0 at $\phi = 0^{\circ}$. M = 0.40.

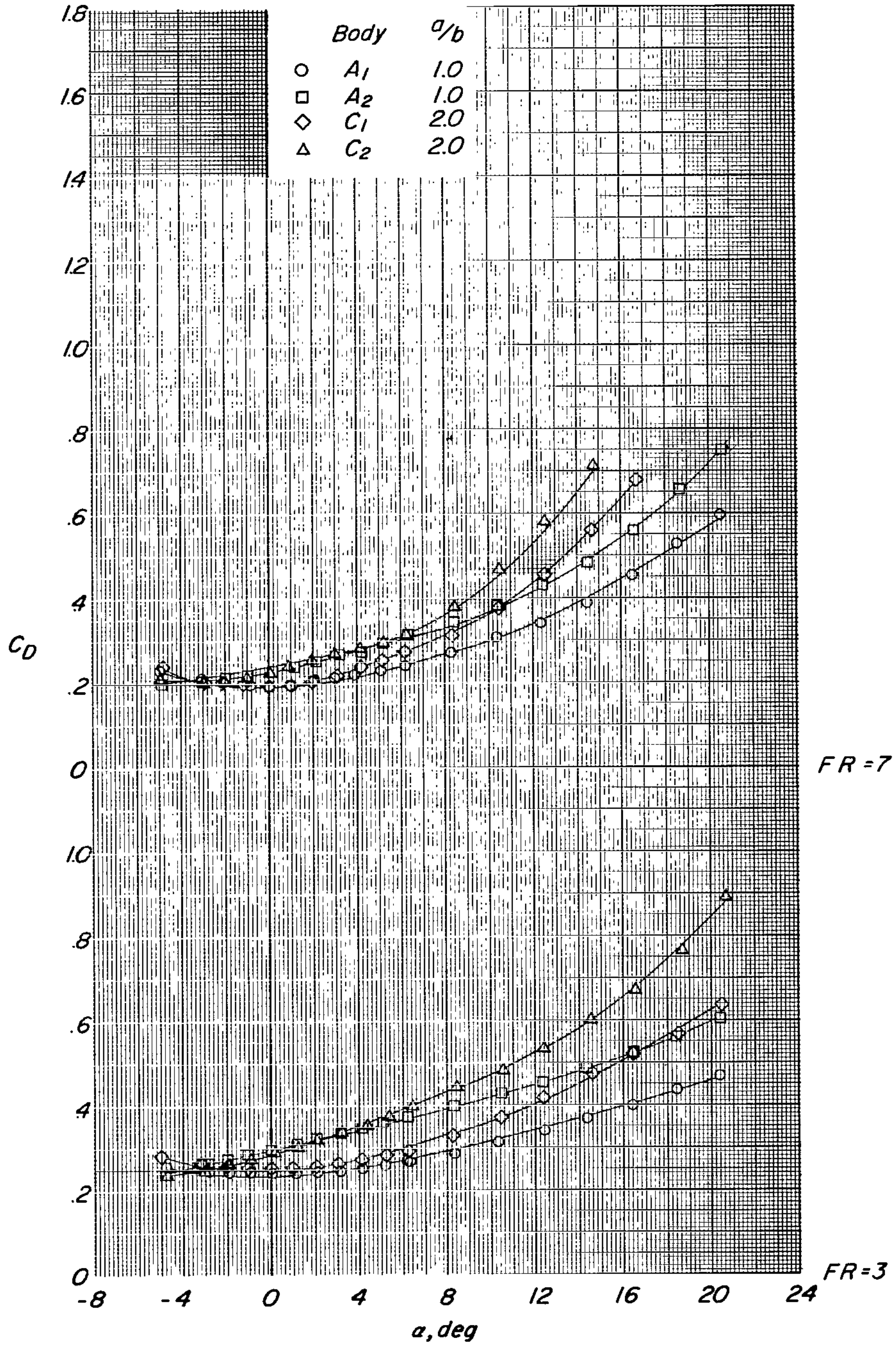

(b) C_D plotted against α.

Figure 9.- Continued.

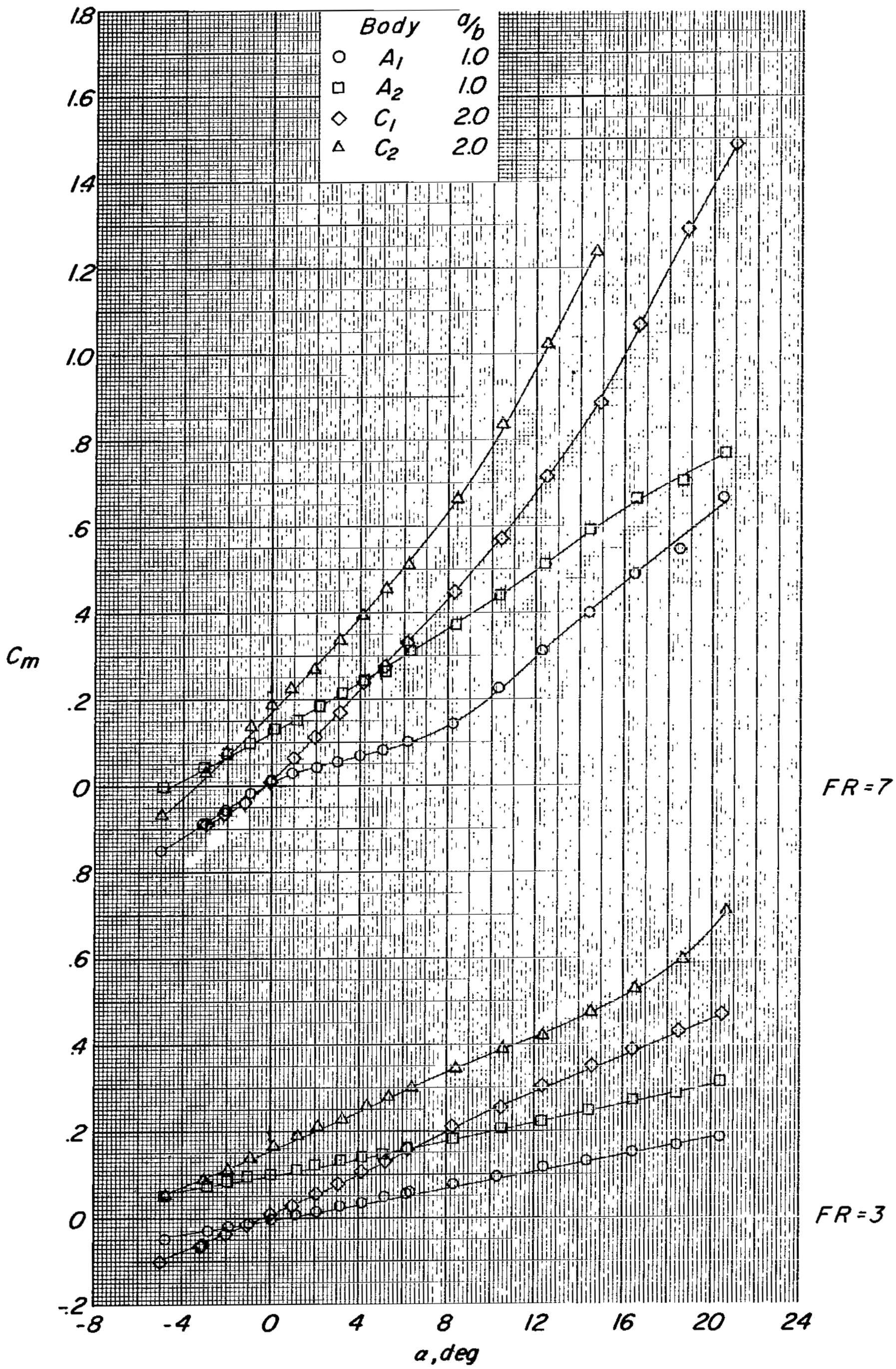

(c) C_m plotted against α.

Figure 9.- Continued.

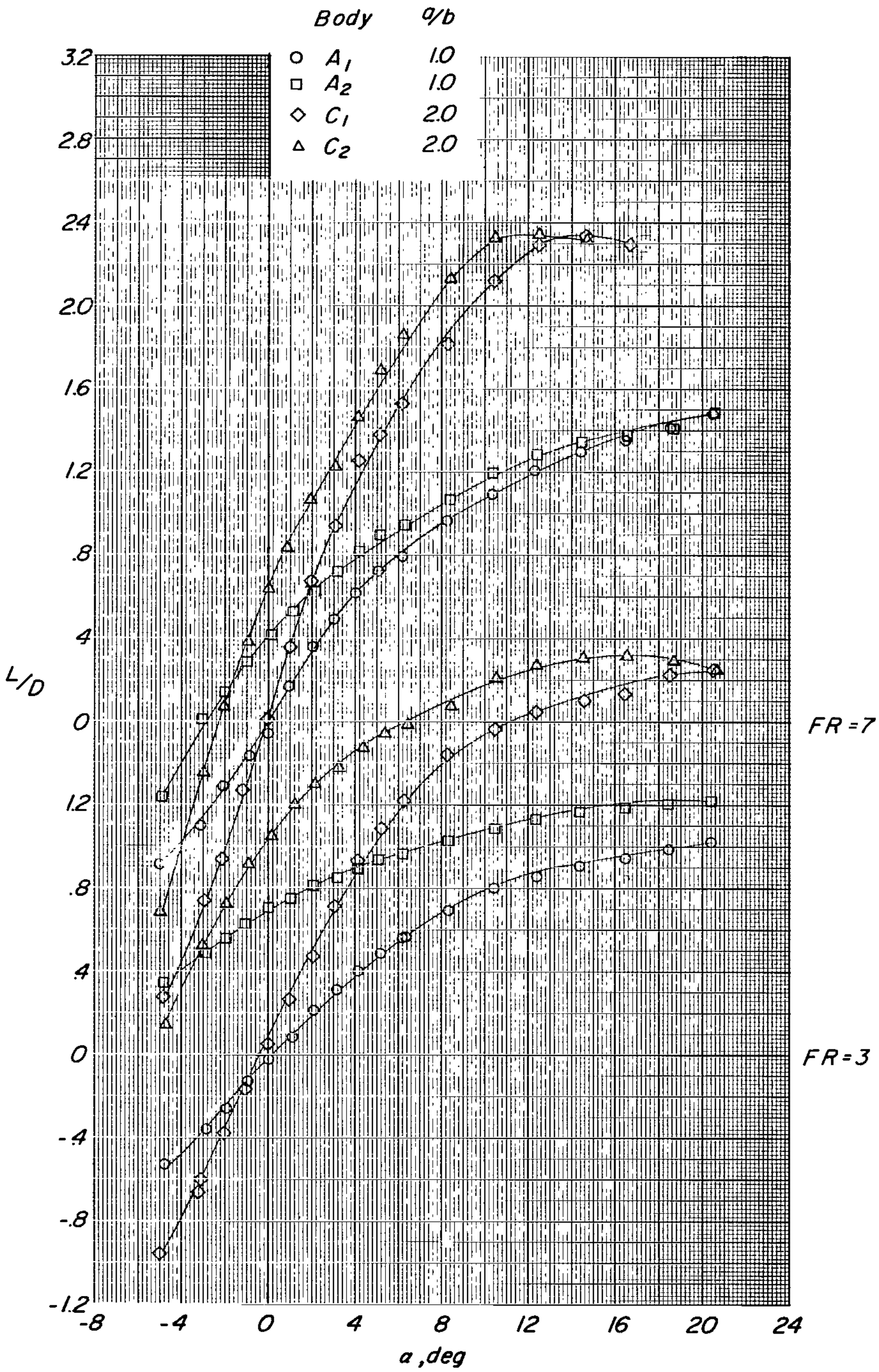

(d) L/D plotted against α.

Figure 9.- Concluded.

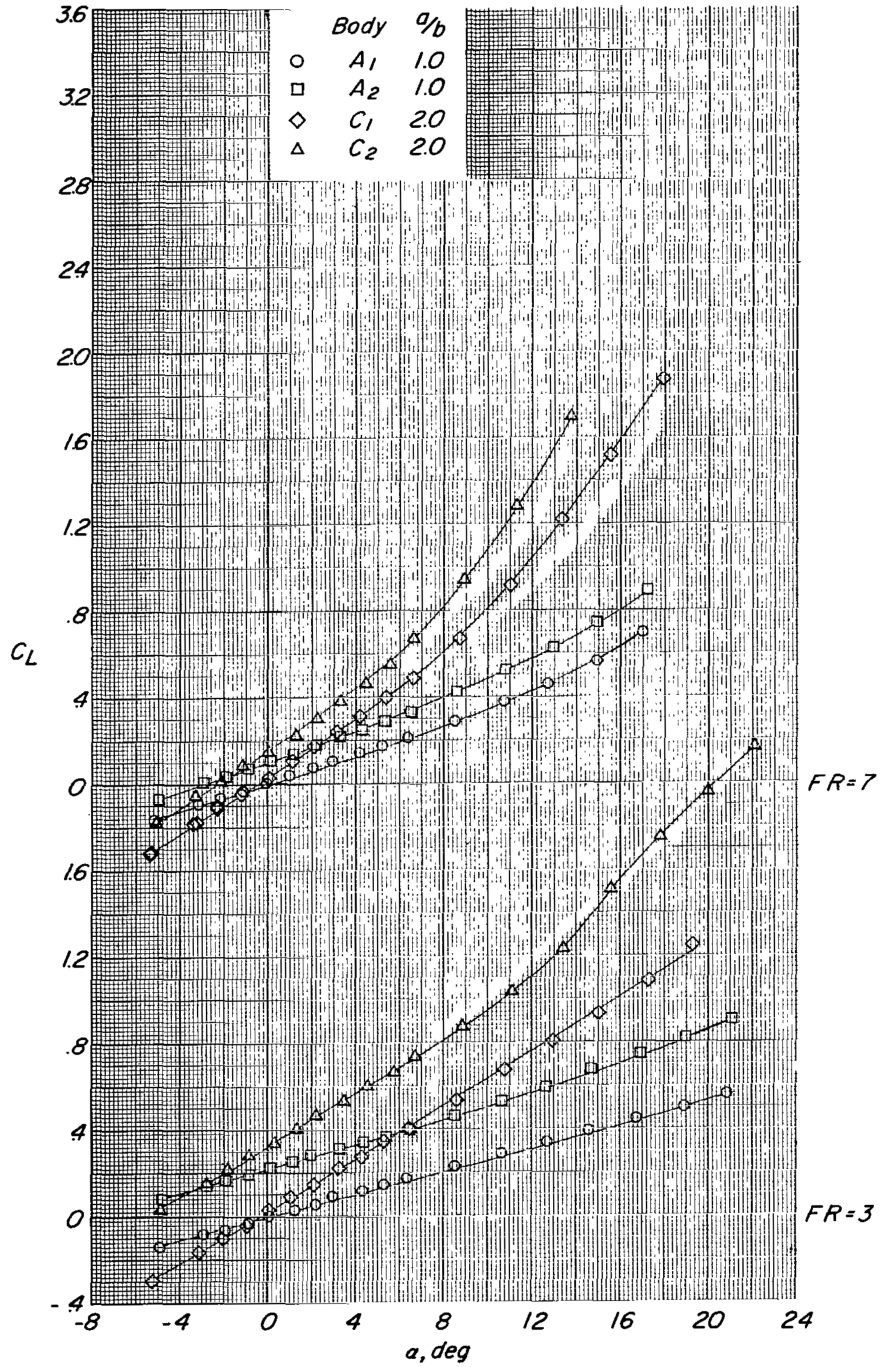

(a) C_L plotted against α.

Figure 10.- Effects of body section displacement on longitudinal aerodynamic characteristics of bodies having a/b = 1.0 and 2.0 at $\phi = 0^{\circ}$. M = 0.80.

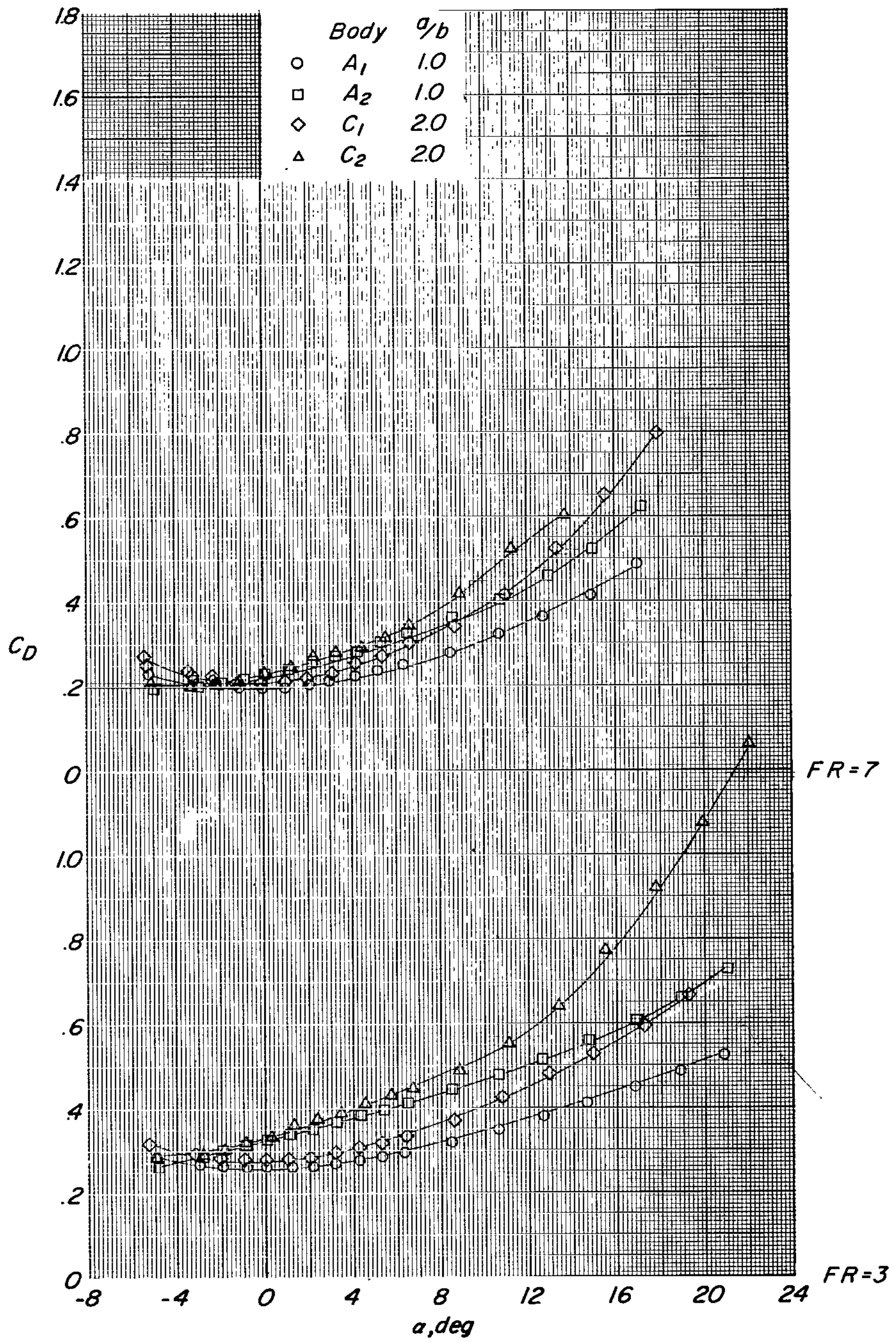

(b) C_D plotted against α.

Figure 10.- Continued.

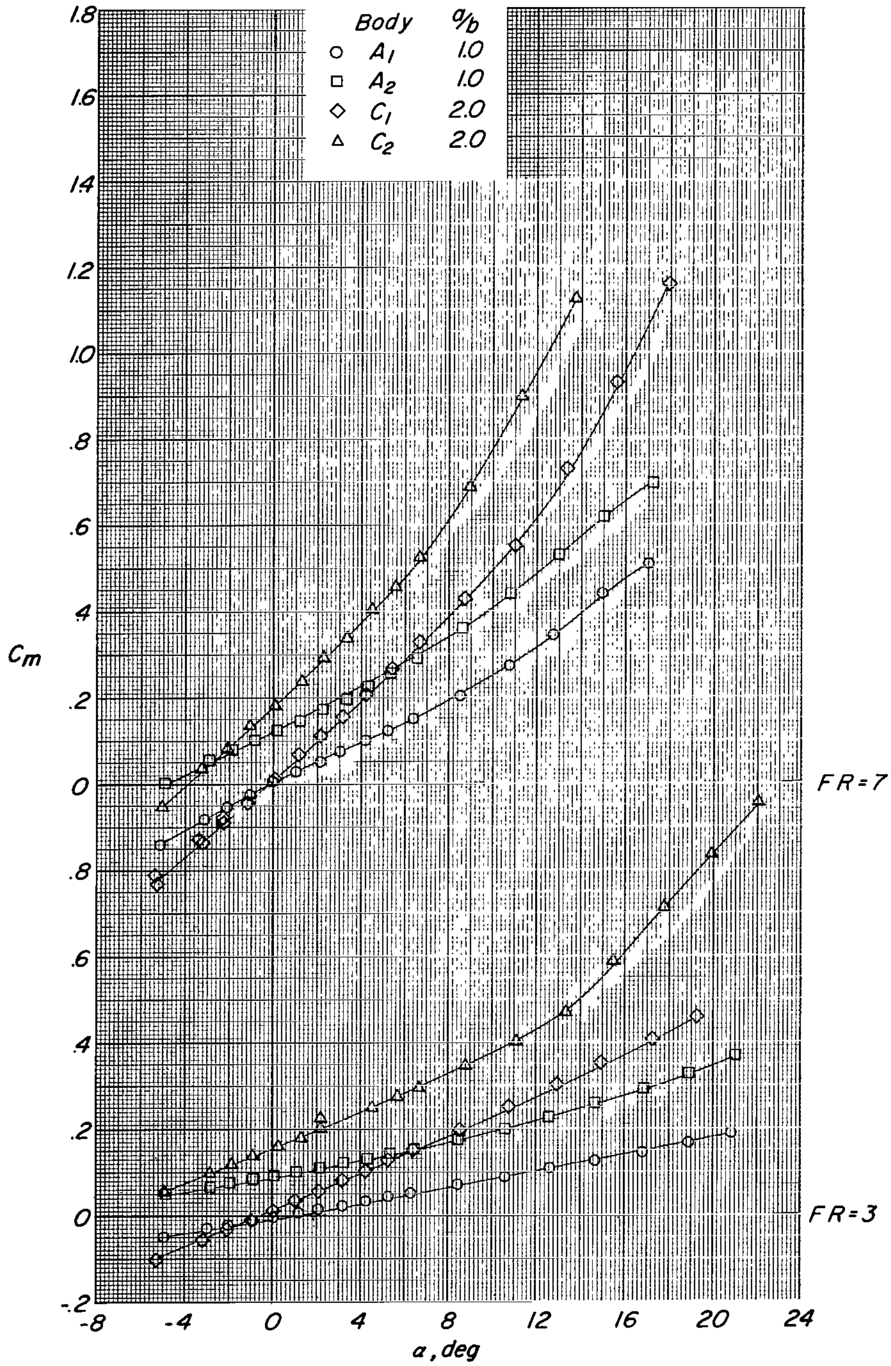

(c) C_m plotted against α.

Figure 10.- Continued.

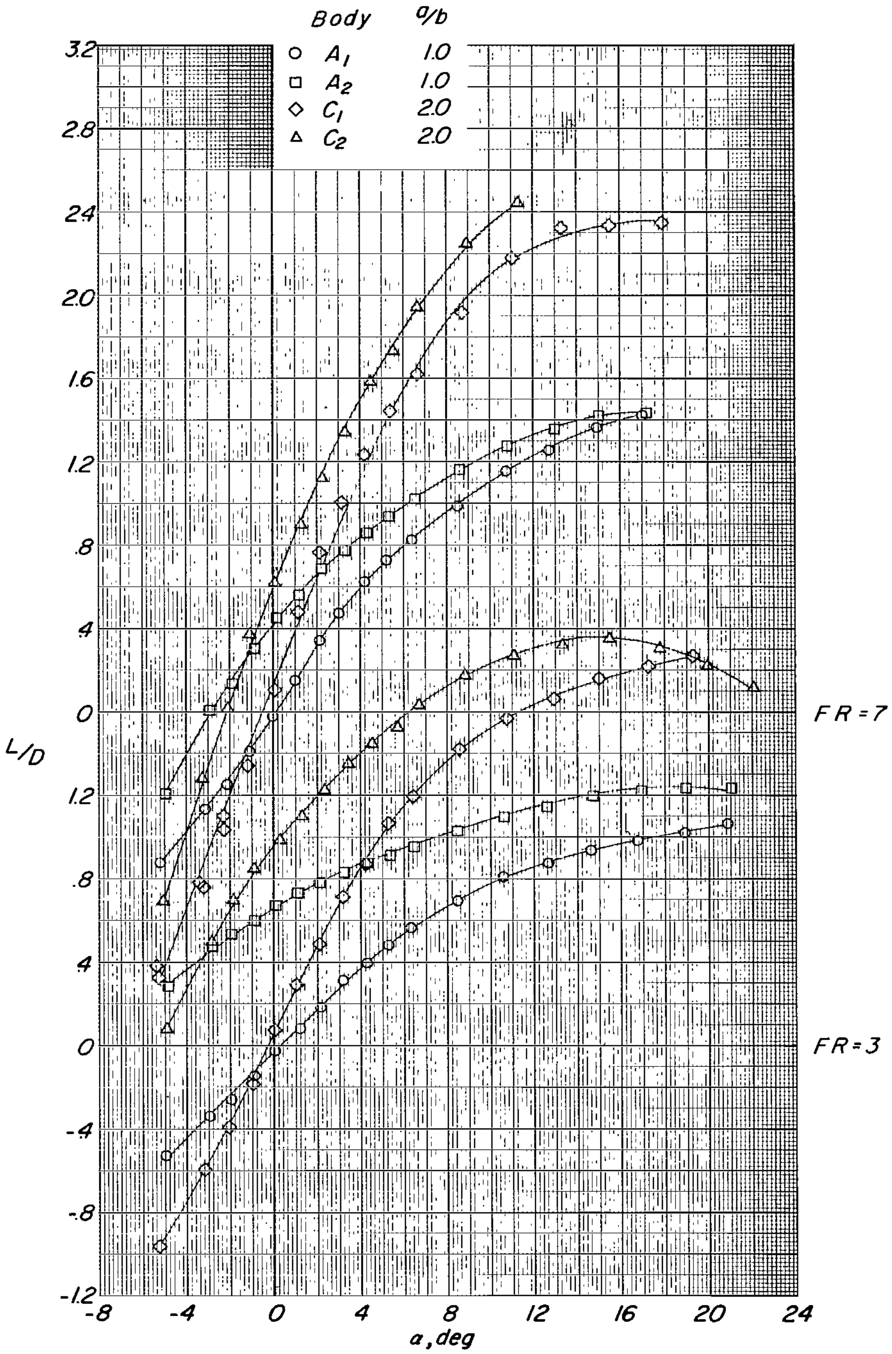

(d) L/D plotted against α.

Figure 10.- Concluded.

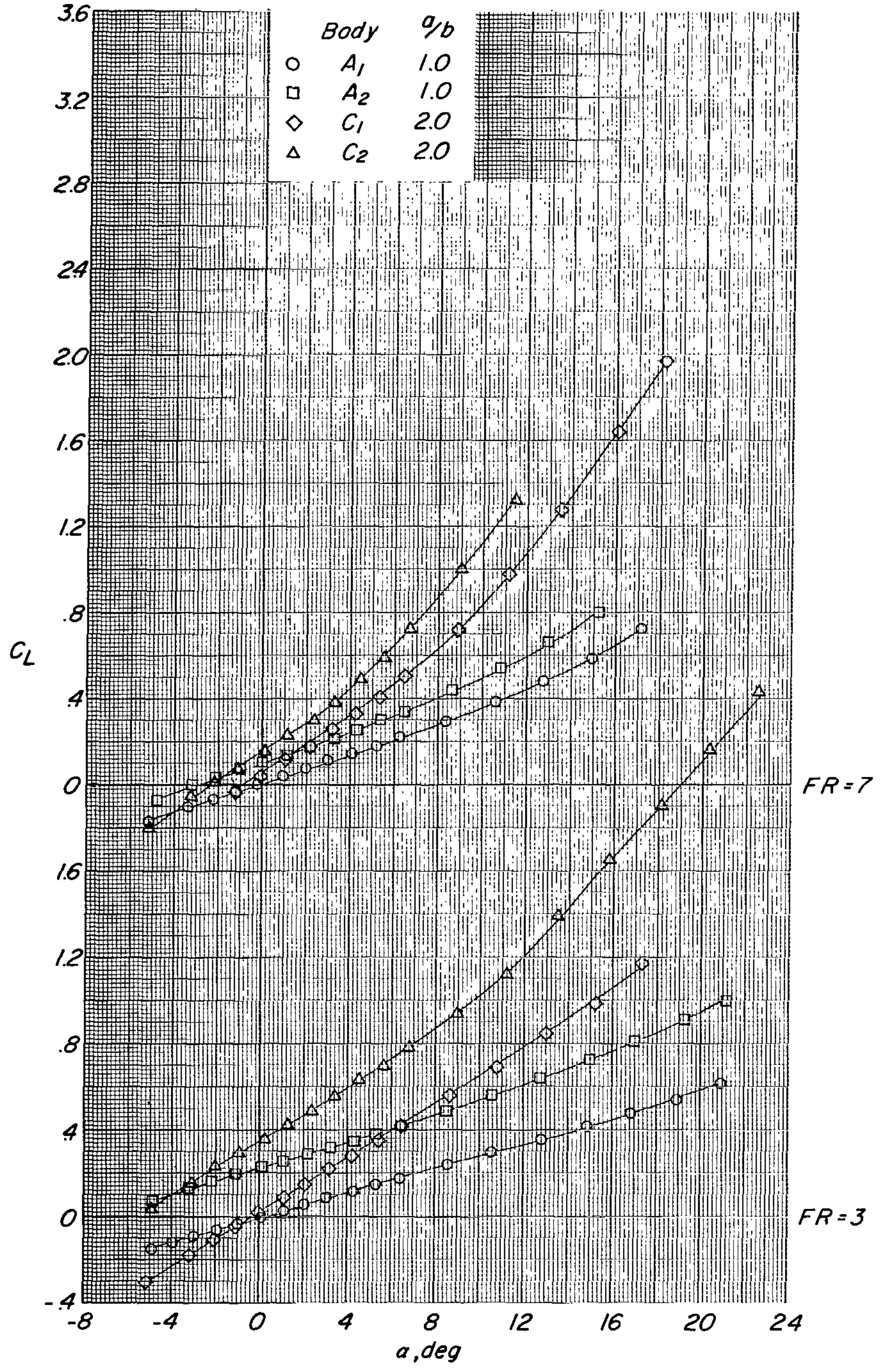

(a) C_L plotted against α.

Figure 11.- Effects of body section displacement on longitudinal aerodynamic characteristics of bodies having a/b = 1.0 and 2.0 at $\phi = 0^{\circ}$. M = 0.90.

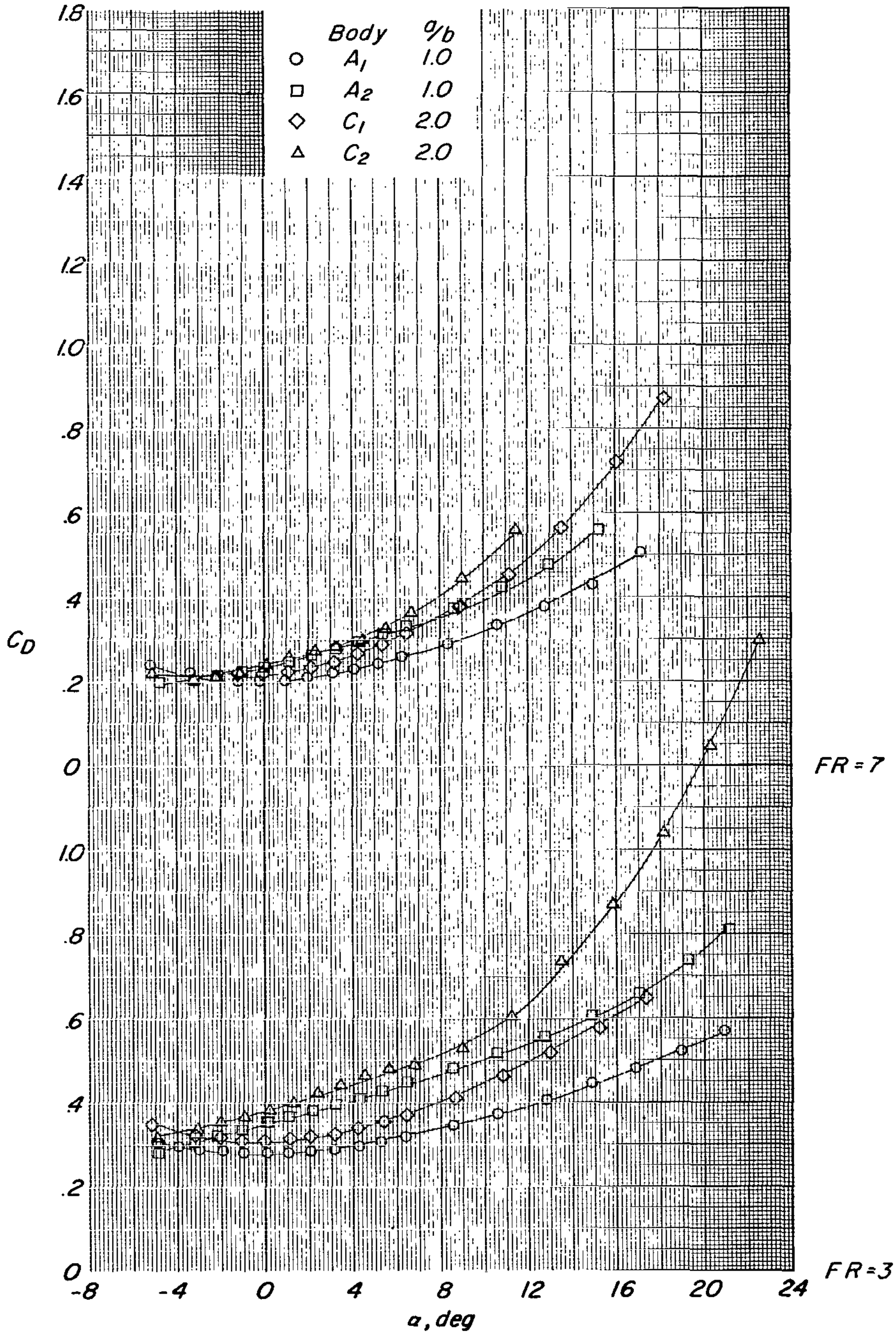

(b) C_D plotted against α.

Figure 11.- Continued.

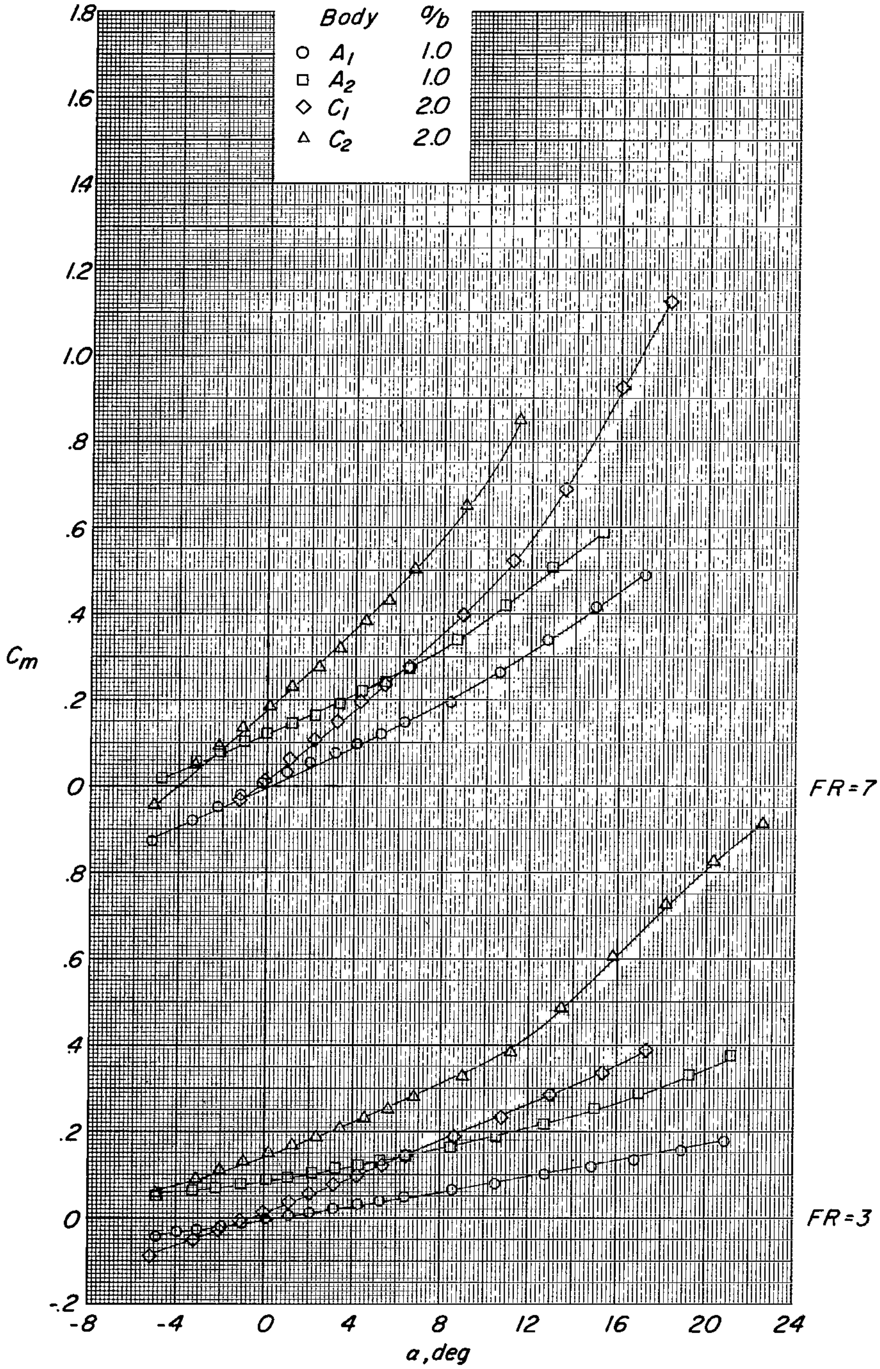

(c) C_m plotted against α.

Figure 11.- Continued.

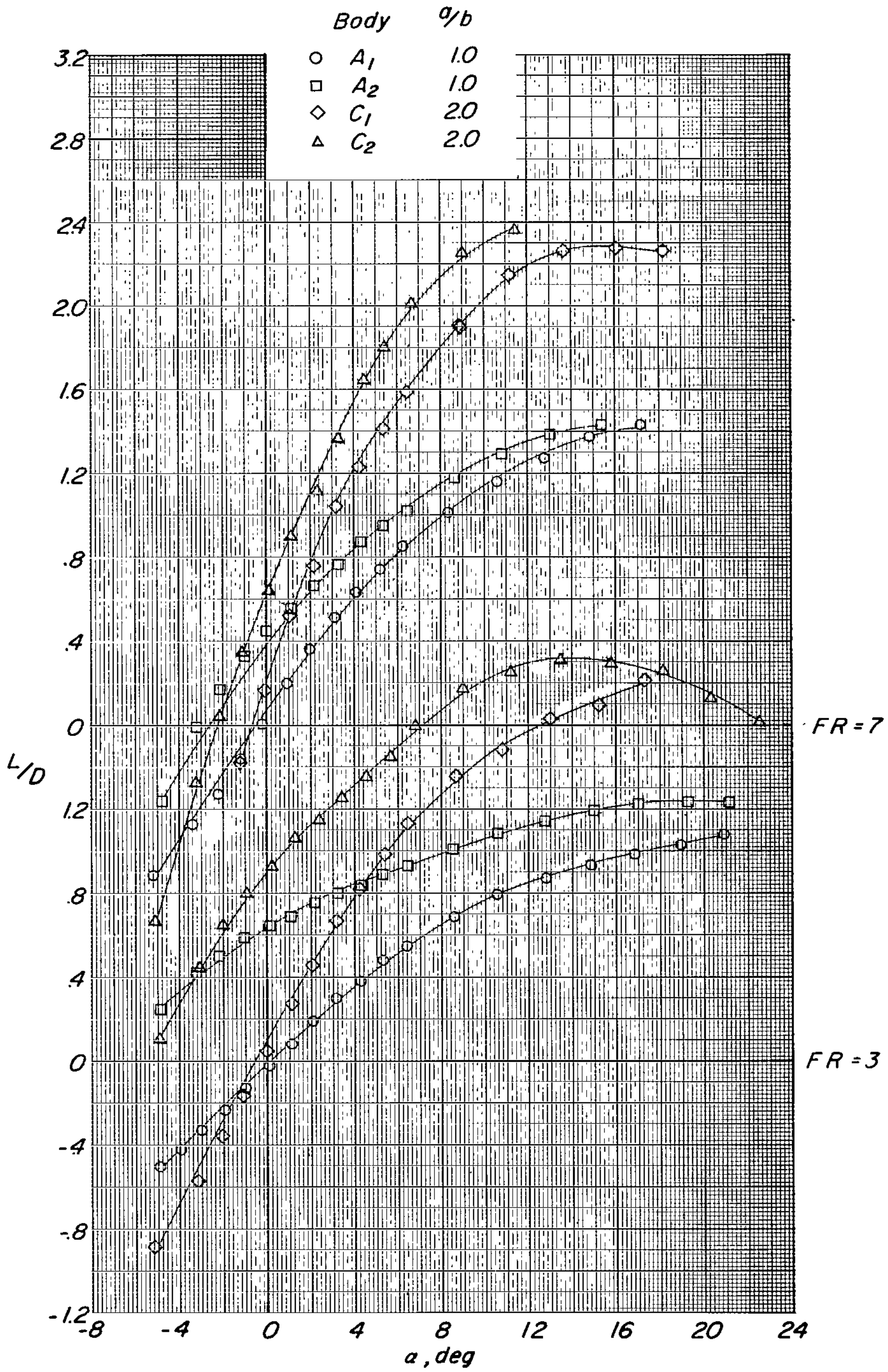

(d) L/D plotted against α.

Figure 11.- Concluded.

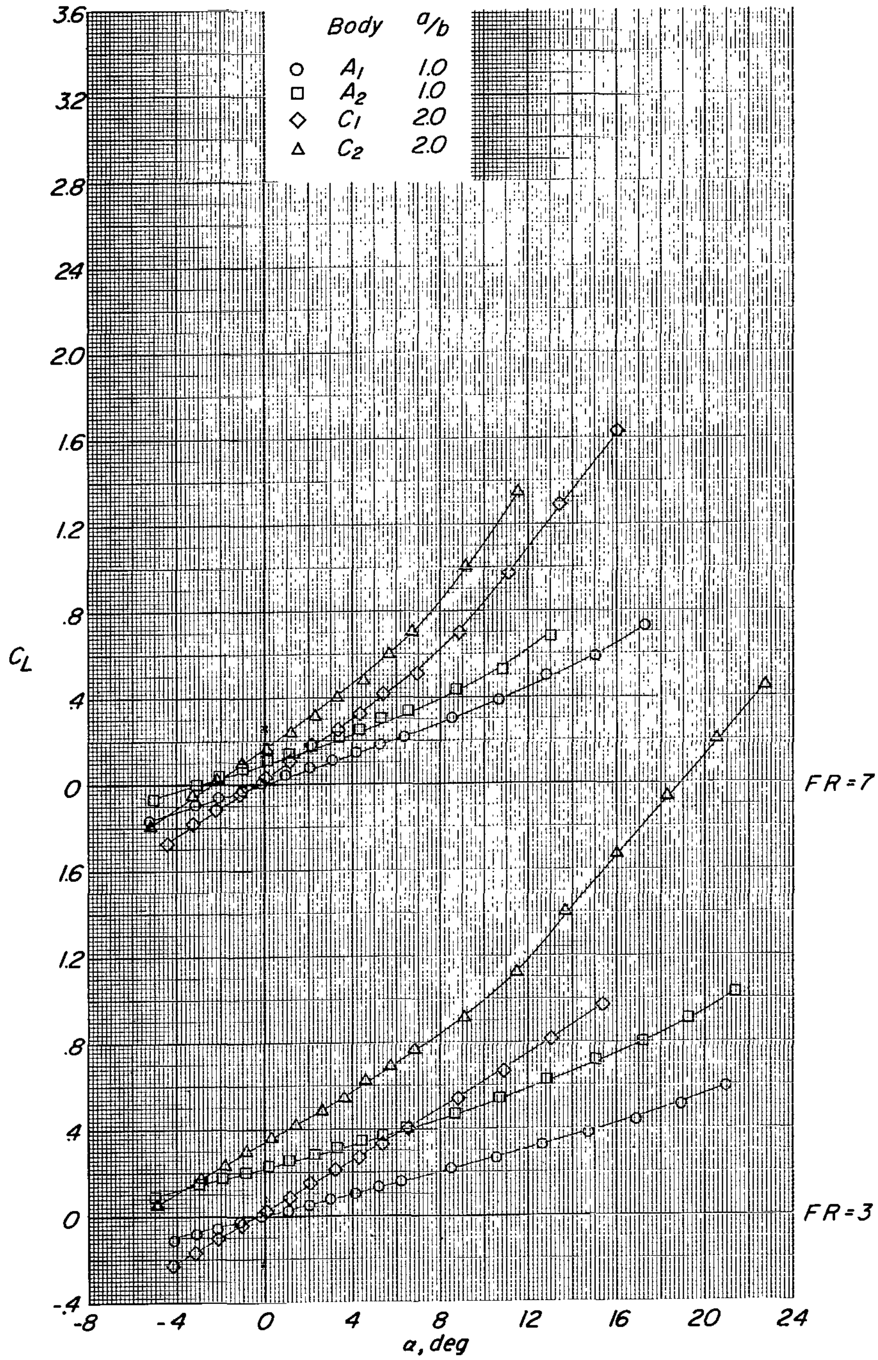

(a) C_L plotted against α.

Figure 12.- Effects of body section displacement on longitudinal aerodynamic characteristics of bodies having $a/b = 1.0$ and 2.0 at $\phi = 0^{\circ}$. $M = 1.00$.

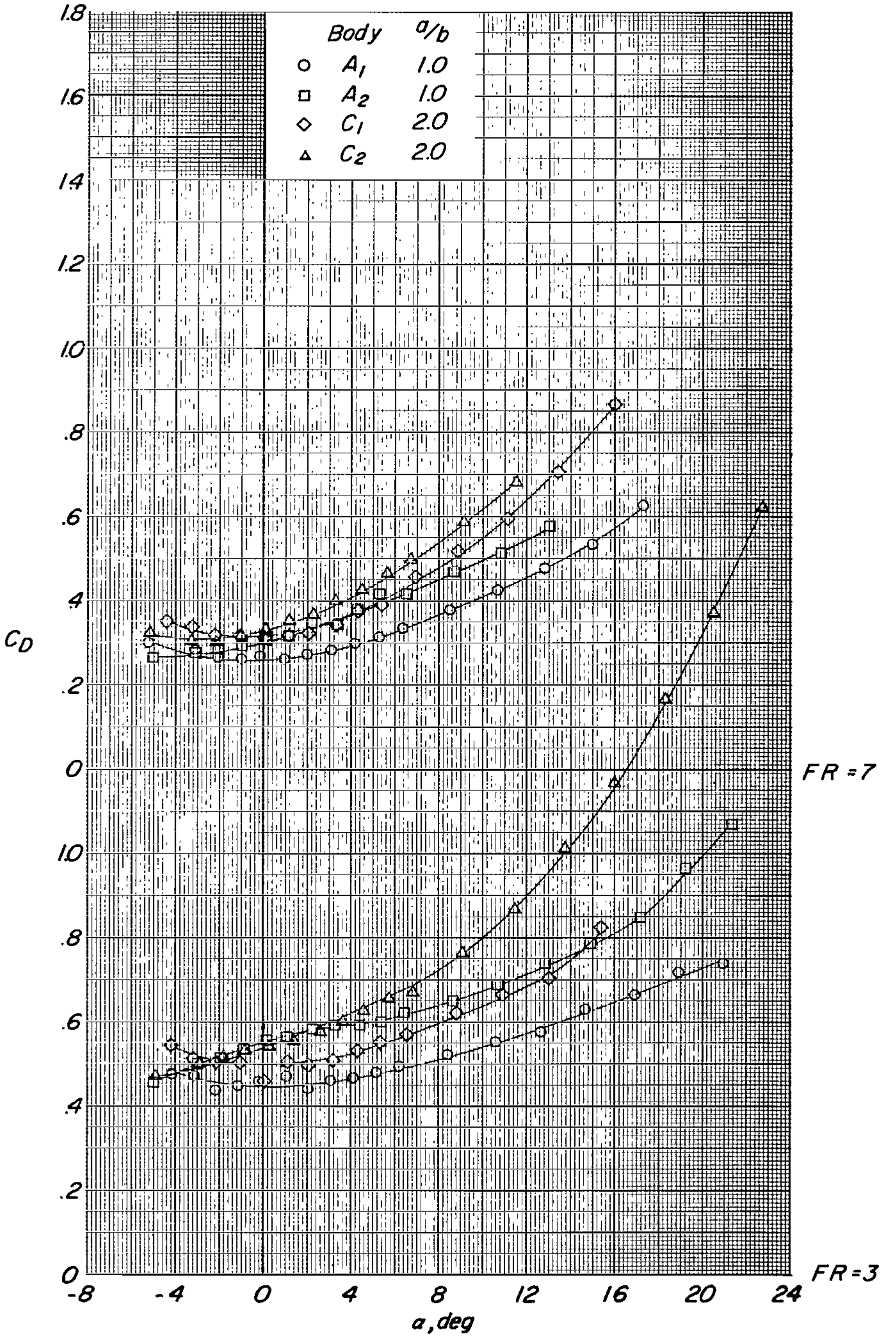

(b) C_D plotted against α.

Figure 12.- Continued.

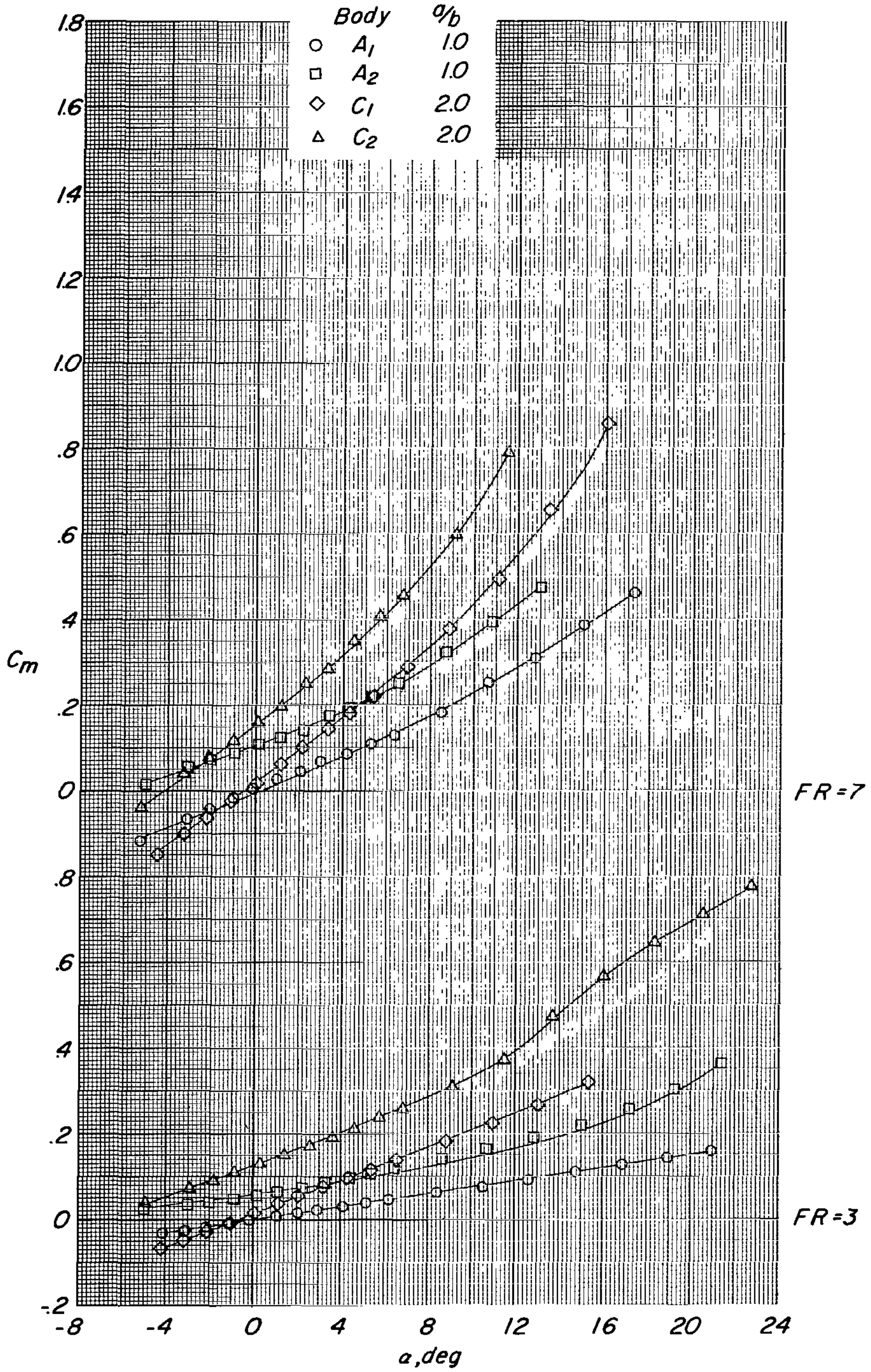

(c) C_m plotted against α.

Figure 12.- Continued.

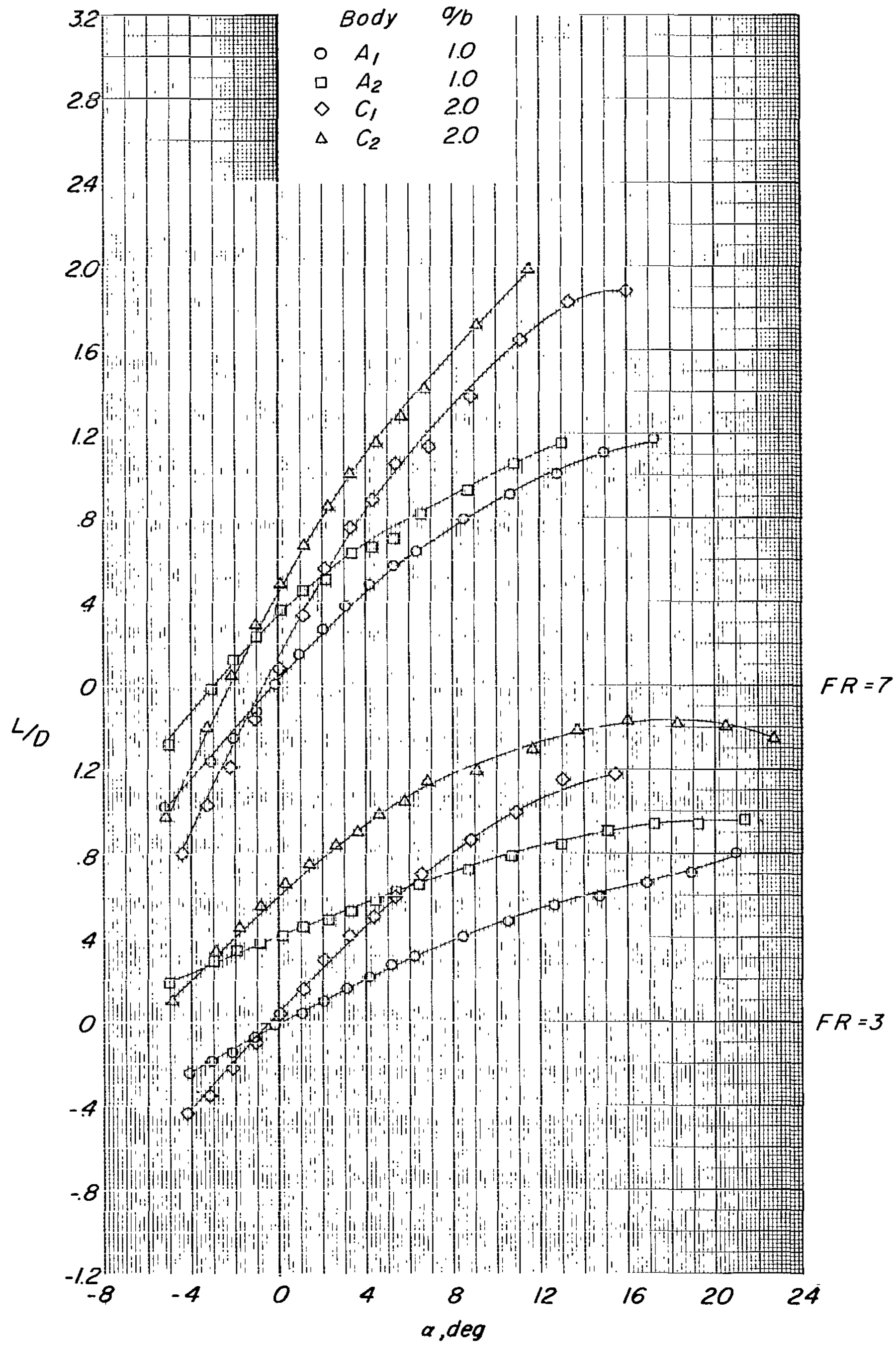

(d) L/D plotted against α.

Figure 12.- Concluded.

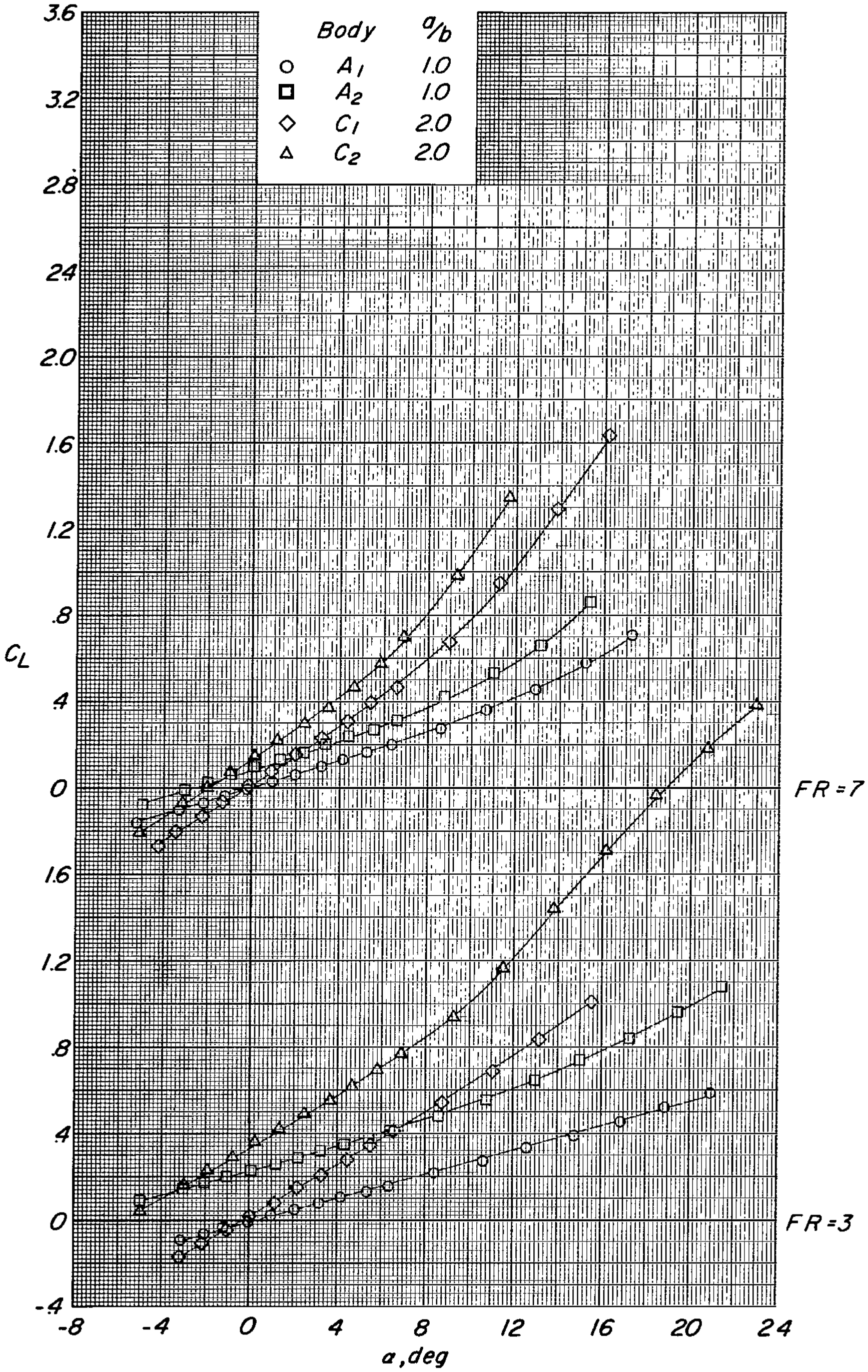

(a) C_L plotted against α.

Figure 13.- Effects of body section displacement on longitudinal aerodynamic characteristics of bodies having $a/b = 1.0$ and 2.0 at $\phi = 0^{\circ}$. $M = 1.14$.

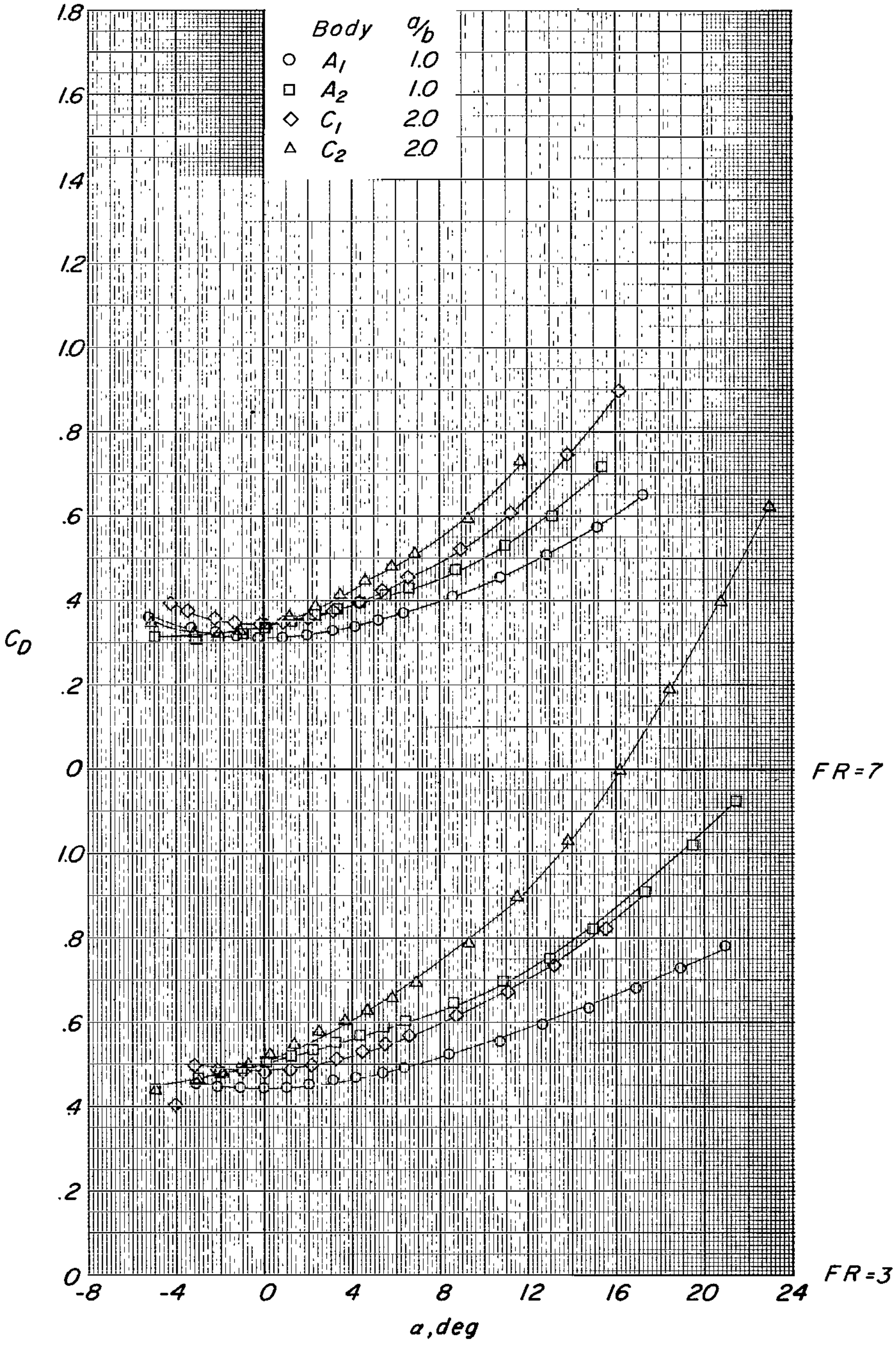

(b) C_D plotted against α.

Figure 13.- Continued.

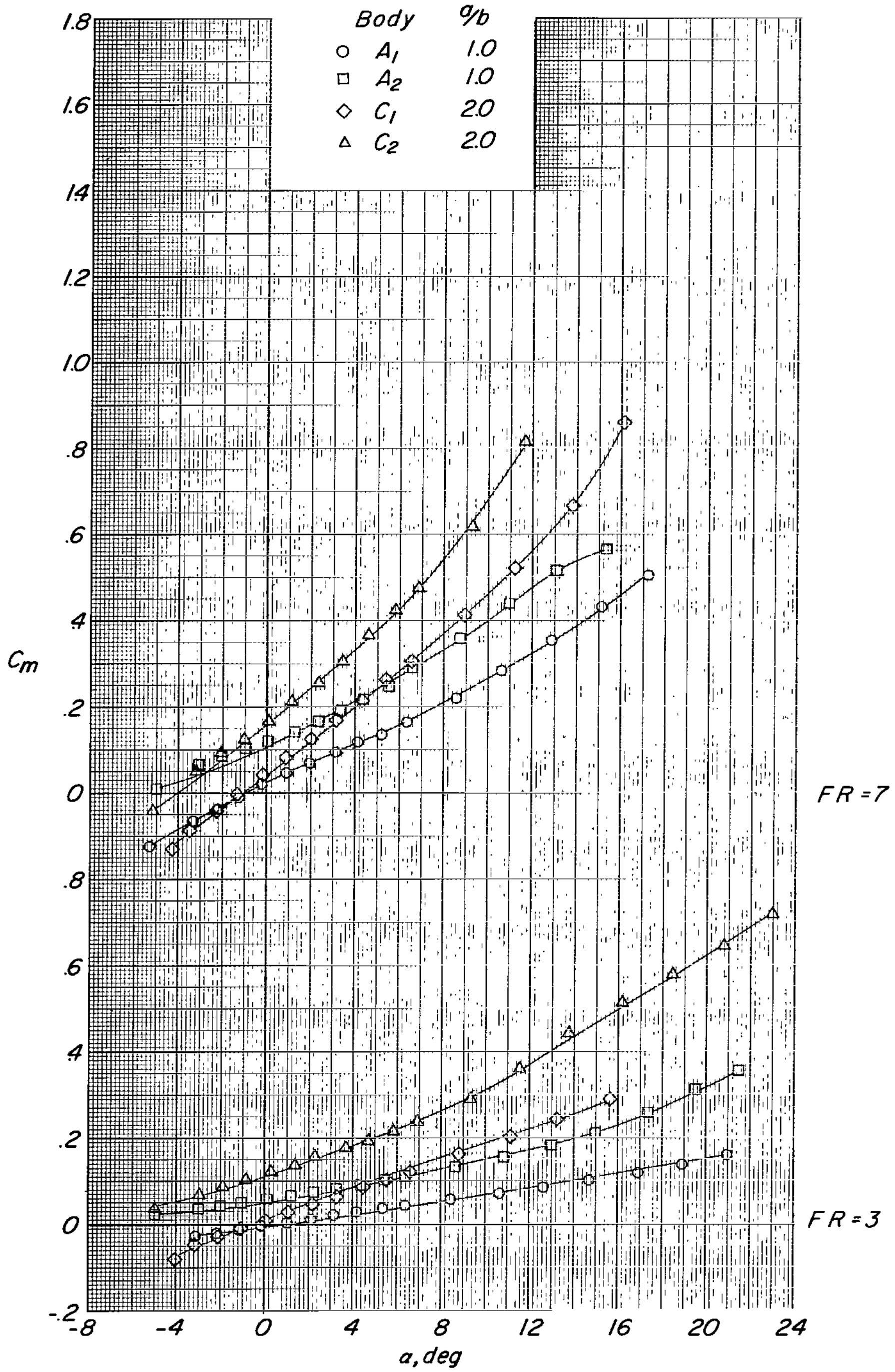

(c) C_m plotted against α.

Figure 13.- Continued.

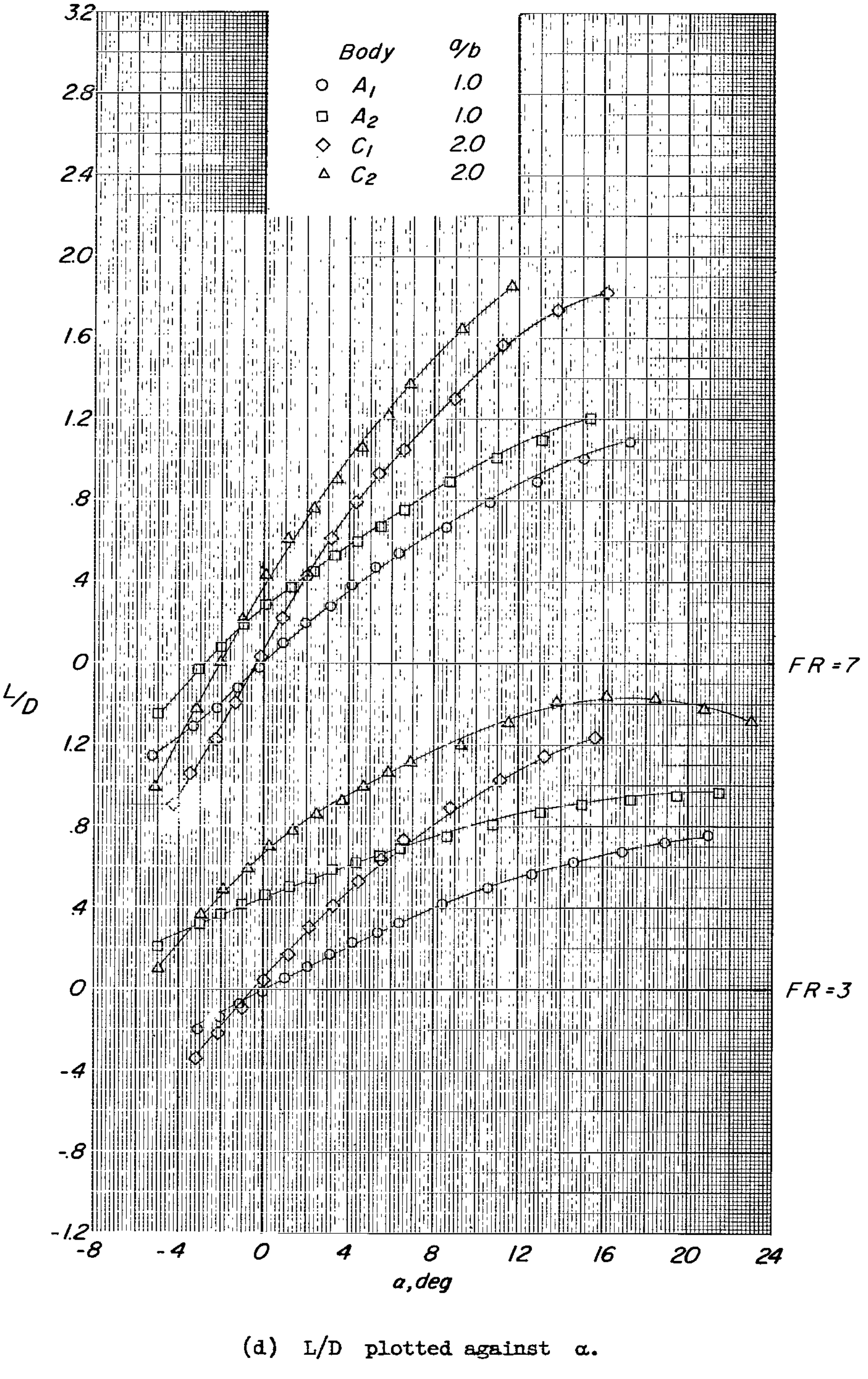

(d) L/D plotted against α.

Figure 13.- Concluded.

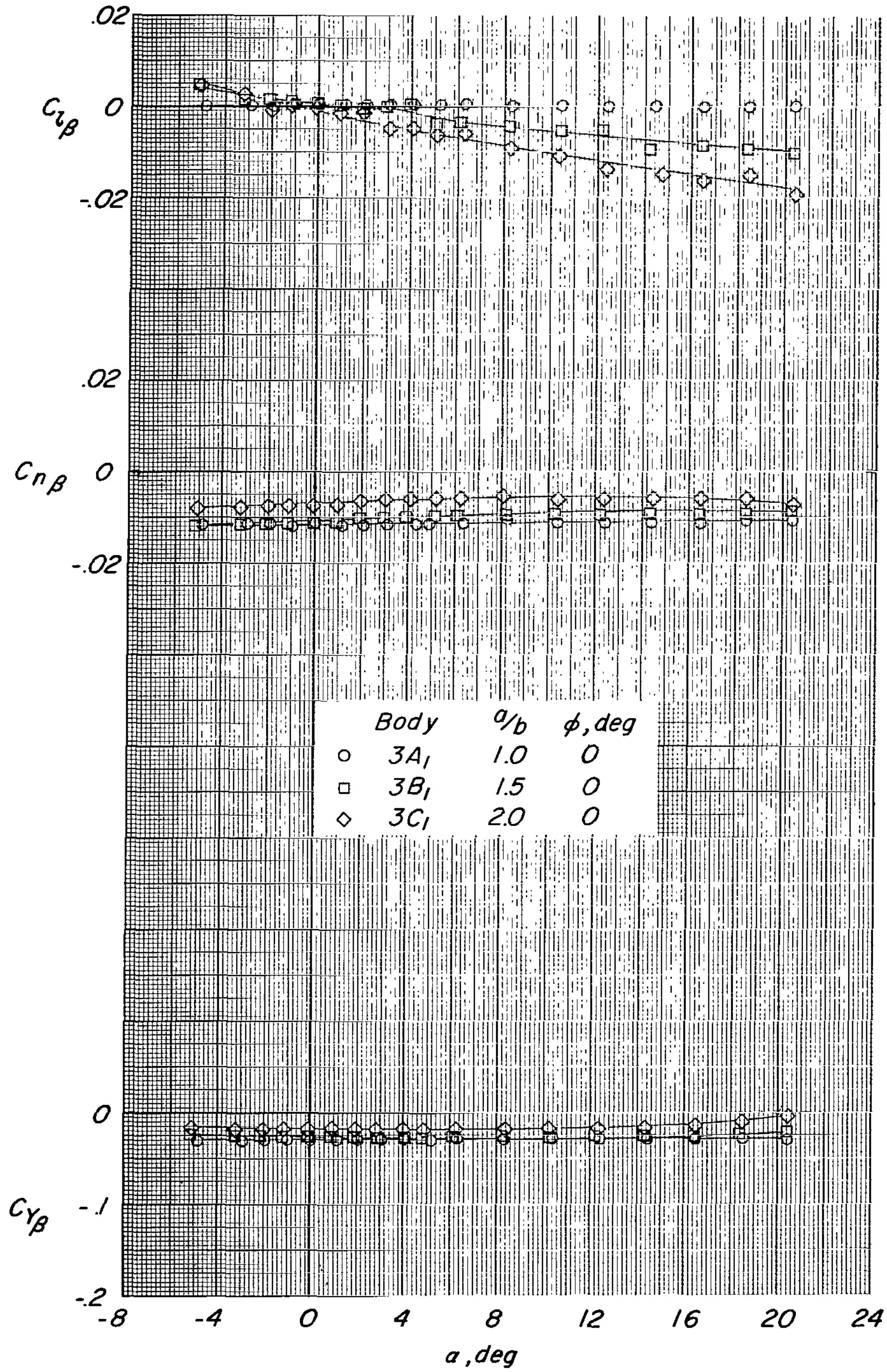

(a) M = 0.40.

Figure 14.- Effects of increasing a/b from 1.0 to 2.0 at $\phi = 0^{\circ}$ on variation of sideslip derivatives with angle of attack for symmetrical bodies having a fineness ratio of 3.

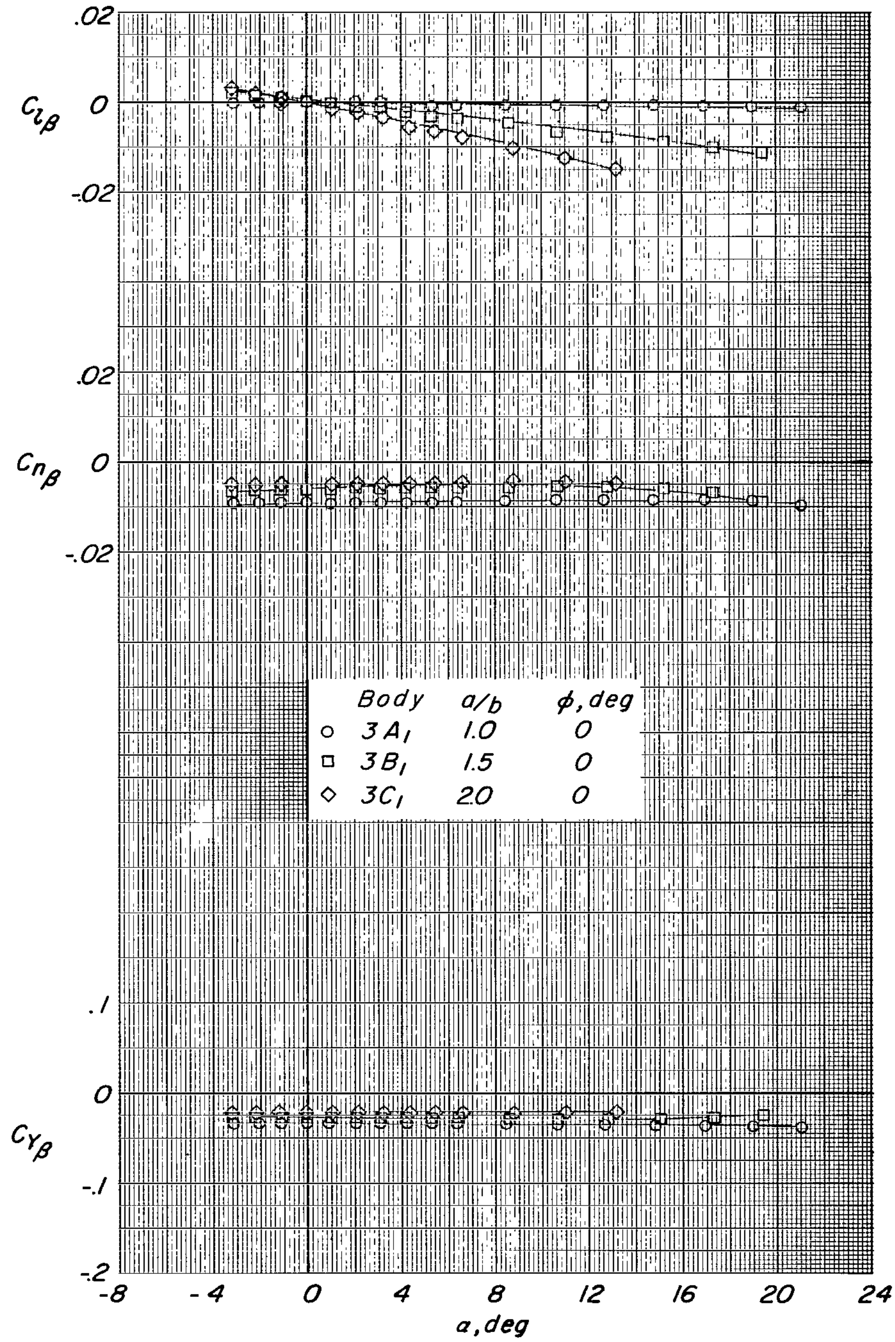

(b) M = 1.14.

Figure 14.- Concluded.

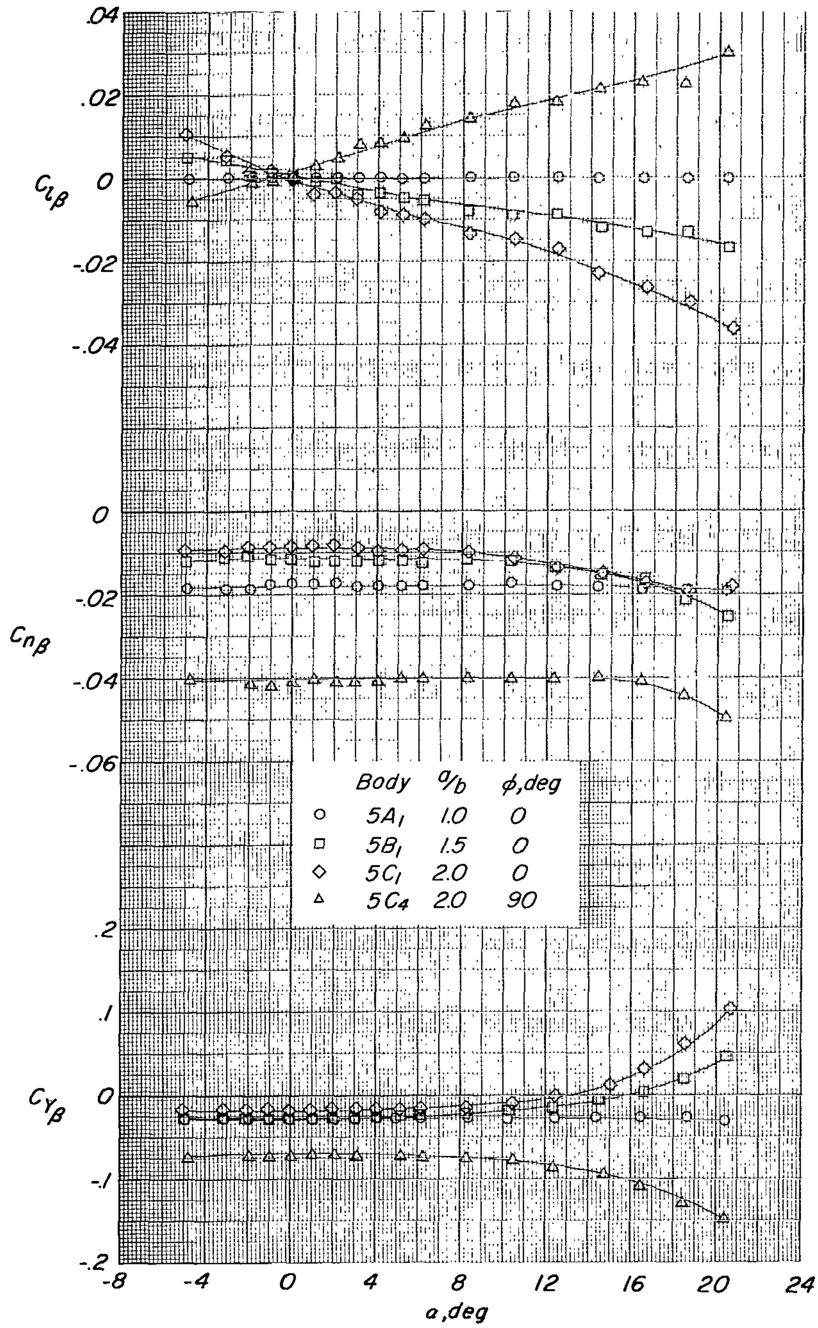

(a) M = 0.40.

Figure 15.- Effects of increasing a/b from 1.0 to 2.0 at ϕ = 0° and 90° on variation of sideslip derivatives with angle of attack for symmetrical bodies having a fineness ratio of 5.

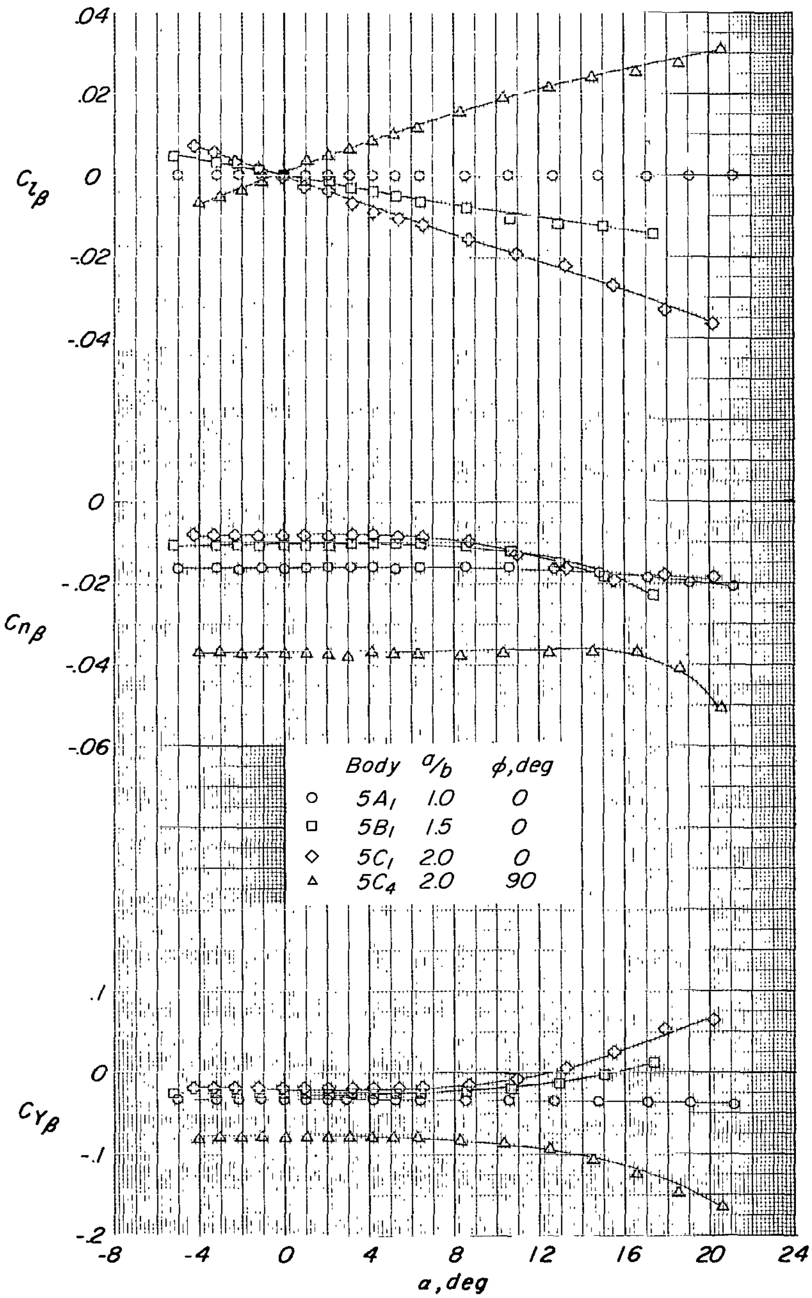

(b) M = 0.90.

Figure 15.- Continued.

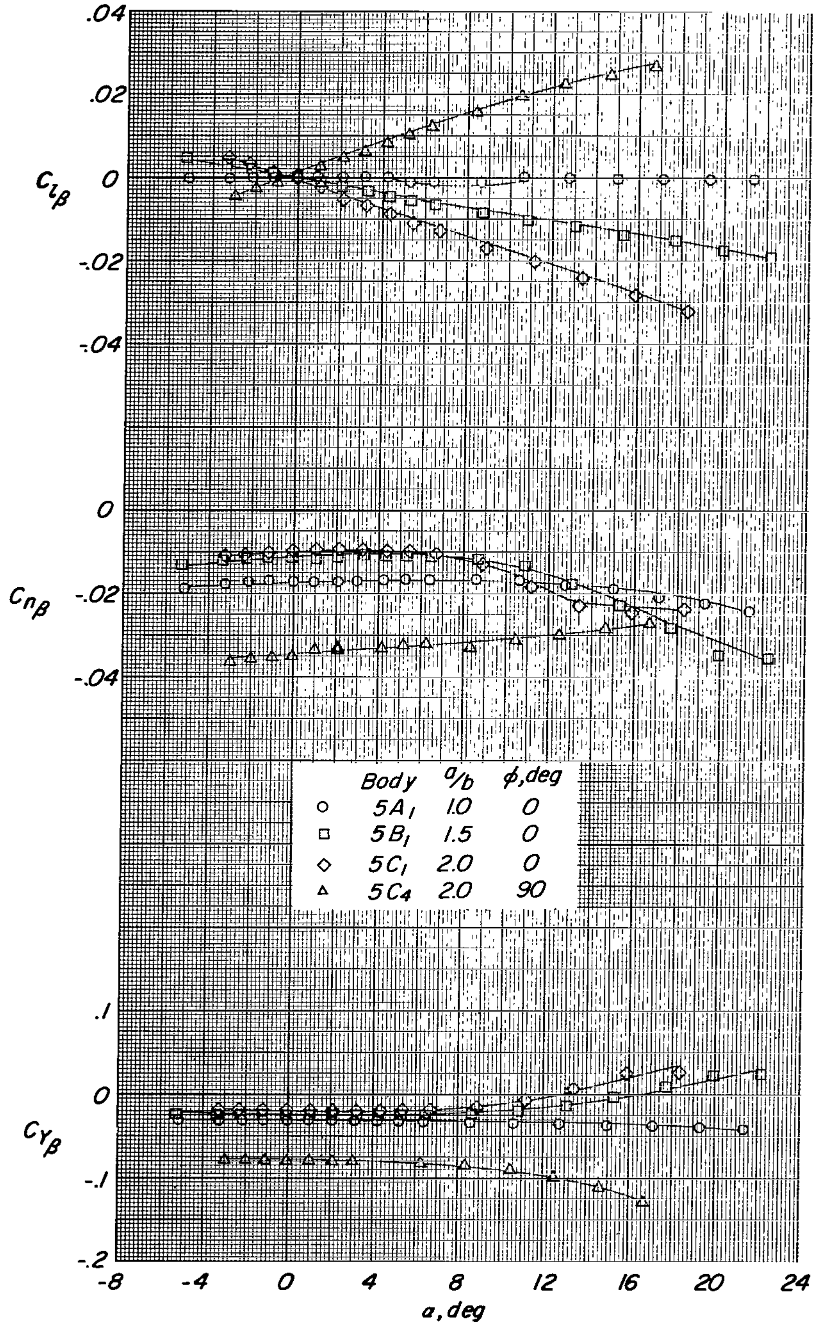

(c) M = 1.14.

Figure 15.- Concluded.

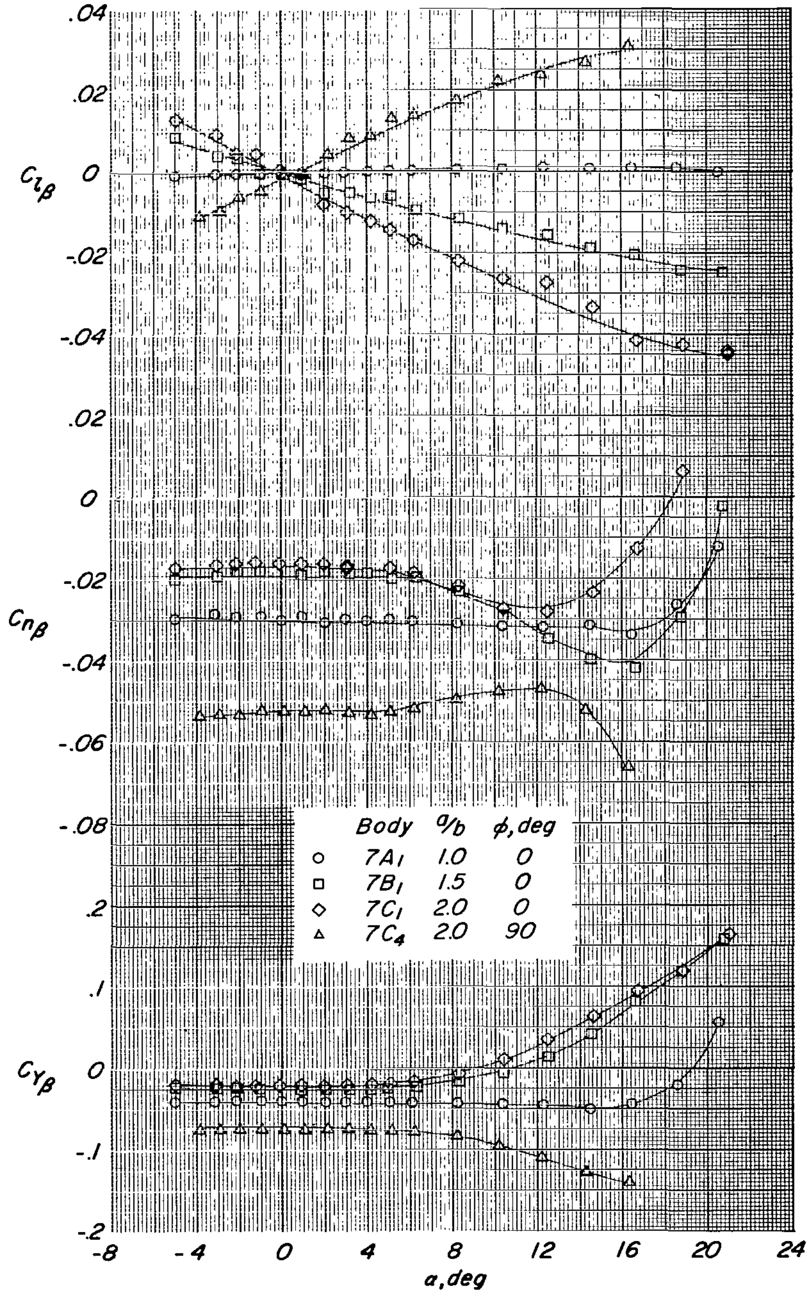

(a) M = 0.40.

Figure 16.- Effects of increasing a/b from 1.0 to 2.0 at $\phi = 0^\circ$ and 90° on variation of sideslip derivatives with angle of attack for symmetrical bodies having a fineness ratio of 7.

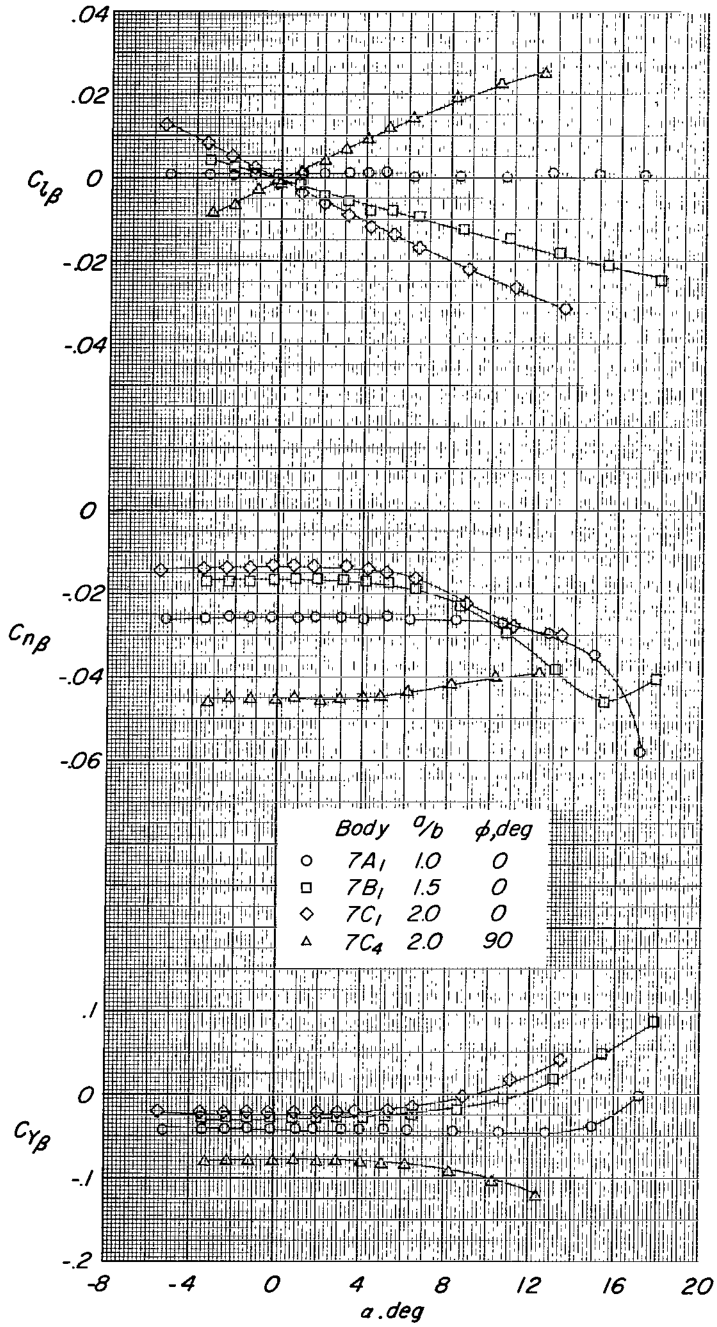

(b) M = 0.90.

Figure 16.- Continued.

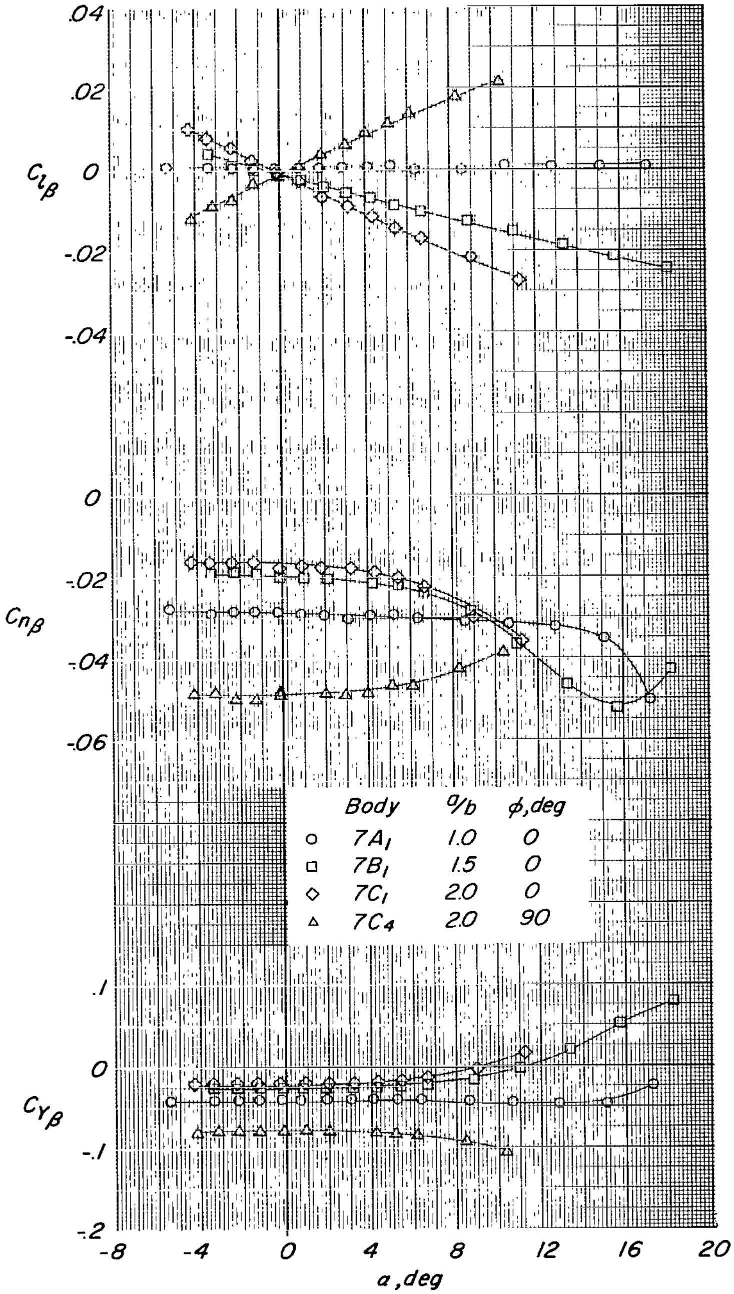

(c) M = 1.14.

Figure 16.- Concluded.

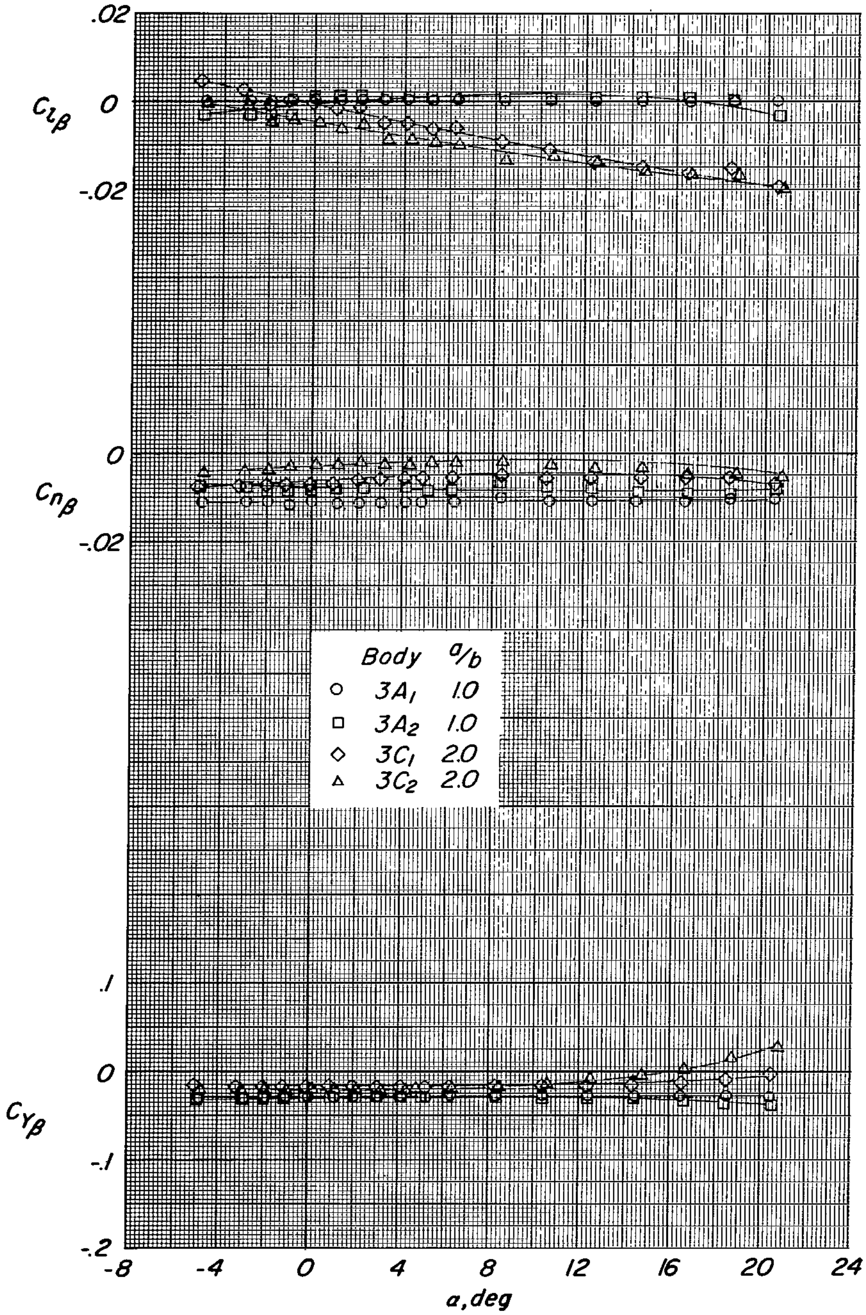

(a) M = 0.40.

Figure 17.- Effects of body section displacement on variation of sideslip derivatives with angle of attack for bodies having $a/b = 1.0$ and 2.0 at $\phi = 0^{\circ}$ and a fineness ratio of 3.

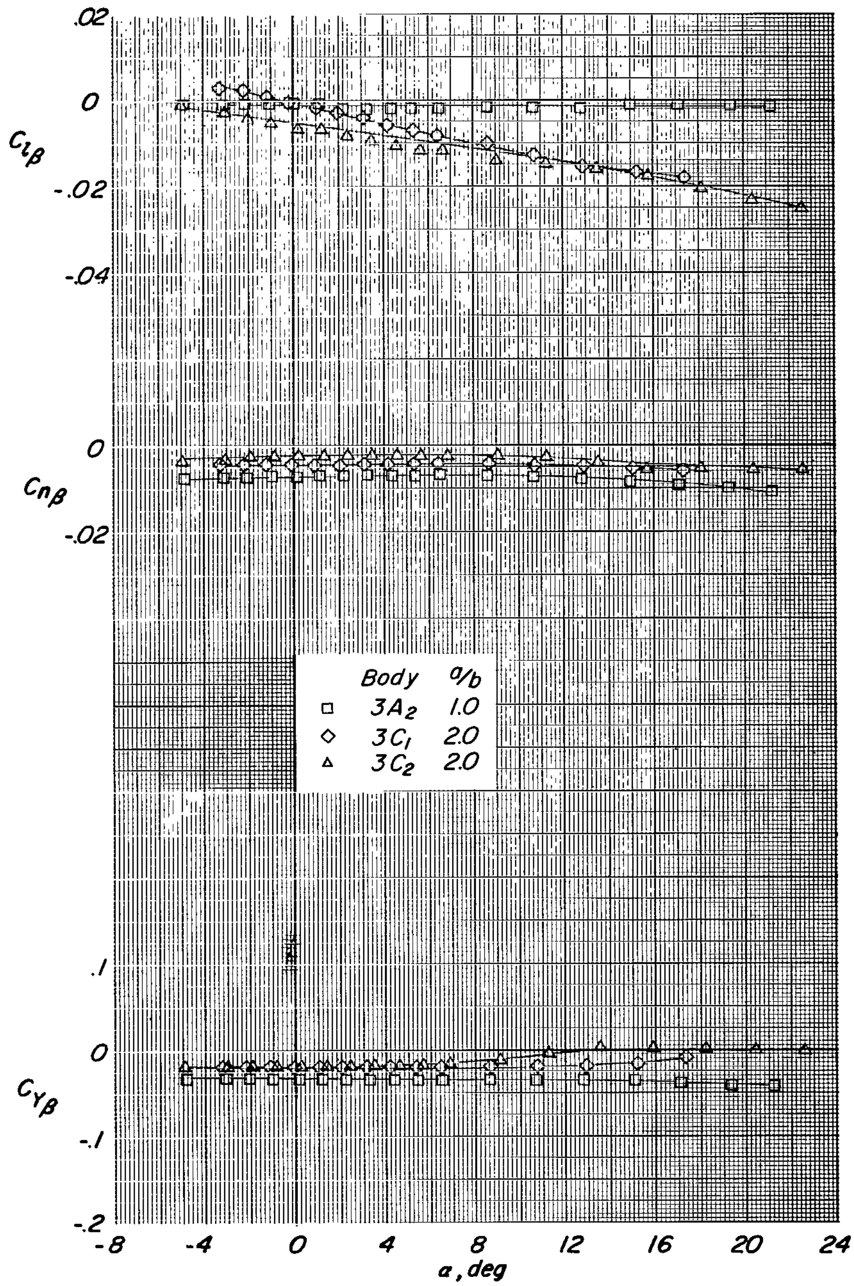

(b) M = 0.90.

Figure 17.- Continued.

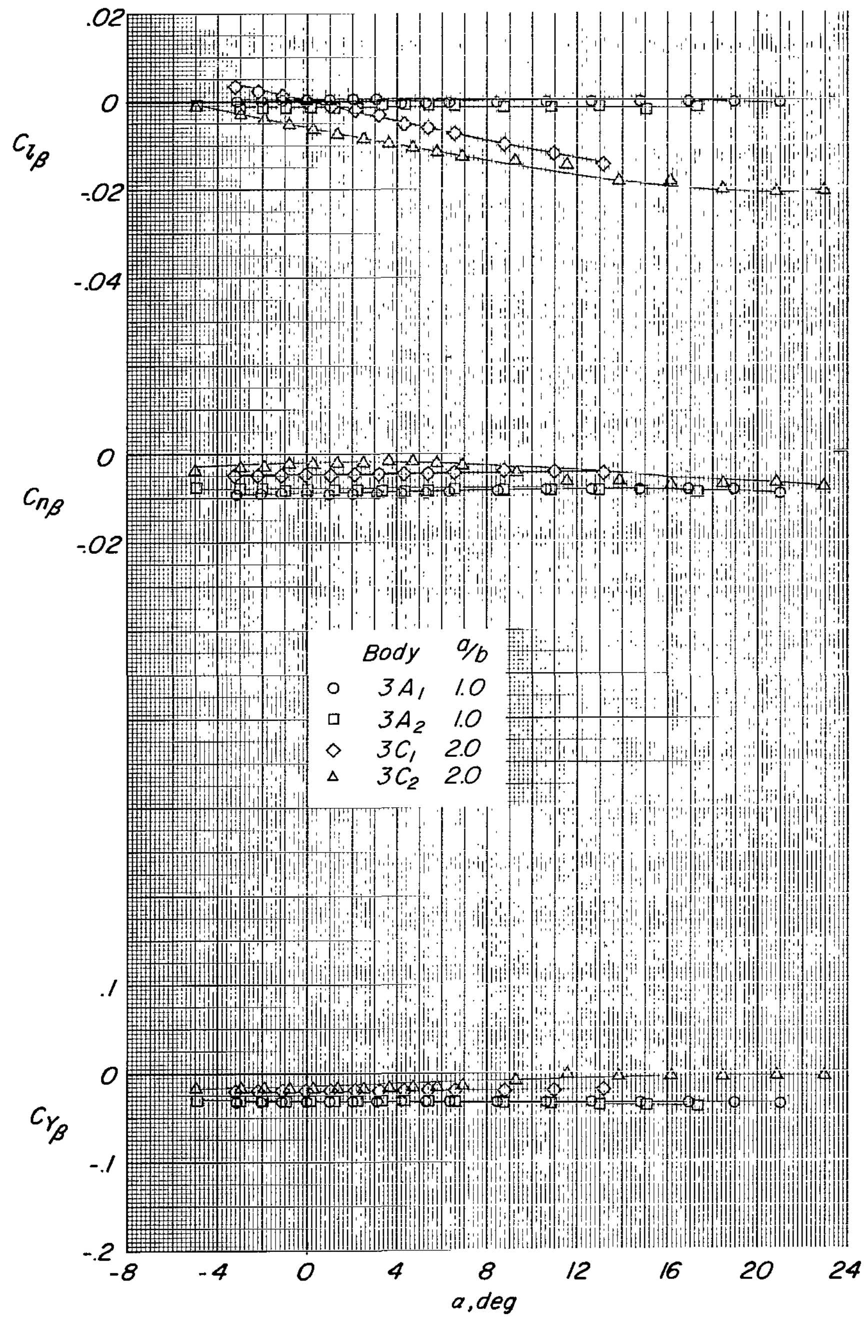

(c) M = 1.14.

Figure 17.- Concluded.

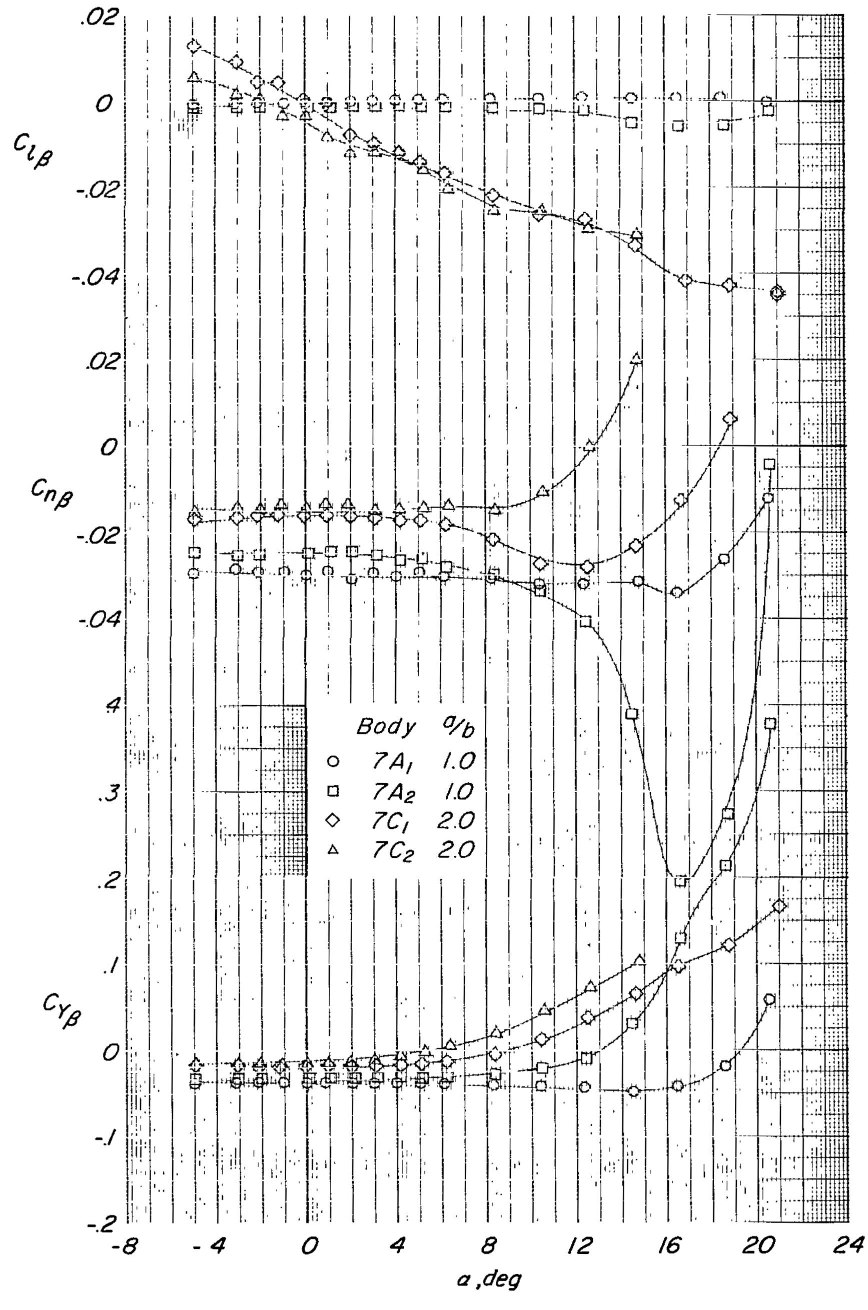

(a) M = 0.40.

Figure 18.- Effects of body section displacement on variation of sideslip derivatives with angle of attack for bodies having a/b = 1.0 and 2.0 at $\phi = 0^\circ$ and a fineness ratio of 7.

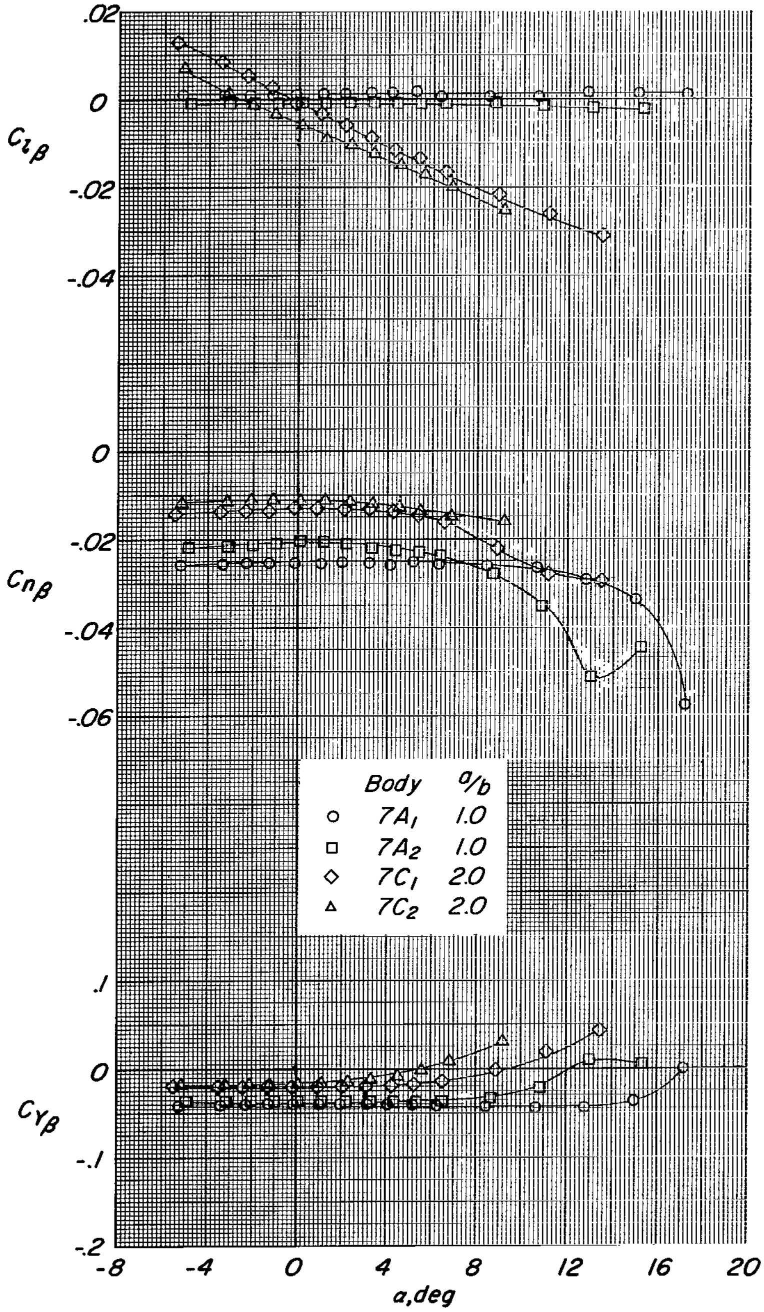

(b) M = 0.90.

Figure 18.- Continued.

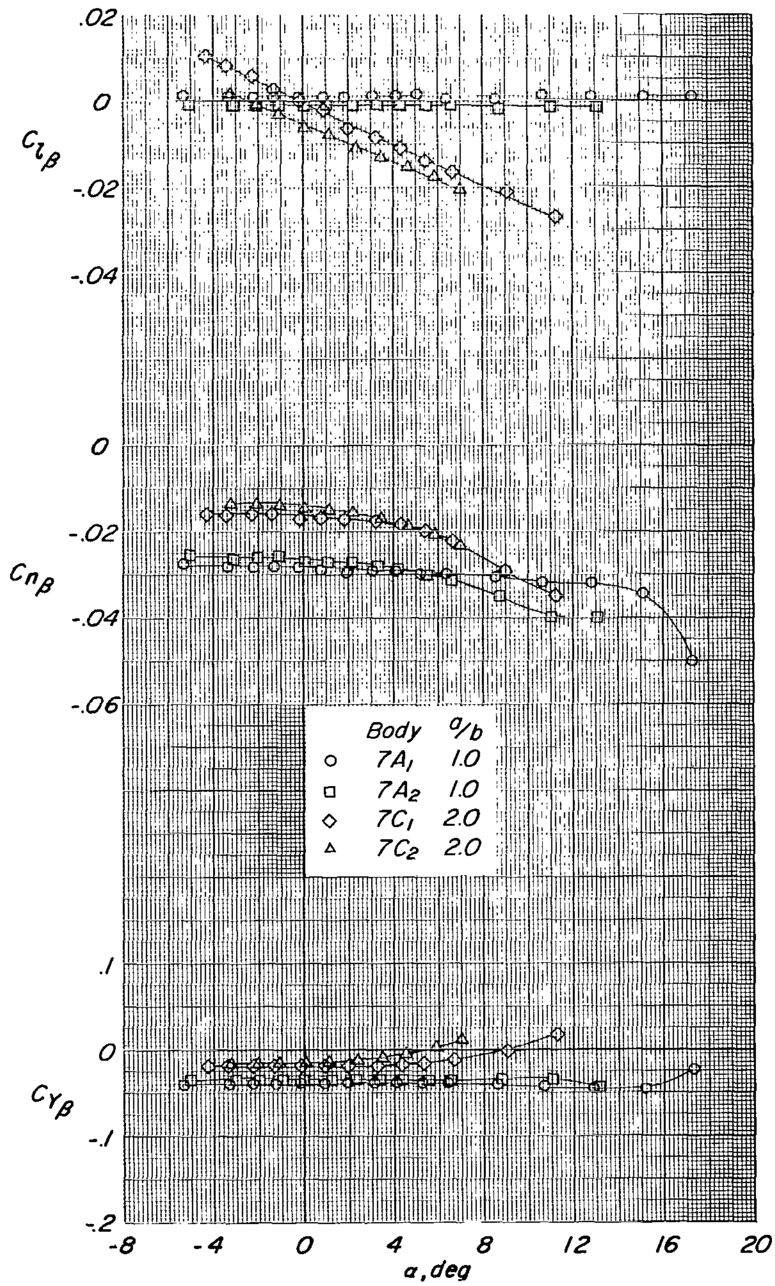

(c) M = 1.14.

Figure 18.- Concluded.

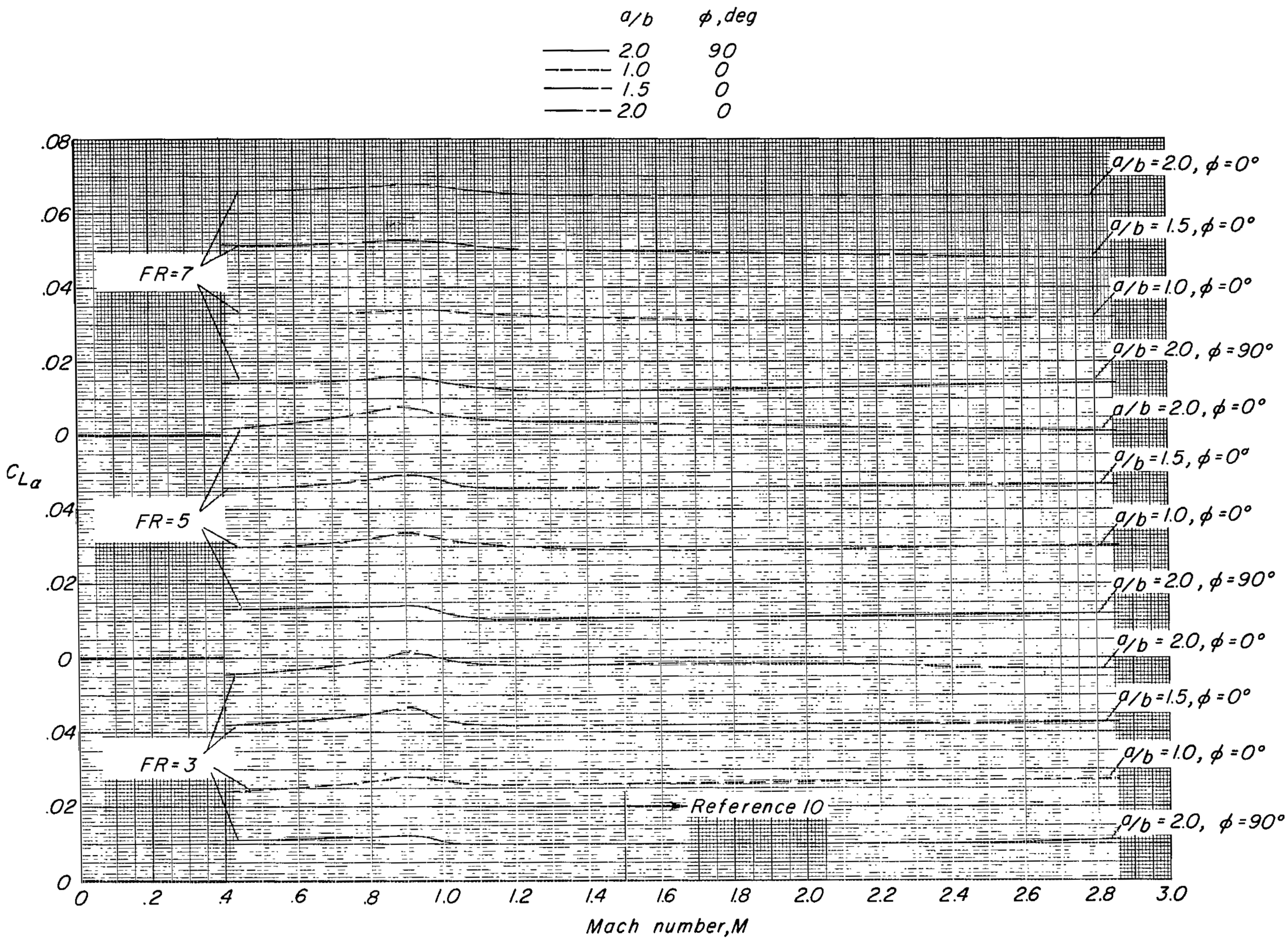

(a) Lift-curve slope based on base area.

Figure 19.- Effects of increasing Mach number on low-angle lift-curve slope for symmetrical bodies having variations in cross-sectional ellipticity.

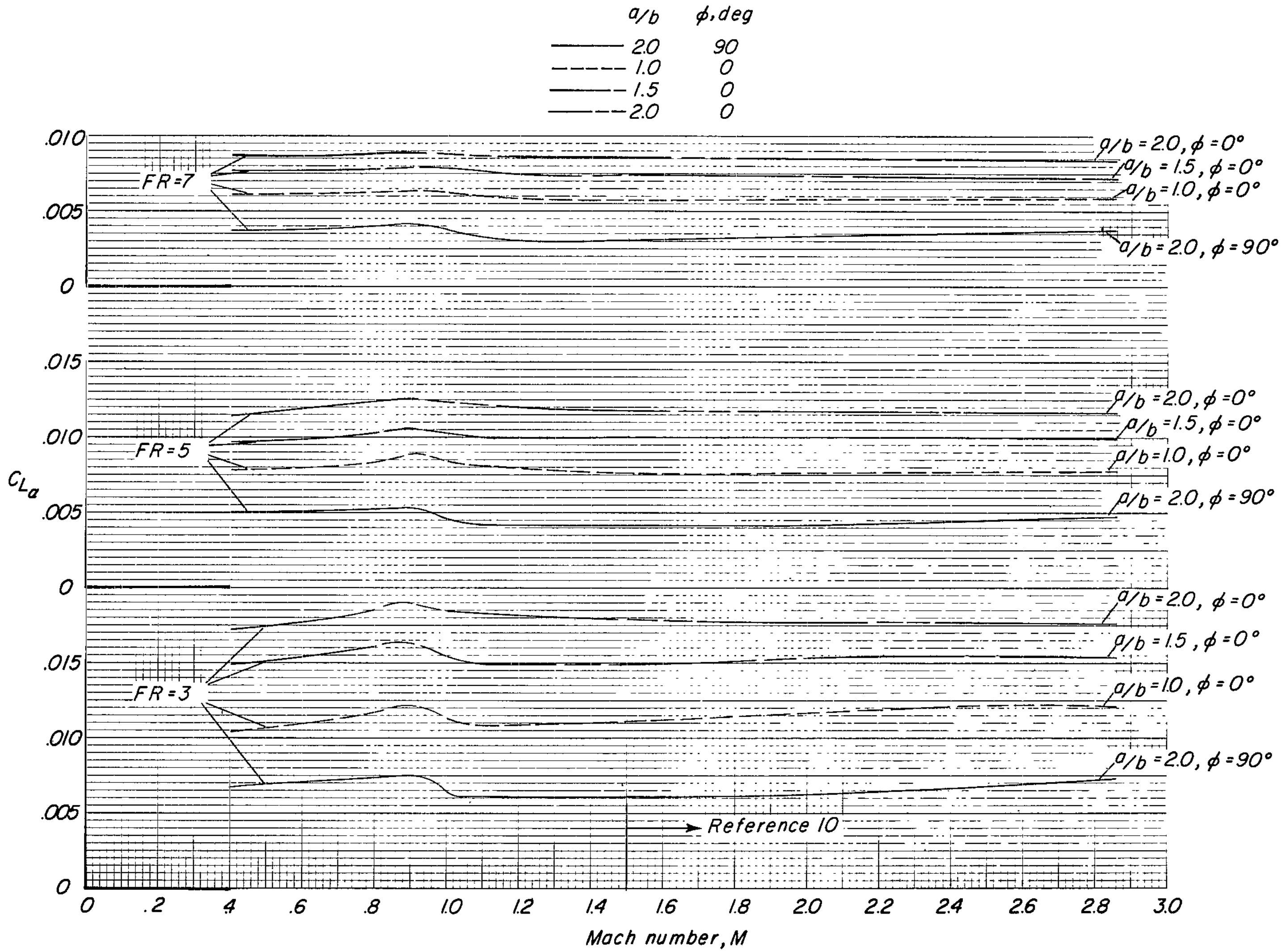

(b) Lift-curve slope based on projected planform area.

Figure 19.- Concluded.

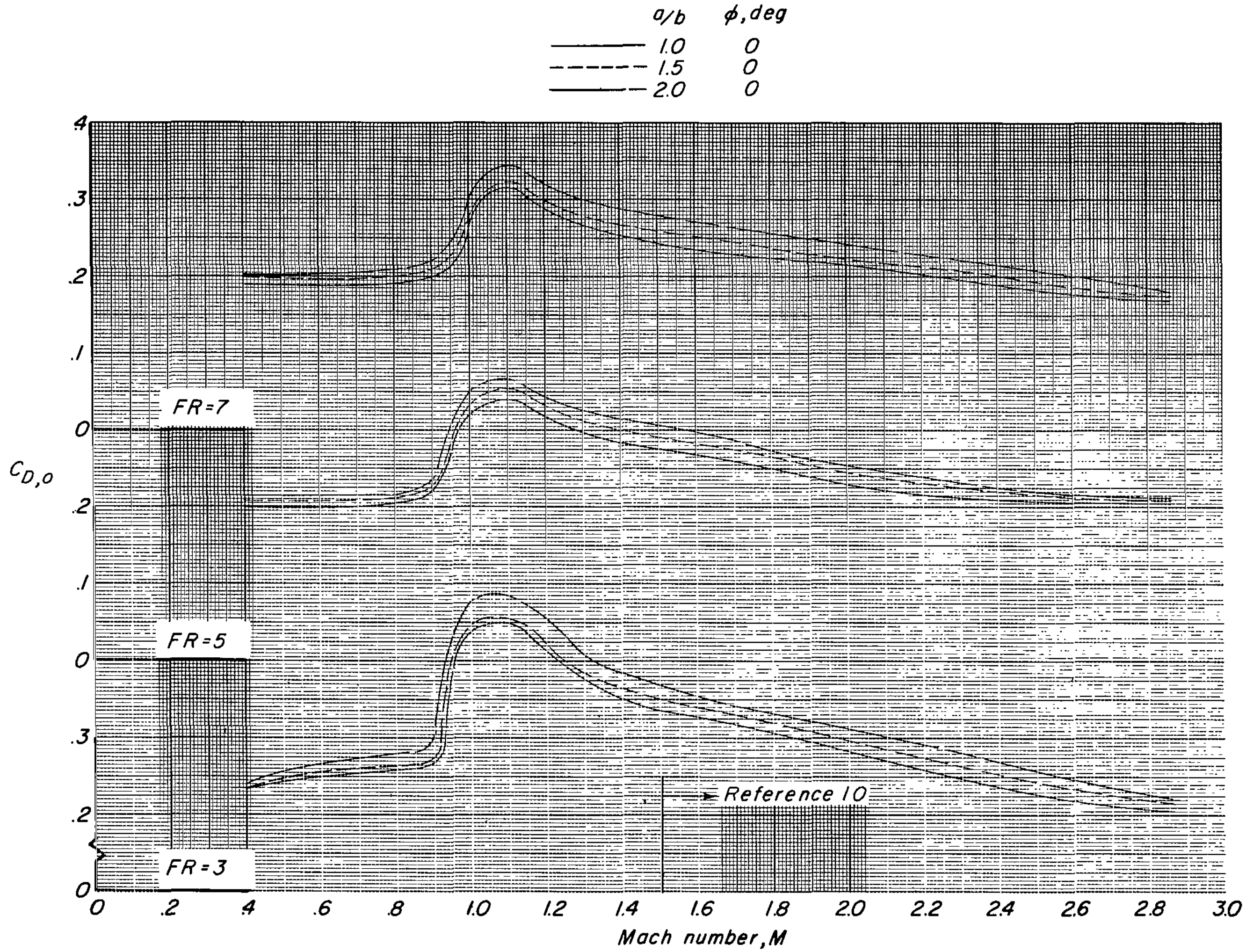

(a) Minimum drag based on base area.

Figure 20.- Effects of increasing Mach number on minimum drag for symmetrical bodies having variations in cross-sectional ellipticity.

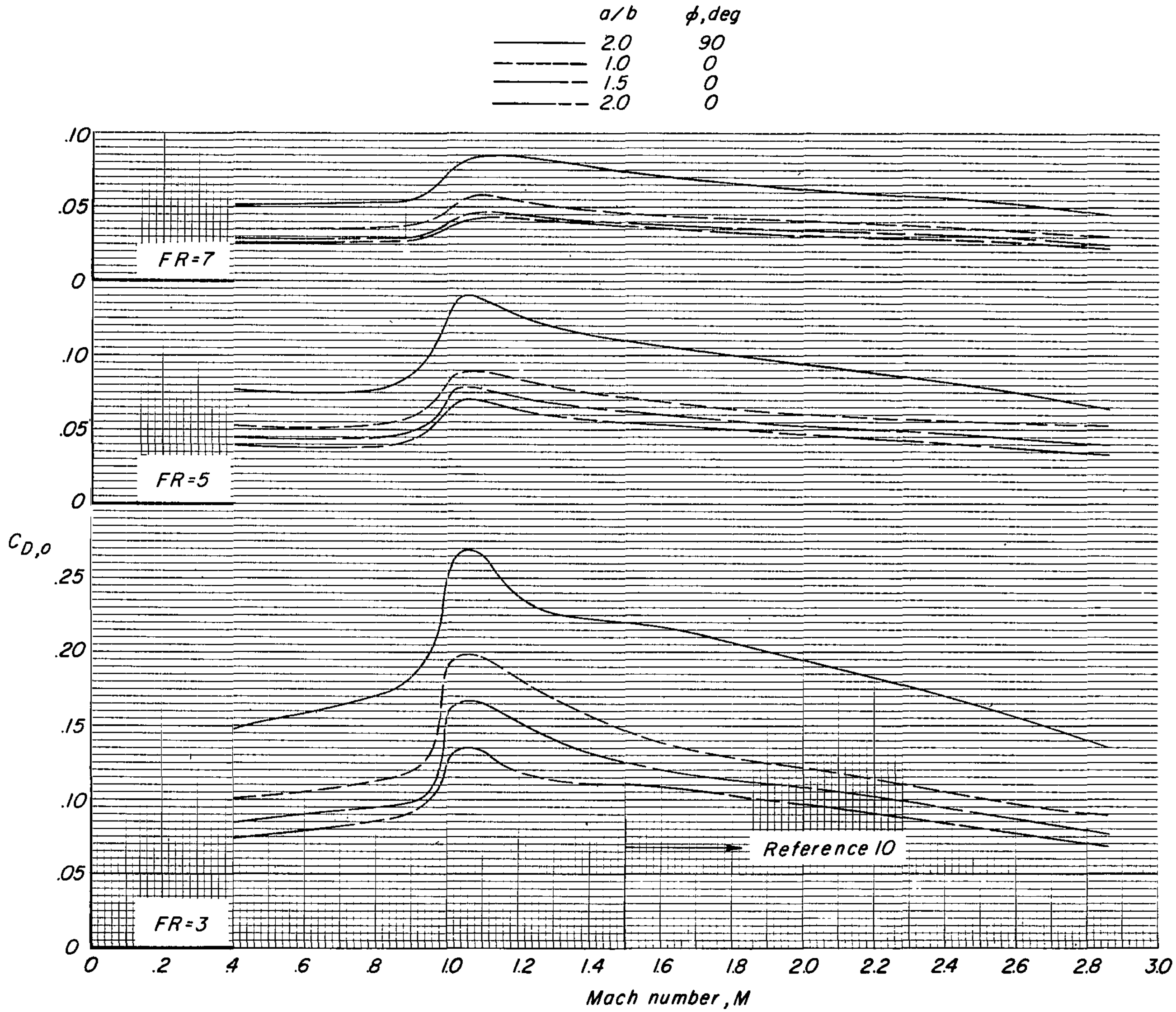

(b) Minimum drag based on projected planform area.

Figure 20.- Concluded.

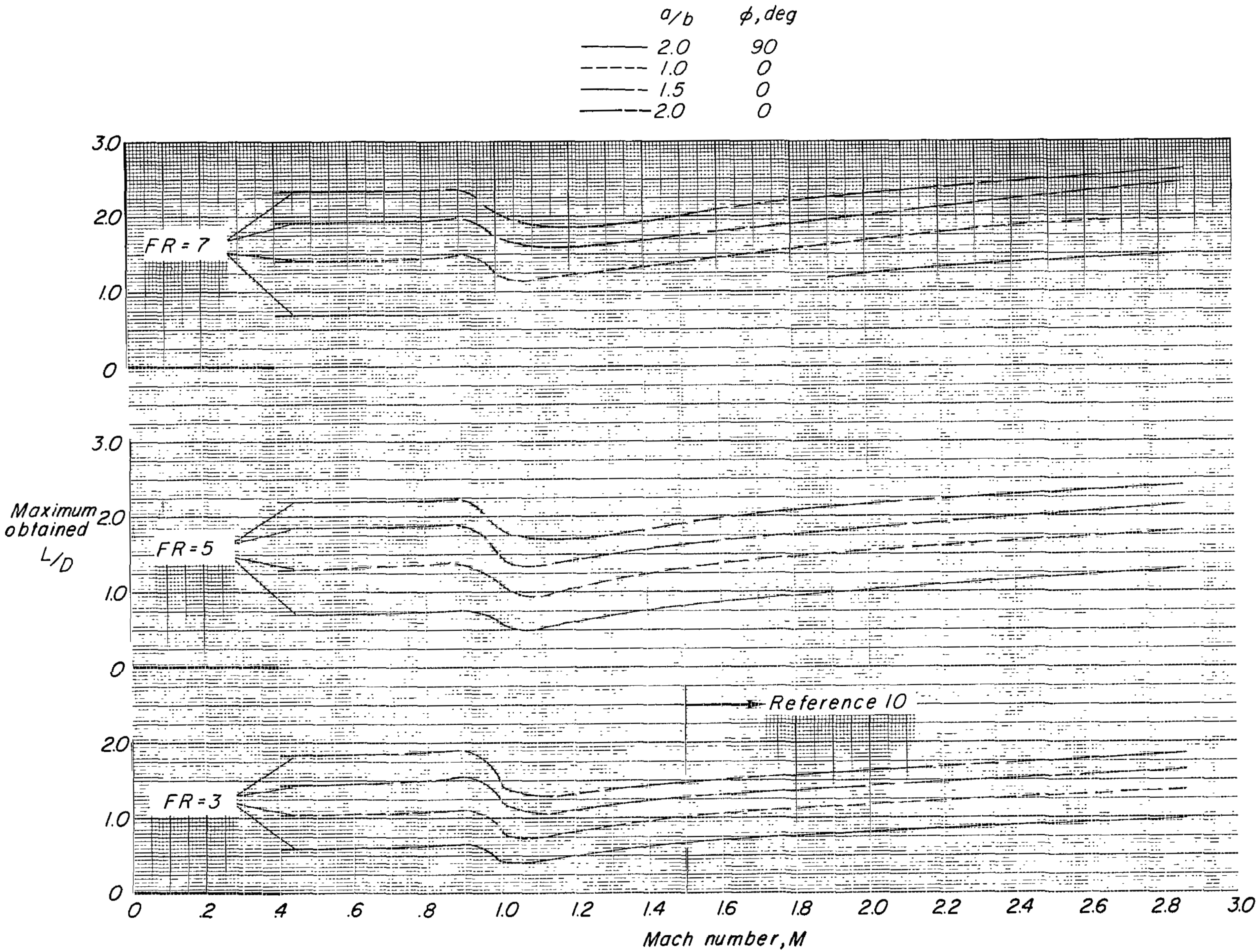

Figure 21.- Effects of increasing Mach number on maximum lift-drag ratio for symmetrical bodies having variations in cross-sectional ellipticity.

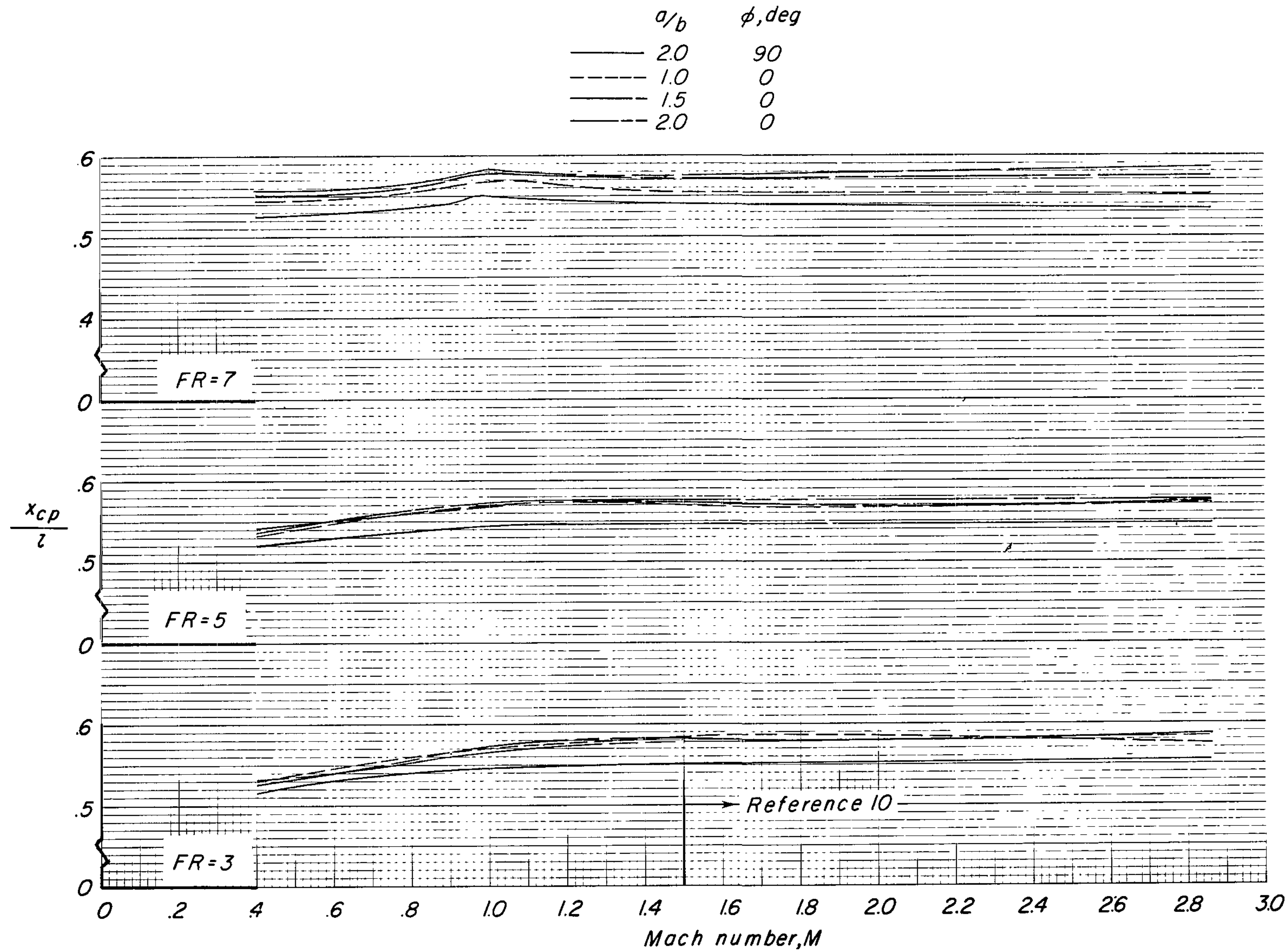

Figure 22.- Effects of increasing Mach number on longitudinal center-of-pressure location for symmetrical bodies having variations in cross-sectional ellipticity.

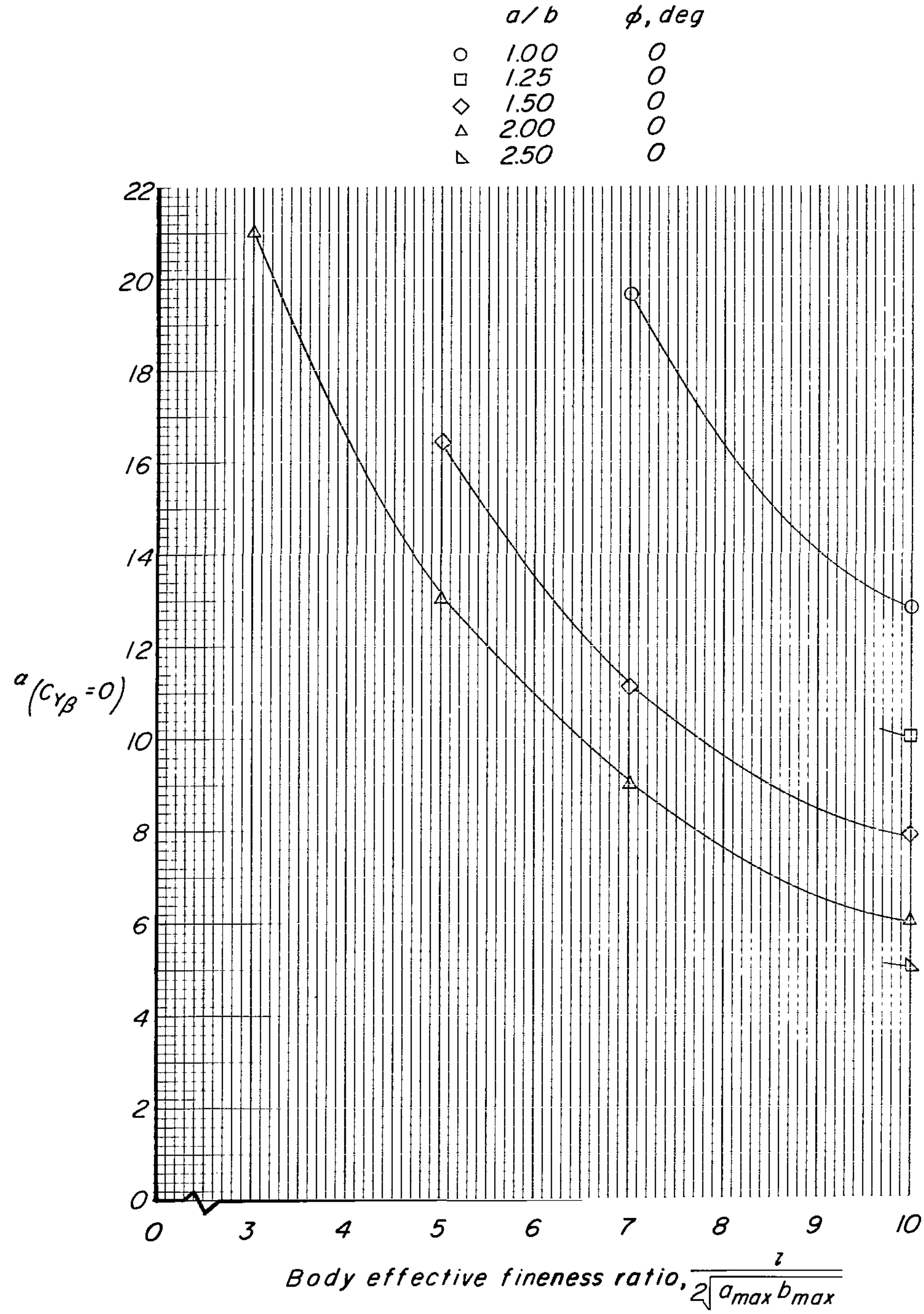

Figure 23.- Effects of ellipticity and effective fineness ratio on angle of attack at which changes in sign of side-force parameter C_{Y_β} occur. M = 0.40. (Data for fineness ratio 10 obtained from ref. 6.)

NASA-Langley, 1965 L-4127

"The aeronautical and space activities of the United States shall be conducted so as to contribute . . . to the expansion of human knowledge of phenomena in the atmosphere and space. The Administration shall provide for the widest practicable and appropriate dissemination of information concerning its activities and the results thereof."

—NATIONAL AERONAUTICS AND SPACE ACT OF 1958

NASA SCIENTIFIC AND TECHNICAL PUBLICATIONS

TECHNICAL REPORTS: Scientific and technical information considered important, complete, and a lasting contribution to existing knowledge.

TECHNICAL NOTES: Information less broad in scope but nevertheless of importance as a contribution to existing knowledge.

TECHNICAL MEMORANDUMS: Information receiving limited distribution because of preliminary data, security classification, or other reasons.

CONTRACTOR REPORTS: Technical information generated in connection with a NASA contract or grant and released under NASA auspices.

TECHNICAL TRANSLATIONS: Information published in a foreign language considered to merit NASA distribution in English.

TECHNICAL REPRINTS: Information derived from NASA activities and initially published in the form of journal articles.

SPECIAL PUBLICATIONS: Information derived from or of value to NASA activities but not necessarily reporting the results of individual NASA-programmed scientific efforts. Publications include conference proceedings, monographs, data compilations, handbooks, sourcebooks, and special bibliographies.

Details on the availability of these publications may be obtained from:

SCIENTIFIC AND TECHNICAL INFORMATION DIVISION

NATIONAL AERONAUTICS AND SPACE ADMINISTRATION

Washington, D.C. 20546